

THE STRUCTURE OF THE OUTER ATMOSPHERE OF COOL STARS

by

Peter Hermann Ulmschneider

A Dissertation Presented to the Faculty
of the Graduate School of Yale University
in Candidacy for the Degree of
Doctor of Philosophy

1966

Abstract

The production of accoustical noise in stellar convection zones is shown to give rise to stellar coronas, stellar winds and U-V radiation. Moreover it is found that the detailed structure of the outer atmospheres of stars is completely determined by this noise flux and that it consequently can be predicted for not too luminous stars of late spectral class.

Contents

	Page
Section 1. Introduction	1
Section 2. Flow and Pressure Equations	4
Section 3. The Shock Front	8
Section 4. Shock Equation	13
a) Shock equation without dissipation term	14
b) Inclusion of a dissipation term	21
c) Complete shock equation	26
d) Comparison with existing theories	27
Section 5. Composition and Thermal Properties of the Stellar Gas	32
a) Abundances	32
b) Internal energy and enthalpy	33
c) Ionization	37
d) The quantities γ , c_p , c_v and H	37
e) Numerical results	39
Section 6. Energy Equation	43
a) General formulation	43
b) Treatment without conduction	45
c) Treatment with conduction	46
Section 7. Radiation Losses	50
a) Temperatures below 7000 °K	50
b) Temperatures exceeding 7000 °K	51
c) Adopted loss function	52
Section 8. Computation of Noise Energy Production from Böhlm-Vitense's Models	55
a) Velocities	55

	Page
b) Production of accoustical noise energy	56
c) Frequency spectrum of the noise	56
d) The cut-off frequency	57
Section 9. Initial Conditions and the Photosphere	62
a) The height at which the shock forms	62
b) Models of stellar photospheres	63
c) Initial pressures	64
d) Shape compression factor	64
e) Initial heights	65
f) The zero reference level	66
g) Initial shock Mach numbers	66
h) Summary of initial values	68
i) Comparison of photospheric models	68
Section 10. The Complete Set of Equations and the Type of Solutions	71
a) Summary of the mathematical problem	71
b) Type of solutions	72
1) Conduction and shock dominated solutions (CD,SD)	72
2) Super- and subcritical solutions	72
3) The three critical solutions (CDC,SDCF,SDCR)	74
c) Selection of the solutions	75
Section 11. Computer Program	76
Section 12. The Principle of Shape Similarity Invariance and the Condition of Complete Shock Dissipation	78
Section 13. Numerical Results	84
a) Recalculation of Bird's results	84

	Page
b) Survey of the different solutions with the full set of equations	84
c) The models	89
Section 14. Discussion of the Solar Results	103
a) Discussion of the model	103
b) Comparison with observation and other models . . .	105
1) Corona temperature	105
2) Pressure and electron density	106
3) Shape compression factor	106
4) Total emission of transition layer and corona .	108
5) Mass flow	109
6) Mechanical energy input	110
7) Comparison with recent models of the transition layer	111
Section 15. Discussion of the Stellar Models	113
a) The amount of convective noise energy produced by different stars	113
b) Coronal temperatures and temperature gradients in the transition layers for different stars . . .	115
c) Comparison with Kuperus	117
Section 16. References	119
Section 17. Acknowledgments	123

	Page
Appendix A: Derivation of the shock equation	124
Appendix B: Principle of shape similarity invariance . . .	126
Appendix C: Entropy difference	130
Appendix D: Expansion for small shock Mach numbers	131
Appendix E: Equation of energy conservation	132
Appendix F: Shock behavior under energy conservation . . .	134
Appendix G: Importance of the bound state energy	135
Appendix H: Agreement with G. B. Field's results	136

Section 1. Introduction

During the last 20 years the existence of a corona, that is, of an extended dilute atmosphere of high temperature overlying the "normal" atmosphere of the sun has been well established.

However, until recently it was not very clear to what extent stars other than the sun possess extended atmospheres of a similar nature. This is somewhat surprising as the internal structure of stars is fairly well known as a function of luminosity and spectral class, and since moreover, quite early the correct mechanism responsible for the appearance of the corona was pointed out.

Qualitatively, the process is as follows: In the large turbulent convection zones of cool, not very luminous stars, accoustical noise is produced which represents at that level in the star only a minute fraction of the total energy contained in radiation and convective mass motion.

This sound energy travels outward into regions of lower and lower density. By the time the atmosphere becomes optically thin, all energy in the mass motion is converted into radiation, while the sound energy is carried by the particles of a more and more dilute gas.* Thus, the amplitude of the waves grow, until shock waves appear and a sudden conversion of sound energy into heat occurs.

*The exact nature of this conversion process including the so-called problem of overshooting [92] does not concern us here.

It is the purpose of this investigation to relate the energetic behavior of the convection zones to the structure of the outer atmospheres. The information required for this endeavor is available for the sun to a quite satisfactory degree. However, even in the stellar cases theoretical data provided by Böhm-Vitense [16] and others are sufficient to predict the transition from the photospheric to the coronal layers. It is nevertheless obvious that the sun serves as the primary test case for this type of work.

Previous models of the outer solar atmosphere have been based largely on the interpretation of observed data, such as the flash spectrum, the radio frequency and ultraviolet spectrum, and the like, thus relating the model atmosphere to the lower boundary, or on the observed solar wind which ties the model to the boundary behavior at infinity.

Computations of the type envisaged here have been carried out for the sun by Bird, Uchida, and others, and most recently by Kuperus who also treated the case of stellar coronas. The primary difficulty in this approach is the determination of the exact balance among the various energy terms, in particular, the shock dissipation, the radiative losses, the heat conduction, and the stellar wind flow. Thus, it presupposes a quite detailed knowledge of a variety of phenomena, in particular, the ones related to the passage of a shock through an atmosphere with variable density. In addition, the presence of radiation terms requires a certain degree of a-priori-information on the structure of the layers involved, and the availability of such quantities as the emission

coefficients for plasmas departing from thermodynamic equilibrium.

It is clear that this investigation is only one step further on the way to a quantitative understanding of outer stellar atmospheres. On the positive side we can say that we applied a more general theory of shock behavior, and that we thus were able to include in the energy balance dissipation, radiation, conduction, and flow terms. On the negative side, we have left out viscosity which is probably of minor importance, but more significantly, we left out magnetic fields. The reasoning in that respect was that for the sun magnetic fields are not the dominant feature outside of areas of activity.* Finally, the atmospheres were treated as homogeneous, so that for instance the spicule structure of the solar atmosphere that determines many of the observational features, such as the "height of the chromosphere," is lost.

We begin by a detailed discussion of the fundamental set of hydrodynamic equations, on which our shock theory is based. After deriving the theoretical relations that determine the energy balance across the outer atmosphere we introduce the numerical procedures and the computer program. Results were obtained for the sun and 3 stars of luminosity classes III- V, and comprise, in particular, the radial variation of electron temperature, gas pressure, and stellar wind velocity.

* This can be seen from arguments, given by Alfvén [5, Eq. (26), p. 95]. If, as is true at least for the upper photosphere in regions with no activity, the magnetic field lines, the direction of wavepropagation and the direction of the gas flow are all directed vertically, no energy is fed into magnetic field disturbances. Thus, no magnetohydrodynamic waves are generated.

Section 2. Flow and Pressure Equations

The behavior of a non-viscous fluid streaming with a velocity \vec{u} can be described by the following equations [58, p. 3]:

Eqn. of Continuity:

$$\frac{\partial \rho}{\partial t} + \nabla \cdot \rho \vec{u} = 0 . \quad (2-1)$$

Eqn. of Motion:

$$\frac{\partial \vec{u}}{\partial t} + (\vec{u} \cdot \nabla) \vec{u} = - \frac{1}{\rho} \nabla p - g \hat{x} . \quad (2-2)$$

Eqn. of Entropy Conservation:

$$\frac{\partial S}{\partial t} + \vec{u} \cdot \nabla S = \frac{\partial S}{\partial t} \Big|_{\text{ext}} . \quad (2-3)$$

These three equations determine the five state functions, \vec{u} (fluid velocity), ρ (density), p (pressure), uniquely if we specify the respective boundary conditions. S is the entropy, $\frac{\partial S}{\partial t} \Big|_{\text{ext}}$ the external entropy influx, g the gravitational acceleration, \hat{x} a unit vector in radial direction, t the time. The pressure p can be removed from the system by the eqn. of state.

In a stationary atmosphere the state functions are not explicit functions of time so that we can write in spherical one dimensional geometry [99]

$$\frac{d\rho}{dx} u + \rho \frac{du}{dx} + \frac{2\rho u}{x} = 0 , \quad (2-4)$$

$$u \frac{du}{dx} + \frac{1}{\rho} \frac{dp}{dx} + \frac{g_0 x_0^2}{x^2} = 0 . \quad (2-5)$$

As shown in Sec. 6 we can write:

$$c^2 = \gamma \frac{p}{\rho} = \gamma \frac{RT}{\mu} , \quad (2-6)$$

where T is the kinetic temperature, c the sound velocity, γ the ratio of specific heats, g_0 the gravitational acceleration at level x_0 .

Defining a dimensionless variable r

$$x = r \cdot r_0 , \quad (2-7)$$

where

$$r_0 = x_0 \quad (2-8)$$

is an arbitrary reference level in the star's atmosphere, and introducing the flow mach number M

$$M = \frac{u}{c} \quad (2-9)$$

we obtain

$$Mc \frac{dp}{dr} + \rho \frac{dMc}{dr} + \frac{2\rho Mc}{r} = 0 , \quad (2-10)$$

$$Mc \frac{dMc}{dr} + \frac{1}{\rho} \frac{dp}{dr} + \frac{g_0 r_0}{r^2} = 0 . \quad (2-11)$$

Differentiating Eq. (2-6) we obtain

$$\frac{dp}{dr} = \frac{c^2}{\gamma} \frac{d\rho}{dr} + \frac{\rho}{\gamma} \frac{dc^2}{dr} - \rho \frac{c^2}{\gamma^2} \frac{d\gamma}{dr} . \quad (2-12)$$

With Eq. (2-12) we eliminate dp/dr from (2-11):

$$\frac{dMc}{dr} (1-\gamma M^2) = \frac{M}{c} \frac{dc^2}{dr} - \frac{Mc}{\gamma} \frac{d\gamma}{dr} + \frac{\gamma M g_o r_o}{c r^2} - \frac{2Mc}{r} , \quad (2-13)$$

or

$$\frac{dM}{dr} = \frac{M}{1-\gamma M^2} \left(\frac{1-\gamma M^2}{2c^2} \frac{dc^2}{dr} - \frac{1}{\gamma} \frac{d\gamma}{dr} + \frac{\gamma g_o r_o}{c^2 r^2} - \frac{2}{r} \right) \quad (2-14)$$

Eq. (2-14) is the well known flow equation [12], [61], [80], [19].

Solving (2-11) for dp/dr yields

$$\frac{dp}{dr} = - \left(Mc^2 \frac{dM}{dr} - \frac{M^2}{2} \frac{dc^2}{dr} - \frac{g_o r_o}{r^2} \right) \rho \quad (2-15)$$

Eq. (2-15) is the pressure equation.

The pressure can also be computed in a different manner.

For this purpose we recall that Eqn. (2-1) in steady state reads

$$\nabla \cdot \rho \vec{u} = 0 . \quad (2-16)$$

Integrating (2-16) over a section of spherical volume bounded by a cone of unit solid angle and by the radii x_o and x we find [19]

$$0 = \int \nabla \cdot \rho \vec{u} \, d\tau = \int \rho \vec{u} \cdot d\vec{\sigma} = \rho u x^2 - \rho_o u_o x_o^2 . \quad (2-17)$$

Using Eqs. (2-6), (2-7) we obtain

$$p = \rho \frac{RT}{\mu} = \frac{p_o \mu_o M_o c_o}{T_o} \frac{T}{\mu M c r^2} . \quad (2-18)$$

In principle, Eqs. (2-18) and (2-15) are identical. In praxi, Eq. (2-15) will be used as a check on the accuracy of the numerical integration. The pressures derived from Eqs. (2-18) and (2-15) indeed agreed very well.

Section 3. The Shock Front

After introducing in the last section the fluid equations in a form suitable to our problem, we now turn to the discussion of the relations that govern the physical behaviour of the gas upon passage of a shock front.

First we have to connect the gas parameters on both sides of the discontinuity that represents the shock front.

Suppose the shock is given in a one dimensional flow. Then we know that mass, momentum and energy have to be conserved in the flow across the shock.

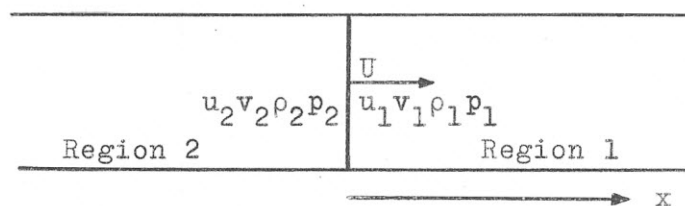


Fig. 1. One dimensional shock discontinuity

Suppose further that relative to the shock the functions of state which describe the flow are (v_1, ρ_1, p_1) , (v_2, ρ_2, p_2) where the subscript 1 refers to the parameters in the front of the shock [58, p. 318]. We have

$$\text{Mass flux:} \quad \rho_1 v_1 = \rho_2 v_2 = j \quad (3-1)$$

$$\text{Momentum flux:} \quad p_1 + \rho_1 v_1^2 = p_2 + \rho_2 v_2^2 \quad (3-2)$$

$$\text{Energy flux:} \quad H_1 + \frac{1}{2} v_1^2 = H_2 + \frac{1}{2} v_2^2 . \quad (3-3)$$

v_1 and v_2 are the velocities relative to the shock, u_1 and u_2 relative to the lab frame. ρ denotes density, p pressure and H enthalpy per gram, U the shock velocity relative to the lab frame.

Introducing the specific volume

$$v = \frac{1}{\rho} \quad (3-4)$$

We can write Eqs. (3-1) to (3-3) in a more convenient form

$$v_1 = jV_1 \quad v_2 = jV_2 \quad (3-5)$$

$$j^2 = \frac{p_2 - p_1}{v_1 - v_2} \quad (3-6)$$

$$v_1 - v_2 = j(V_1 - V_2) = \sqrt{(p_2 - p_1)(v_1 - v_2)} \quad (3-7)$$

$$H_1 - H_2 = \frac{1}{2} (v_2^2 - v_1^2) j^2 = \frac{1}{2} (v_1 + v_2)(p_1 - p_2) \quad (3-8)$$

Eq. (3-8) is the so-called shock adiabat [58, p. 320].

At this point we ought to emphasize that the actual shock structure in a gas is much more complicated as indicated by the above simple relations. We can summarize a more realistic picture [97], [117] leaving electric and magnetic effects aside, by distinguishing the following regions of a shock front:

1) External (kinetic) Relaxation Region.

This region immediately follows the shock front. The kinetic temperatures T_a , T_i , T_e of atoms, ions and electrons

respectively rise to an equal and very high value:

$$T_e = T_i = T_a$$

2) Internal (ionization and excitation) Relaxation Region.

Following kinetic relaxation, the electrons spend their energy in excitation and ionization; their kinetic temperature decreases:

$$T_e < T_i \approx T_a .$$

3) Radiative Recombination Region.

Here inelastic collisions between atoms, ions and electrons predominate and give rise to an ionizing radiation (which may penetrate to the front of the shock producing the precursors). At the same time, it leads to an equalization of the kinetic temperatures.

$$T_e = T_i = T_a .$$

For our purpose of main importance is the fact that the ratio of specific heats γ is the same from in front of the shock and in the front itself through the end of the kinetic relaxation region, where ionization starts to change γ . (See Section 5)

With these remarks in mind we now suppose that the specific heats c_p , c_v (per gram) depend only on the (kinetic) temperature (cf. Eqs. (5-15) to (5-17)).

We then can write:

$$H = c_p T = \frac{\gamma p V}{\gamma - 1}, \quad (3-9)$$

$$c_p - c_v = \frac{R}{\mu}, \quad (3-10)$$

$$\gamma = \frac{c_p}{c_v}. \quad (3-11)$$

where T is the temperature, R the gas constant in erg per degree K, μ the mean molecular weight. Hence,

$$\frac{v_1}{v_2} = \frac{\rho_1}{\rho_2} = \frac{v_2}{v_1} = \frac{(\gamma+1)p_1 + (\gamma-1)p_2}{(\gamma-1)p_1 + (\gamma+1)p_2}, \quad (3-12)$$

$$j^2 = \frac{1}{2v_1} \left((\gamma-1)p_1 + (\gamma+1)p_2 \right), \quad (3-13)$$

$$v_1^2 = \frac{1}{2} v_1 \left((\gamma-1)p_1 + (\gamma+1)p_2 \right). \quad (3-14)$$

With the flow velocities u relative to the lab frame and the sound velocity c_1 of the gas in front of the shock we can write the above equations in terms of the shock Mach number M_s ,

$$M_s = \frac{U - u_1}{c_1} = - \frac{v_1}{c_1}, \quad (3-15)$$

where

$$v_1 = u_1 - U \quad (3-16)$$

$$v_2 = u_2 - U \quad (3-17)$$

$$c_1^2 = \gamma \frac{p_1}{\rho_1} = \gamma p_1 v_1 \quad (3-18)$$

As a small disturbance in region 1 travels always with velocity c_1 we see that always

$$M_s \geq 1 \quad (3-19)$$

Thus we have as a final result [58, p. 331]

$$\frac{p_2}{p_1} = \frac{2\gamma M_s^2 - (\gamma - 1)}{\gamma + 1} \quad (3-20)$$

$$\frac{\rho_2}{\rho_1} = \frac{v_1}{v_2} = \frac{(\gamma + 1) M_s^2}{(\gamma - 1) M_s^2 + 2} \quad (3-21)$$

where γ is now a function of the temperature.

Section 4. Shock Equation

We are now ready to derive the relations which determine the behavior of the shock passing through the nonuniform medium described by the system of equations reviewed in Section 2.

The solutions have to conform to the conservation conditions derived in the last section which connect the parameters behind the shock front with those of the undisturbed steady state flow in front of the shock.

There are three different methods in the literature, to find the development of the shock Mach number M_s during the passage of the front through the medium.

- 1) The approach developed by Brinkley and Kirkwood [17] for underwater and atomic explosions. Here a shock of arbitrary strength is considered, and use is made of the "principle of shape similarity invariance" which is based essentially on experimental results.

This approach has been adopted by Schatzmann [93], Weymann [115] and Osterbrock [76] to the solar atmosphere for small shock Mach numbers.

- 2) The approach treating shocks as the result of the development of large amplitude sound waves which has been given by Landau and Lifshitz [58, p. 372].

This approach was adopted by Kuperus [54] to stellar coronas, again for small shock Mach numbers.

- 3) The approach based on the theory for shock tube experiments that was developed by Whitham [116] and Bird [11],[12],[14]

and adopted by Bird [13],[14] to the solar atmosphere for arbitrary shock Mach numbers.

We shall follow in our discussion Bird's treatment, however expand it to include the variability of γ and include the influence of dissipation terms on the shock Mach number as suggested by methods 1) and 2). We shall subsequently show that our treatment reduces to the above methods in their proper domain of validity.

a) Shock equation without dissipation.

First, let us modify Bird's treatment to account for a variable γ , but still without dissipation term.

All unsteady flow processes have one characteristic property in common. A disturbance at a point P of the x,t plane can be felt at a later instant only within a limited region, the so-called region of influence, bounded by the two characteristics C^+ , C^- that are defined respectively by the equations [72]

$$\frac{dx}{dt} = u \pm c \quad (4-1)$$

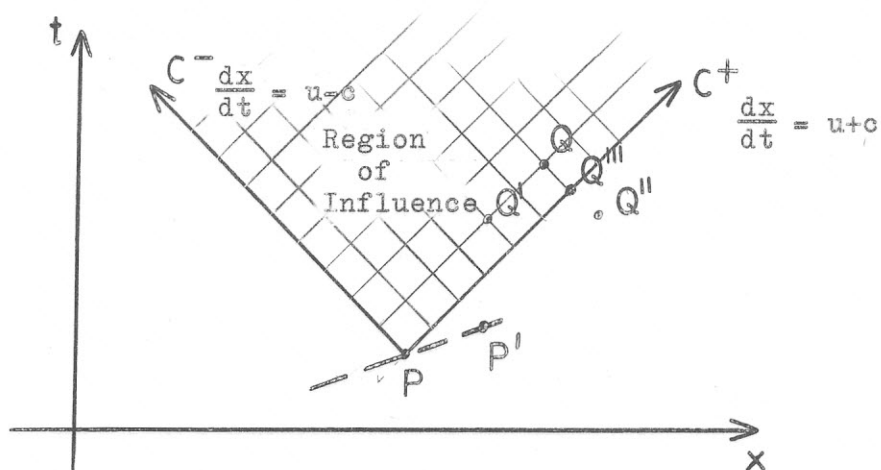


Fig. 2. Distance-time plot of a gas flow

dx/dt is the velocity of a disturbance, u the flow velocity, c the sound velocity as before.

The 3 equations of continuity, of momentum and energy conservation connect the 3 state functions ρ , p , u at the point Q with those at the point Q' . But under no circumstances can they connect the state functions at Q with those at Q'' , as Q'' is outside the region of influence.

Indeed P could be the seat of a discontinuity, and if the discontinuity propagates with velocity c , as for instance is the case with weak discontinuities or very weak shocks, the state functions would jump discontinuously at Q''' when we cross from Q to Q'' . At the point Q''' our time and space derivatives have to behave therefore in such a way that all derivatives across C^+ vanish.

In a gravitating atmosphere of spherical symmetry with outward mass flow we can write the basic equations in the form:
(See Sec. 2)

Eq. of Continuity

$$\frac{\partial \rho}{\partial t} + u \frac{\partial \rho}{\partial x} + \rho \frac{\partial u}{\partial x} + \frac{2u\rho}{x} = 0 \quad (4-2)$$

Eq. of Motion

$$\frac{\partial u}{\partial t} + u \frac{\partial u}{\partial x} + \frac{1}{\rho} \frac{\partial p}{\partial x} + g_0 \frac{x}{2} = 0 \quad (4-3)$$

Adiabatic eqs:*

*The use of this equation behind the shock front is somewhat problematic. The huge increase in entropy by the discontinuity is followed by an entropy loss due to recombination radiation. (cont.)

$$\frac{\partial p}{\partial t} + u \frac{\partial p}{\partial x} = c^2 \left(\frac{\partial \rho}{\partial t} + u \frac{\partial \rho}{\partial x} \right) \quad (4-4)$$

Again u is the flow velocity and x_0 , g_0 are defined like in section 2.

Eliminating ρ from Eq. (4-2) by Eq. (4-4) and using Eq. (4-3) we get

$$0 = \frac{\partial p}{\partial x} + \frac{1}{u \pm c} \frac{\partial p}{\partial t} \pm c \rho \left(\frac{\partial u}{\partial x} + \frac{1}{u \pm c} \frac{\partial u}{\partial t} \right) \pm \frac{c \rho}{u \pm c} g_0 \frac{x_0^2}{x^2} + \frac{c^2 \rho u^2}{(u \pm c)x} \quad (4-5)$$

and with the definition of the sound velocity

$$\frac{\partial p}{\partial x} \pm \frac{1}{u \pm c} \frac{\partial p}{\partial t} = c^2 \left(\frac{\partial \rho}{\partial x} + \frac{1}{u \pm c} \frac{\partial \rho}{\partial t} \right) \quad (4-6)$$

where the $\left\{ \begin{matrix} + \\ - \end{matrix} \right\}$ sign is valid in (4-5) and (4-6) if we are on $\left\{ \begin{matrix} C^+ \\ C^- \end{matrix} \right\}$.

The characteristic equations (4-5), (4-6) exhibit that there are only derivatives along the respective characteristics C^+ , C^- viz.

$$\left(\frac{\partial g}{\partial x} \right)_{\left\{ \begin{matrix} C^+ \\ C^- \end{matrix} \right\}} = \frac{\partial g}{\partial x} + \frac{\partial g}{\partial t} \frac{\partial t}{\partial x} \quad \left| \quad \left\{ \begin{matrix} C^+ \\ C^- \end{matrix} \right\} = \frac{\partial g}{\partial x} + \frac{\partial g}{\partial t} \frac{1}{u \pm c} \quad (4-7)$$

To show how these equations are applied in deriving the shock equation we consider the case of a shock generated by a piston

However this loss is small if the pressure and thus the temperature drops very rapidly to the equilibrium value. Whether this drop is indeed sufficiently rapid could only be ascertained by a detailed investigation of the ionization relaxation region which at present appears impossible to carry out.

moving into a tube. It is assumed that the gas is at rest in front of the shock.

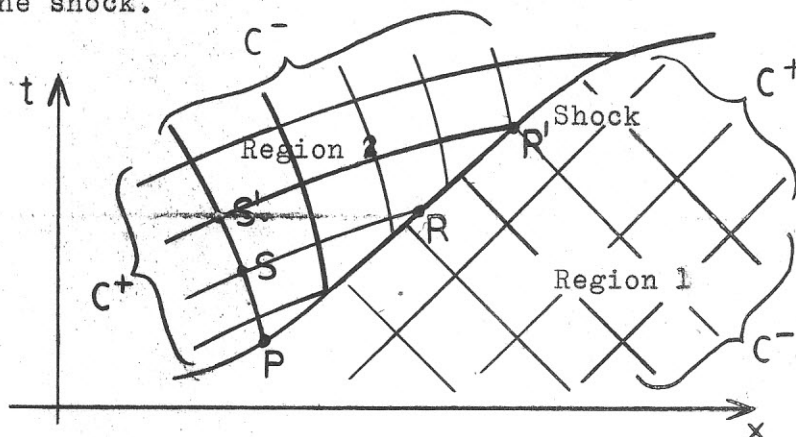


Fig. 3. Distance-time plot of a shock wave

The characteristics C^+ , C^- are drawn for both regions. The slope of C^+ in region 1 is larger than the slope of the shock world line that indicates the supersonic propagation of the shock into region 1.

Consider now a point P on the shock world line. From P disturbances travel along C^- until they get reflected on density variations at S and S' . They travel along C^+ to catch up with the shock and modify it at R , R' .

These so-called re-reflected waves should be taken into account at every point if we want to use the characteristic equations in region 2.

The effort is greatly reduced if we neglect the effect of the re-reflected waves altogether as has been done by Bird [11], [12] and Whitham [116]. This procedure will be called BW approximation.

Bird [11] has compared the BW approximation with exact calculations and found that there is very good agreement when

shocks propagate toward lower densities. We feel that the reason for this good agreement is the fact that disturbances travelling towards regions of higher density such as those travelling along C^- are damped out as already Lamb [57] has shown for an isothermal atmosphere.

With the BW approximation we can use the characteristic equation along C^+ until it meets the shock. There the quantities are connected across the shock with the flow in front via the equations derived in Section 3.

We have:

$$(4-5): \quad \frac{dp_2}{dx} + c_2 \rho_2 \frac{du_2}{dx} + \frac{c_2 \rho_2}{u_2 + c_2} \left(g_0 \frac{x_0^2}{x^2} + \frac{2c_2 u_2}{x} \right) = 0 \quad (4-8)$$

$$(3-20): \quad \frac{p_2}{p_1} = \frac{2\gamma M_s^2 - (\gamma - 1)}{\gamma + 1} = \phi \quad (4-9)$$

$$(3-21): \quad \frac{\rho_2}{\rho_1} = \frac{(\gamma + 1) M_s^2}{(\gamma - 1) M_s^2 + 2} = \theta \quad (4-10)$$

$$\frac{u_2 - U}{u_1 - U} = \frac{(\gamma - 1) M_s^2 + 2}{(\gamma + 1) M_s^2} = \frac{1}{\theta} \quad (4-11)$$

$$M_s = \frac{U - u_1}{c_1} \quad M = \frac{u_1}{c_1} \quad (4-12)$$

$$\frac{c_2}{c_1} = \left(\gamma \frac{p_2}{\rho_2} / \gamma \frac{p_1}{\rho_1} \right)^{1/2} = \left(\frac{\phi}{\theta} \right)^{1/2} = \zeta \quad (4-13)$$

Now it is true identically that:

$$\frac{u_2}{u_1} = \frac{u_2 - U}{u_1 - U} \cdot \frac{u_1 - U}{c_1} = \frac{u_1 - U}{c_1} + \frac{u_1}{c} \quad (4-14)$$

$$= \left(1 - \frac{1}{\theta}\right) M_s + M$$

or

$$\frac{u_2}{c_1} = \xi + M, \quad (4-15)$$

$$\xi = \frac{2M_s^2 - 2}{(\gamma + 1)M_s}. \quad (4-16)$$

Going over to the dimensionless variable v as in Sec. 2 we obtain after some manipulations (cf. Appendix A)

$$\begin{aligned} \frac{dM_s}{dr} = & \frac{\zeta \eta M_s}{1 - \gamma M^2} \left\{ - \frac{(\xi + 2M - (\gamma \xi + 2\zeta)M^2)}{2} \frac{1}{c^2} \frac{dc^2}{dr} + \right. \\ & + \frac{1}{\xi + \zeta + M} \left((\zeta(\xi + \zeta) - 1 + (\zeta - \gamma(\xi + \zeta))M) \frac{g_o r_o}{c^2 r^2} - \right. \\ & - \frac{1}{\xi + \zeta + M} \left(\zeta \xi - \xi M + (\zeta^2 - 1 - (\gamma - 1)\zeta \xi)M^2 - (\gamma - 1)\zeta M^3 \right)^2 r - \\ & \left. - (\delta - M + (\zeta - \gamma \delta)M^2) \frac{1}{\gamma} \frac{d\gamma}{dr} \right\}, \quad (4-17) \end{aligned}$$

where

$$\eta = \frac{(\gamma+1)/2}{\frac{2}{\gamma+1} \left((\gamma-1)M_s^2 + 2 \right) + \zeta \left(\frac{M_s^2 + 1}{M_s} \right)} \quad (4-18)$$

and

$$\delta = \frac{\xi}{\gamma+1} \left(\frac{M_s}{\theta\zeta} - \gamma \right) \quad (4-19)$$

Equation (4-17) is identical with Bird's [12] result except for the additional term proportional to $\frac{1}{\gamma} \frac{dy}{dr}$.

Letting $dc^2/dr \rightarrow 0$, $g_0 \rightarrow 0$, $2/r \rightarrow 0/r$ (plane geometry), $dy/dr \rightarrow 0$ we see that the right hand side of Eq. (4-17) goes to zero, and as $M_s \geq 1$

$$\frac{dM_s}{dr} \rightarrow 0. \quad (4-20)$$

We thus have shown that Bird's theory is a constant flux theory where the energy loss by dissipation is resupplied from a reservoir such as a piston moving with constant velocity into a pipe. In our case where we have shocks of a given shape (triangular shape) the energy is carried in this shape of the shock and the shock thus becomes the smaller the more it dissipates.

This effect of modification of the shock Mach number by dissipation is the dominant feature of the approach by Brinkley and Kirkwood [17] which we will discuss now.

b) Inclusion of a dissipation term.

To calculate the rate of dissipation of a shock we consider a shock pulse of arbitrary shape in a gas at rest:

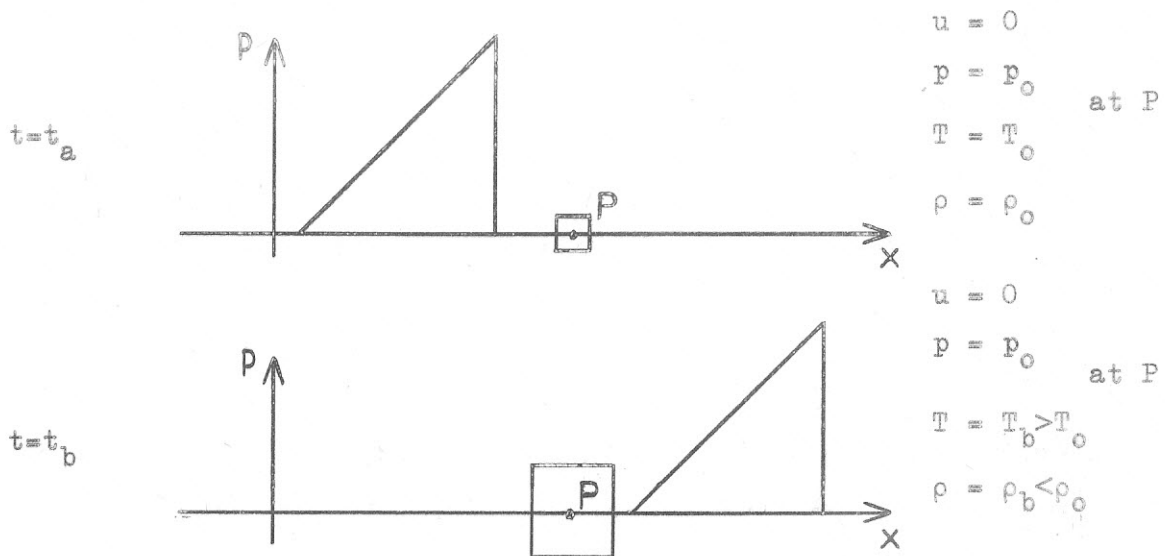


Fig. 4. Fluid element before (top) and after (bottom) arrival of a shock pulse.

The total work done on the small volume element at P is

$$\Delta W = \Delta E + p_0 \Delta V = \Delta H, \quad (4-21)$$

i.e., we have increased the internal energy and the volume against the pressure p_0 . H is the enthalpy per gram.

If $D(x)$ is the total energy of the shock per unit area of initial surface in our spherical geometry, then

$$\frac{dD(x)}{dx} = -\rho_0 \Delta H \frac{x^2}{x_0^2} \quad (4-22)$$

where

$$D(x) = \frac{x^2}{x_0^2} \int_{t_0}^{\infty} (p - p_0) u dt \quad (4-23)$$

Here pressure p and flow velocity u refer to the shock profile, t_x is the time of arrival of the shock front at the point x .

We can rewrite this integral using the "principle of shape similarity invariance" as defined in Appendix B and obtain

$$D(x) = \frac{x^2}{x_0^2} p_m u_m \pi \nu \quad (4-24)$$

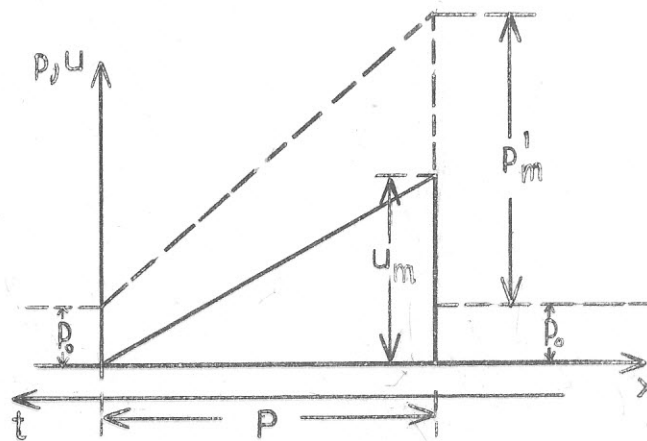


Fig. 5. Triangle shock pulse.

p_m is the maximum pressure difference, u_m the maximum velocity difference, π the time scale, ν the form factor and

$$\pi = \begin{cases} \frac{P}{2} & \text{for triangular shocks} \\ \frac{P}{2} & \text{for exponential shocks} \\ \frac{P}{4} & \text{for sawtooth shocks} \end{cases} \quad (4-25)$$

with:

$$v = \left\{ \begin{array}{l} \frac{2}{3} \text{ for triangular} \\ 1 \text{ for exponential} \\ \frac{1}{3} \text{ for sawtooth} \end{array} \right\} \text{ shocks} \quad (4-26)$$

and P the period of the shock.

Now ΔH is the total enthalpy change after the pressure has come back to equilibrium

$$\Delta H = T \Delta S + V \Delta p. \quad (4-27)$$

Using the results of Appendix C we have

$$\Delta H = T c_v \ln \frac{p}{p_0} \left(\frac{\rho}{\rho_0} \right)^{-\gamma} \quad (4-28)$$

or with Eqs. (4-9) and (4-10):

$$\Delta H = T c_v \ln \phi \theta^{-\gamma} \quad (4-29)$$

From Eqs. (3-9) to (3-11) we know that

$$c_v = \frac{c^2}{\mu(\gamma-1)} = \frac{c^2}{T\gamma(\gamma-1)} \quad (4-30)$$

so that

$$\Delta H = \frac{c^2}{\gamma(\gamma-1)} \ln \phi \theta^{-\gamma} \quad (4-31)$$

Thus

$$\frac{dD(x)}{dx} = -\rho \frac{x^2 c^2}{x_0^2 \gamma(\gamma-1)} \ln \phi \theta^{-\gamma} \quad (4-32)$$

and with Eqs. (4-16) and (4-9)

$$D(x) = \frac{x^2}{x_0^2} (\phi-1) p \xi c \mu \nu \quad (4-33)$$

where we neglected $M \approx 10^{-4}$ against $\xi \approx 1$.* This neglect is permissible in most of our applications, except close to the critical point. However, there almost all shock energy is dissipated already.

Holding x^2/x_0^2 , p , c constant and differentiating only the terms contributing to the dissipation term as we have already treated all the other contributions, we obtain

$$\frac{dD(x)}{dx} = \frac{x^2}{x_0^2} p c \mu \nu \left(\xi \frac{d(\phi-1)}{dx} + (\phi-1) \frac{d\xi}{dx} \right) \quad (4-34)$$

Using the definitions of ϕ and ξ again and

$$p = \rho \frac{c^2}{\gamma}$$

we find instead of (4-34):

* One might think that as dM/dr is large, it should contribute to (4-34), however even when M changes from 10^{-4} to 10^{-2} it is still much smaller than ξ .

$$\frac{dD(x)}{dx} = \rho \frac{x^2}{x_0^2} c^3 \left[\frac{4}{(\gamma+1)^2} (3M_s^2 - 2 - \frac{1}{M_s^2}) \frac{dM_s}{dx} \right] \quad (4-35)$$

Comparison with (4-32) yields:

$$\frac{dM_s}{dx} = - \frac{1}{4c} \frac{(\gamma+1)^2}{\gamma(\gamma-1)} \frac{\ln \phi \theta^{-\gamma}}{(3M_s^2 - 2 - \frac{1}{M_s^2})} \quad (4-36)$$

or with the dimensionless variable r from Sec. 2:

$$\frac{dM_s}{dr} = - \frac{1}{4} \frac{r_0 x}{c_1} \left[\frac{1}{M_s^2} \right] \quad (4-37)$$

where

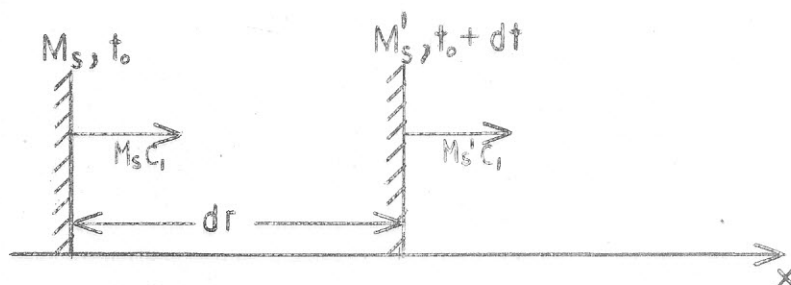
$$x = \frac{(\gamma+1)^2}{\gamma(\gamma-1)} \frac{\ln \phi \theta^{-\gamma}}{(3M_s^2 - 2 - \frac{1}{M_s^2})} \quad (4-38)$$

There is one more minor correction to be applied to (4-37).

So far we assumed that there is no flow in front of the shock.

To include such a flow we consider the following situation:

a) $u = Mc_1 = 0$



$$b) \quad u = Mc_1 \neq 0$$

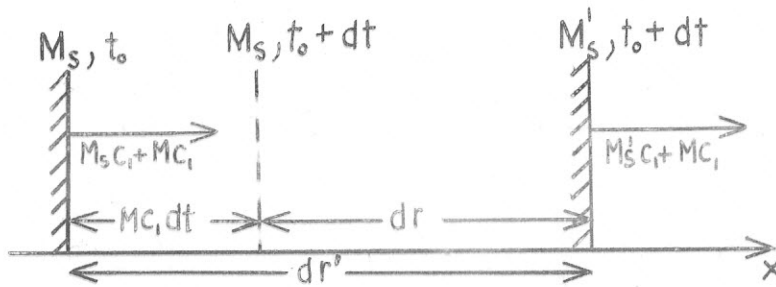


Fig. 6. Influence of fluid flow on the shock dissipation.

$$\text{Now: } dr' = dr + Mc_1 dt \quad dr = M_s c_1 dt \quad \text{or } dr' = dr \left(1 + \frac{M}{M_s}\right)$$

Thus instead of (4-37) we have

$$\frac{dM_s}{dr'} = \frac{dM_s}{dr} \cdot \frac{1}{1 + \frac{M}{M_s}} = -\frac{1}{4} \frac{\chi r_0}{c^2 \nu \left(1 + \frac{M}{M_s}\right)} \quad (4-39)$$

c) Complete shock equation

The complete shock equation can now be written as

$$\begin{aligned} \frac{dM_s}{dr} &= \frac{\zeta \eta M_s}{1 - \gamma M^2} \left\{ -\frac{(\xi + 2M - (\gamma \xi + 2\zeta)M^2)}{2} \frac{1}{c^2} \frac{dc^2}{dr} + \right. \\ &+ \frac{1}{\xi + \zeta + M} \left((\zeta(\xi + \zeta) - 1 + (\zeta - \gamma(\xi + \zeta))M) \frac{g_0 r_0}{c^2 r^2} - \right. \\ &- \frac{1}{\xi + \zeta + M} \left(\zeta \xi - \xi M + (\zeta^2 - 1 - (\gamma - 1)\zeta \xi)M^2 - (\gamma - 1)\zeta M^3 \right) \frac{2}{r} - \\ &\left. \left. - (\delta - M + (\zeta - \gamma \delta)M^2) \frac{1}{\gamma} \frac{d\gamma}{dr} \right\} - \frac{1}{4} \frac{\chi r_0}{c^2 \nu \left(1 + \frac{M}{M_s}\right)}, \quad (4-40) \end{aligned}$$

with η , δ , χ defined by Eqs. (4-18), (4-19) and (4-38) respectively.

d) Comparison with existing theories

1) Bird [12]:

Putting $\gamma = \text{constant}$, $\mu = 1$ and neglecting the dissipation term leads immediately back to Bird's theory.

2) Schatzmann [93], Weymann [115], Osterbrock [76]:

These theories are valid only for weak shocks see Osterbrock [76, p. 369], $\gamma = \text{const.}$ and no mass motion.

For weak shocks we can define a "shock strength $\bar{\eta}$ " by the relation

$$\rho_2 - \rho_1 = \bar{\eta} \rho_1, \quad \bar{\eta} \ll 1, \quad (4-41)$$

where again the indices 1 and 2 refer to the regions in front of and behind the shock respectively. With Eq. (3-21) we get

$$\bar{\eta} = 2 \frac{M_s^2 - 1}{(\gamma - 1)M_s^2 + 2} \approx \frac{4\alpha}{\gamma + 1}, \quad (4-42)$$

where for weak shocks the shock Mach number is written as

$$M_s = 1 + \alpha. \quad (4-43)$$

Suppose now that there is no mass motion in the atmosphere. We can expand Eq. (4-40) in terms of α up to terms of order α^2 (See Appendix D):

$$\frac{1}{\alpha} \frac{d\alpha}{dr} = -\frac{1}{4} \frac{1}{c} \frac{dc^2}{dr} + \frac{r_0}{2h} - \frac{1}{6} \frac{r_0 \alpha}{c \mu v}, \quad (4-44)$$

where:

$$H_s = \frac{RT}{\mu g_0} \frac{x^2}{x_0^2} = \frac{c^2 r^2}{\gamma g_0}$$

is the scale height.

Using the more familiar relation

$$x = r \cdot r_0$$

from Sec. 2 and (4-42) we have

$$\frac{1}{\bar{\eta}} \frac{d\bar{\eta}}{dx} = \frac{1}{4} \frac{1}{c^2} \frac{dc^2}{dx} + \frac{1}{2H_s} - \frac{\gamma+1}{24} \frac{1}{c \bar{\mu} \bar{\nu}} \bar{\eta} \quad (4-45)$$

Inserting $\bar{\mu} \bar{\nu} = P/12$ from Eqs. (4-25), (4-26) for sawtooth shocks (4-45) becomes identical with Osterbrock's result in the absence of an external magnetic field.

It is interesting to note that the first and second term arise purely from energy conservation. This fact shows again that Bird's theory is one applying energy conservation. The first term modifies the shock strength such that energy is conserved when the shock enters a region with different sound velocity, but equal pressure. (See Appendix F). The shock strength decreases as the sound velocity increases. The second term modifies the shock strength such that energy is conserved when a shock travels down a density gradient produced by a gravitational field. (See Appendix F). Here the shock strength gets longer with decreasing density.

The third term is the Brinkley-Kirkwood dissipation term, the only term proportional to $\bar{\eta}$.

2) Landau-Lifshitz [58], Kuperus [54].

This approach too is restricted to weak shocks as only small amplitude waves remain simple waves in second approximation, cf. Landau-Lifshitz [58, p. 377].

For weak shock waves we know the energy in a sawtooth wave: (Problem 1 [58, p. 377]) to be:

$$E = E_0 / (1 + av_0 t / l_0)^2, \quad (4-46)$$

where

$$a = \frac{1}{2} (\gamma + 1).$$

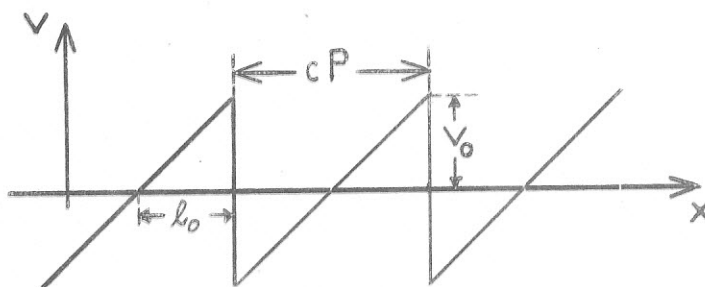


Fig. 7. Sawtooth shock

Now:

$$E = E_0 (1 + bx)^{-2}, \quad b = \frac{1}{2} (\gamma + 1) \frac{2v_0}{2l_0 c} \quad (4-47)$$

or:

$$\frac{1}{E(0)} \frac{dE(0)}{dx} = -2b = -\frac{(\gamma+1)\bar{\eta}}{cP} \quad (4-48)$$

where we used Eq. (2) of Appendix F, that is:

$$u = 2v_0 = \bar{\eta}c \quad (4-49)$$

and:

$$2\lambda_0 = cP = \frac{c}{\nu} \quad (4-50)$$

Here P is the period, ν the frequency of the shock waves.

According to Eq. (4-24) the energy in the shock wave can be written

$$E = p' u \pi \nu \quad (4-51)$$

or with

$$p' = \gamma \bar{\eta} p_0 \quad (4-52)$$

from (3-20) using

$$M_s = 1 + \alpha = 1 + \frac{\gamma+1}{4} \bar{\eta} ,$$

we get:

$$E = \gamma c p_0 \pi \nu \bar{\eta}^2 . \quad (4-53)$$

Hence

$$\frac{1}{E} \frac{dE}{dx} = 2 \frac{1}{\bar{\eta}} \frac{d\bar{\eta}}{dx} \quad (4-54)$$

Since for sawtooth shocks $\mu v = P/12$ we finally obtain:

$$\frac{1}{\bar{\eta}} \frac{d\bar{\eta}}{dx} = - \frac{\gamma+1}{24} \frac{1}{c \mu v} \bar{\eta} \quad (4-55)$$

This is identical with our Eq. (4-45). The energy conservation terms have to be added in Eq. (4-55).

Section 5. Composition and Thermal Properties of the Stellar Gas

Before we derive the third and last major relation required for our problem, we would like to show how γ , μ and H may be computed in stellar atmospheres.

a) Abundances

We considered the ten most abundant elements according to Aller [4] i.e. H, He, C, N, O, Ne, Mg, Si, S, Fe with the following abundances:

Element	ϵ_i
H	1,000,000
He	157,000
C	400
N	891
O	100
Ne	500
Mg	32
Si	27
S	20
Fe	9

Table 1. Abundances by number

Atomic parameters such as ionization potentials, etc. were taken from Allen [2].

b) Internal energy and enthalpy.

Under conditions of thermodynamic equilibrium, internal energy E , enthalpy H and the adiabatic coefficient γ are functions of temperature and density or pressure.

In the regions of interest of our problem thermal equilibrium is not established, and we have to reformulate the expressions for E , H and γ .

For this purpose we consider a gas of N_0 neutral particles of which $v_1 N_0$ are H atoms, $v_2 N_0$ are He atoms, $v_3 N_0$ are C atoms etc., then we have:

$$v_i = \frac{\epsilon_i}{\sum_i \epsilon_i} \quad \sum_i v_i = 1 \quad (5-1)$$

where the ϵ_i 's are the abundances by number. At a given temperature we define

$$x_{i0} = 1 - \sum_{r=1}^{f_i} x_{ir} \quad \text{fraction of element } i \text{ in neutral state}$$

$$x_{i1} \quad \text{fraction of element } i \text{ in first ionized state}$$

.

.

.

$$x_i f_i \quad \text{fraction of element } i \text{ in fully ionized state}$$

Let χ_{ir} be the ionization potentials of element i in stage of ionization r .

The internal energy can now be written as the sum of the translation, ionization and excitation energies:

$$E = E_{\text{transl.}} + E_{\text{ioniz.}} + E_{\text{excit.}} \quad (5-2)$$

According to Rosa and Unsöld [89] and making explicit use of the one to one correspondence of thermodynamics to statistical mechanics in our problem which is possible for particles with a Maxwellian velocity distribution.

$$\begin{aligned} E_{\text{ioniz.}} &= N_0 \sum_i v_i \{ x_{i1} x_{i1} + x_{i2} \{ x_{i1} + x_{i2} \} + \dots \} \\ &= N_0 \sum_i v_i \sum_{r=1}^{f_i} x_{ir} \sum_{l=1}^r x_{il} \end{aligned} \quad (5-3)$$

$$\begin{aligned} E_{\text{trans.}} &= N_0 \frac{3}{2} k T_e \sum_i v_i \{ 1 + x_{i1} + 2x_{i2} + \dots + f_i x_{if_i} \} \\ &= N_0 \frac{3}{2} k T_e \left\{ 1 + \sum_i v_i (x_{i1} + 2x_{i2} + \dots + f_i x_{if_i}) \right\} \\ &= N_0 \frac{3}{2} k T_e (1 + \bar{x}) \end{aligned} \quad (5-4)$$

where

$$\bar{x} = \sum_i v_i \sum_{r=1}^{f_i} r x_{ir} \quad (5-5)$$

These two terms are formally identical with the corresponding equilibrium terms, if we insert for "the" temperature the kinetic temperature T_e which we assume to be the same for all particles. The actual departures from equilibrium are of course hidden in the

expressions to be given for the x_{ir} 's.

Turning now to the bound states, we have similarly [89]

$$E_{\text{excit.}} = N_0 \sum_i v_i \sum_{r=0}^f x_{ir} \sum_{s=0}^{n_i^*} x_{irs} N_{irs} \quad (5-6)$$

where:

$$N_{irs} = b_{irs} N_{irs}^* \quad (5-7)$$

with:

$$N_{irs}^* = \frac{g_{irs} e^{-\chi_{irs}/kT_e}}{n_i^* \sum_{s=0} g_{irs} e^{-\chi_{irs}/kT_e}} \quad (5-8)$$

For n_i^* the number of the shell limit because of the Stark effect one may take:

$$\log n_i^* = 1.620 + \frac{2}{3} \log Z_i - \frac{1}{6} \log P_e \quad (5-9)$$

given by Unsöld [106]. χ_{irs} denotes an excitation potential, b_{irs} describes the departure from equilibrium in conventional notation, N_{irs}^* is the comparison population in equilibrium at T_e , Z_i the ionic charge, P_e the electron pressure.

It is convenient to use the notation

$$E_{\text{excit.}} = N_0 \sum_i v_i \sum_{r=0}^{f_i} x_{ir} h_{ir} \quad (5-10)$$

with:

$$h_{ir} = \left(\sum_{s=0}^{n_i^*} \chi_{irs} b_{irs} g_{irs} e^{-\chi_{irs}/kT_e} \right) / \left(\sum_{s=0}^{n_i^*} g_{irs} e^{-\chi_{irs}/kT_e} \right) \quad (5-11)$$

If we write internal energy and enthalpy in terms of one atom of the original gas of N_0 atoms, we have

$$H/a = E/a + \frac{pV}{N_0} = E/a + (1+\bar{x})kT_e \quad (5-12)$$

where from Eqs. (5-2) to (5-4) and (5-10) follows

$$E/a = \frac{3}{2} kT_e (1+\bar{x}) + \sum_i v_i \sum_{r=1}^{f_i} x_{ir} \sum_{l=1}^r \chi_{il} + \sum_i v_i \sum_{r=0}^{f_i} x_{ir} h_{ir} \quad (5-13)$$

Thus

$$H/a = \frac{5}{2} kT_e (1+\bar{x}) + \sum_i v_i \sum_{r=1}^{f_i} x_{ir} \sum_{l=1}^r \chi_{il} + \sum_i v_i \sum_{r=0}^{f_i} x_{ir} h_{ir} \quad (5-14)$$

with \bar{x} and b_{ir} defined respectively by Eqs. (5-5) and (5-11).

In an extremely dilute atmosphere we have [49]:

$$b_{i0} \text{ very large, } b_{irs} \rightarrow 1 \text{ for } s \gg 0.$$

However, we note that $\chi_{i0} = 0$ so that the major overpopulated term does not enter the energy balance.

We have neglected the bound energy E_{excit} altogether in our calculation as sufficient accuracy can be achieved without this complicated term. A numerical check on the influence of this

neglected term has been carried out and is given in Appendix G and shown in Fig. 8.

c) The Ionization

Low pressures and small optical depth make it possible to use an ionization formula resulting from the balancing of collisional ionization and radiative recombination. These assumptions are valid roughly for the regions above the level where H becomes largely neutral. We used the approximation even in deeper layers in order to keep machine computations within reasonable limits. The actual computation was carried out analogous to the procedure adopted by House [34].

d) The quantities γ , c_p , c_v and H.

In the above approximation, the ionization ratios depend only on T_e and not P_e or the density.

We have:

$$H/a = \frac{5}{2} kT_e (1+\bar{x}) + \sum v_i \sum_{r=1}^{f_i} x_{ir} \sum_{l=1}^r \chi_{il} \quad (5-15)$$

$$E/a = \frac{3}{2} kT_e (1+\bar{x}) + \sum v_i \sum_{r=1}^{f_i} x_{ir} \sum_{l=1}^r \chi_{il} \quad (5-16)$$

and

$$c_p/a = \frac{dH/a}{dT_e} \quad c_v/a = \frac{dE/a}{dT_e} \quad \gamma = \frac{c_p/a}{c_v/a} \quad (5-17)$$

Thus

$$\gamma = \frac{\frac{5}{2}(1+\bar{x}) + T_e \left\{ \sum_i \nu_i \sum_{r=1}^{f_i} \left(r \cdot \frac{5}{2} + \left(\sum_{\ell=1}^r \chi_{i\ell} \right) / kT_e \right) \frac{dx_{ir}}{dT_e} \right\}}{\frac{3}{2}(1+\bar{x}) + T_e \left\{ \sum_i \nu_i \sum_{r=1}^{f_i} \left(r \cdot \frac{5}{2} + \left(\sum_{\ell=1}^r \chi_{i\ell} \right) / kT_e \right) \frac{dx_{ir}}{dT_e} \right\}} \quad (5-18)$$

with \bar{x} defined by Eq. (5-5).

The mean molecular weight reads:

$$\mu = \frac{\mu_0}{1+\bar{x}} \quad \text{where } \mu_0 = \frac{\sum_i \mu_i \epsilon_i}{\sum_i \epsilon_i} \quad (5-19)$$

μ_i is the atomic weight of element i .

In regions of constant γ , μ , $T \leq 6 \cdot 10^3$ °K and $T \geq 7 \cdot 10^5$ °K we get

$$c_p = \frac{\gamma R}{\mu(\gamma-1)} \quad (5-20)$$

since,

$$c_p - c_v = R/\mu \quad \text{or } c_p/a - c_v/a = k\mu_0/\mu = k(1+\bar{x}) \quad (5-21)$$

Similarly,

$$H = c_p T_e = \frac{\gamma R T_e}{\mu(\gamma-1)} \quad (5-22)$$

$$H/a = H \mu_0 m_H \quad (5-23)$$

As the sound velocity depends only on quantities affected by the kinetic temperature, it is simply:

$$c^2 = \left. \frac{\partial p}{\partial \rho} \right|_{\text{ad}} = \gamma \frac{p}{\rho} = \gamma \frac{RT_e}{\mu} . \quad (5-24)$$

e) Numerical results.

Figs. 9 and 10 give γ , u and H as functions of T_e .

It is seen that contributions from elements other than H and He can be neglected, leaving $\gamma = 5/3$ except in regions where H, He and He^+ ionize.

The enthalpy is dominated by the translatory energy:

$$H/a = \frac{5}{2} kT_e (1+\bar{x}) \quad (5-25)$$

except in the regions where H, He and He^+ ionize. At those regions not only \bar{x} increases but also the ionization energy Eq. (5-15). However as the ionization energy and \bar{x} do not increase after full ionization is achieved, the translatory term Eq. (5-25) proportional to T slowly begins again to dominate.

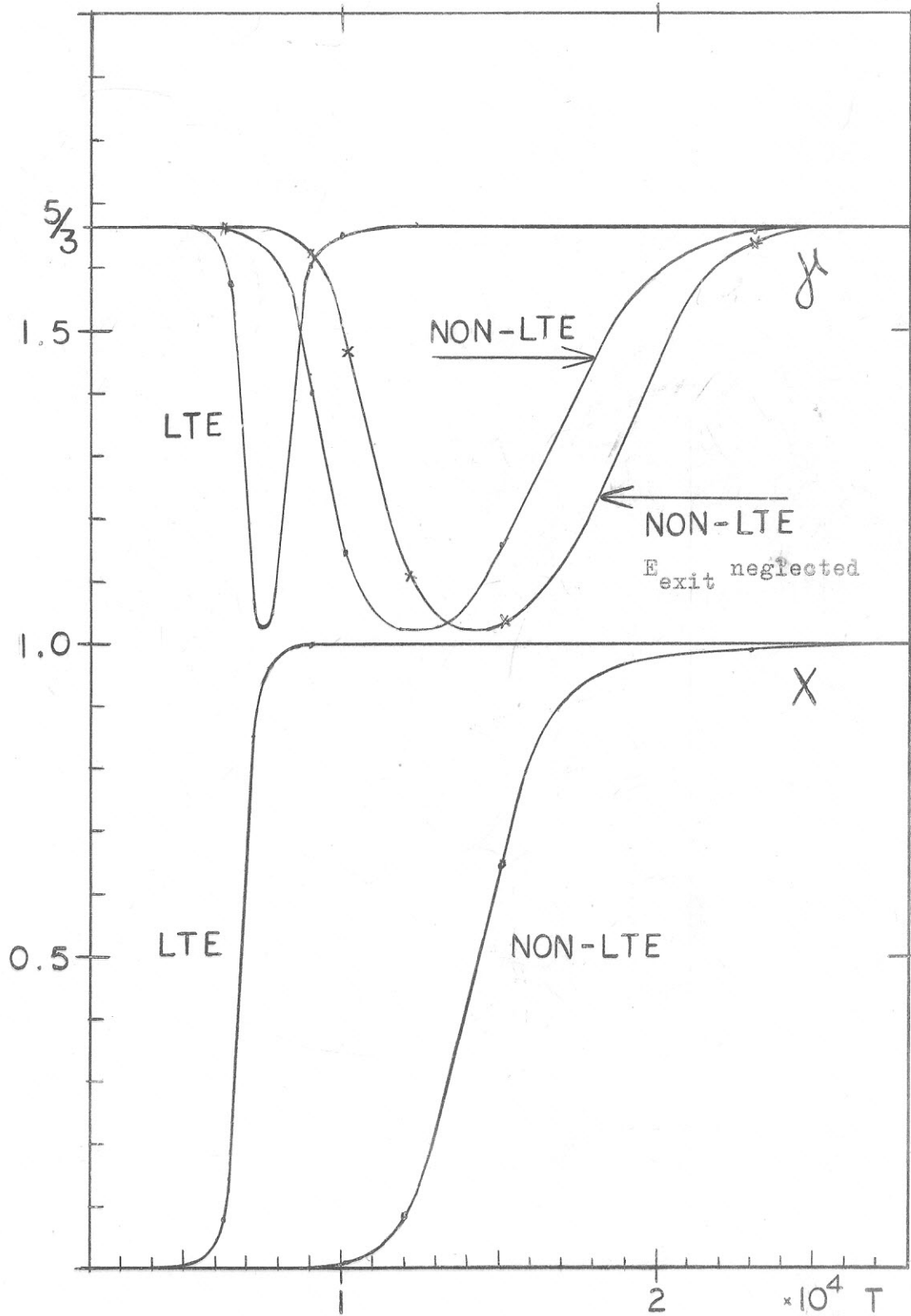


Fig. 8. $\gamma = c_p/c_v$ and the ionization ratio x versus temperature T . Influence of bound energy.

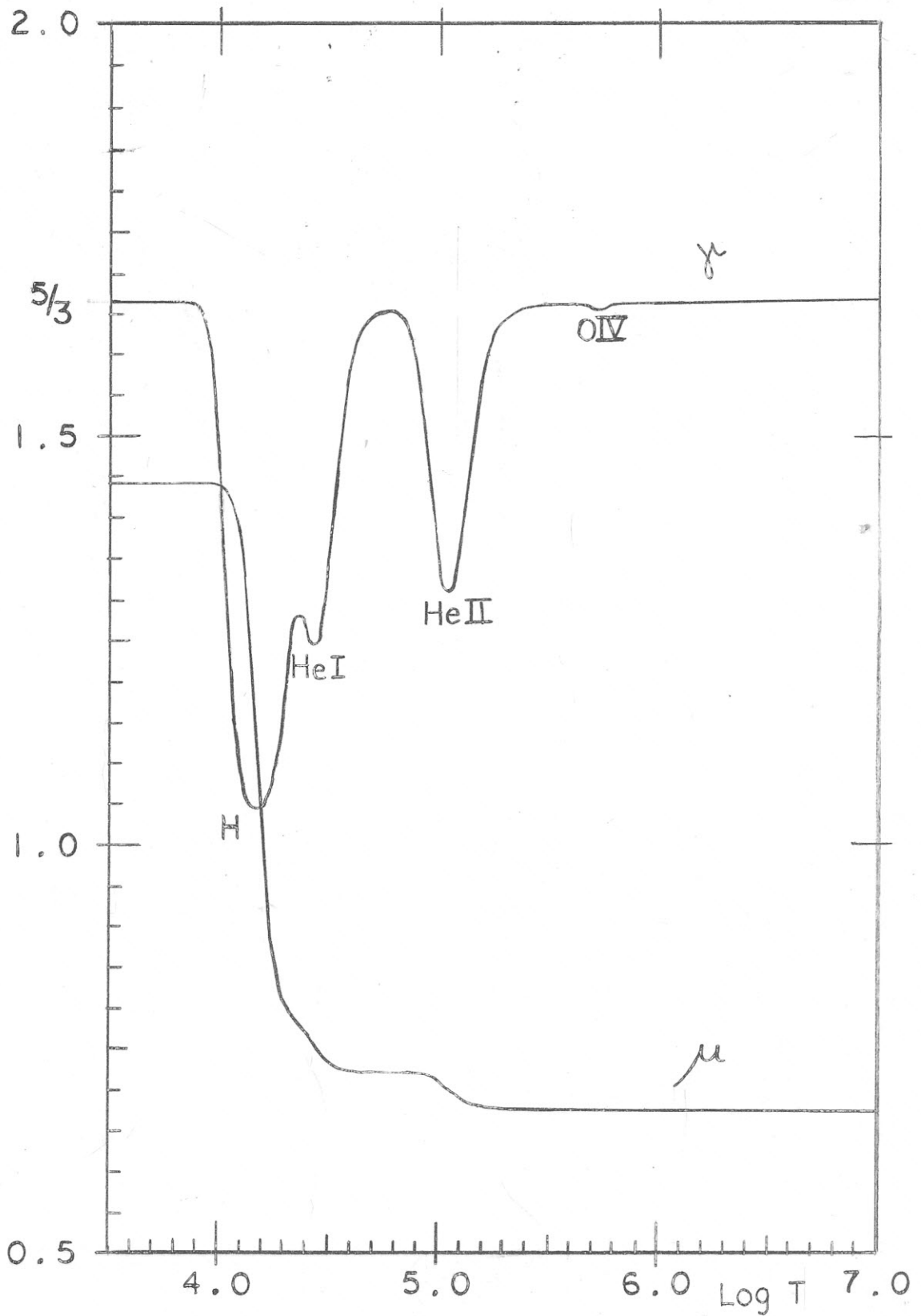


Fig. 9. $\gamma = c_p/c_v$ and mean molecular weight μ as functions of T .

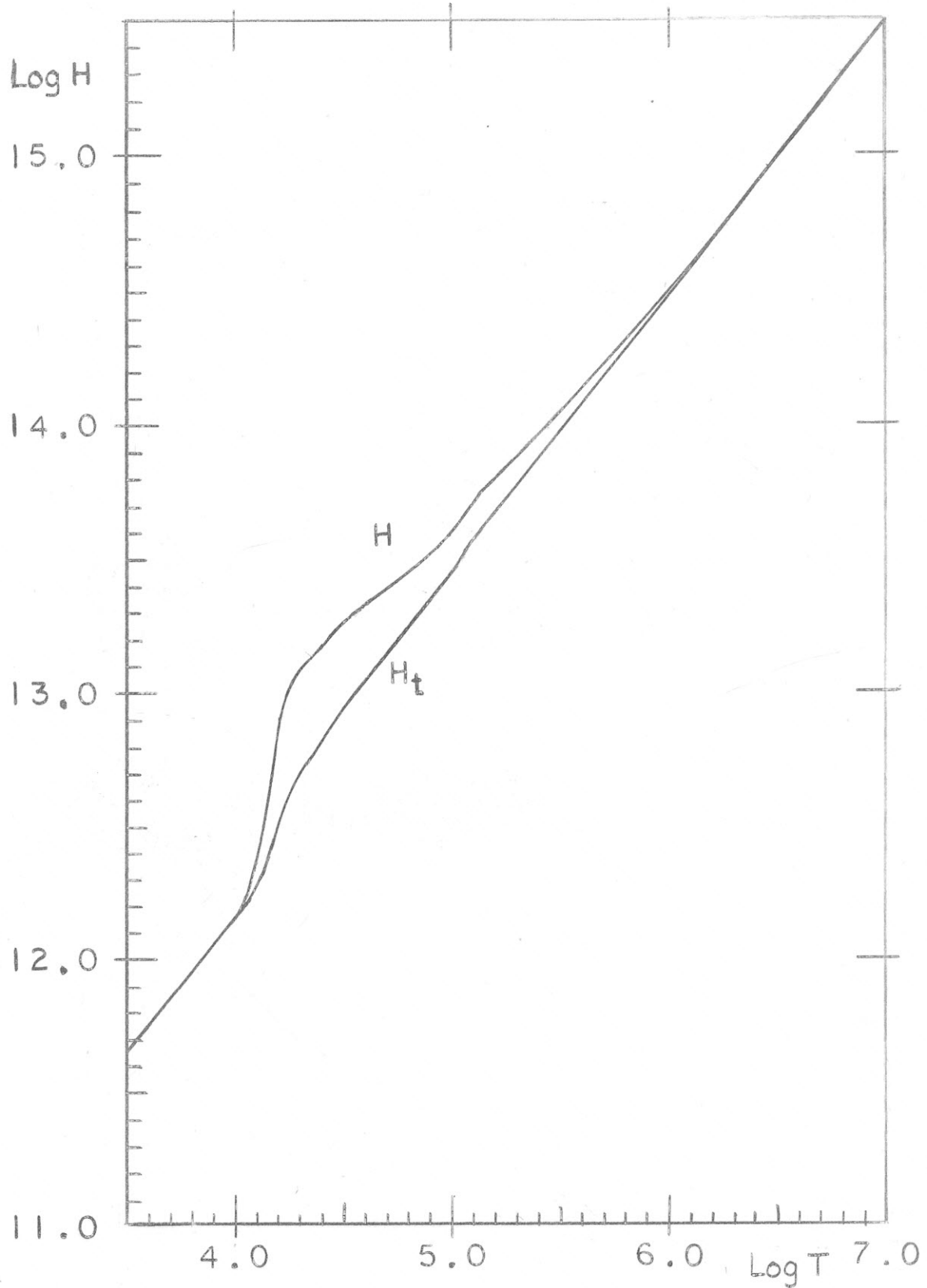


Fig. 10. Enthalpy H per gram as function of T . The curve $H_{\text{trans}} = 2.5RT/\mu$ shows the translatory part of the enthalpy only.

Section 6. Energy Equation

From the three basic differential equations that we wrote down in Section 2: (2-1), (2-2), (2-3) the first two were used to derive the flow equation (2-14), while the first two, a restricted form of the third and additional information about the shock structure was used to derive the shock equation (3-40).

a) General Formulation

We now turn to Eq. (2-3) and consider the energy balance. Recalling from earlier that:

$$V = \frac{1}{\rho} \quad (6-1)$$

$$dE = TdS - pdV \quad (6-2)$$

$$dH = TdS - Vdp \quad (6-3)$$

As before V represents the specific volume per gram, S the entropy per gram, E the internal energy per gram and H the enthalpy per gram.

Using equations (2-1) to (2-3) and (6-4) to (6-6) we show in Appendix E that they can be combined to yield

$$\frac{\partial}{\partial t} \left(\frac{1}{2} \rho u^2 + \rho \epsilon \right) = - \nabla \cdot \rho \vec{u} \left(\frac{1}{2} u^2 + H \right) - \rho \vec{u} \cdot \vec{g} + \rho T \left. \frac{\partial S}{\partial t} \right|_{\text{ext}} \quad (6-4)$$

This is the same result as given by [58, p. 11] except that there are the additional terms representing gravitation and external energy sources and sinks.

Adding moreover conduction we get [58, p. 184]

$$\frac{\partial}{\partial t} \left(\frac{1}{2} \rho u^2 + \rho \epsilon \right) = - \nabla \cdot \left\{ \rho \vec{u} \left(\frac{1}{2} u^2 + H \right) - u \nabla T \right\} - \rho \vec{u} \cdot \vec{g} + \rho \dot{Q}_{\text{ext}} \quad (6-5)$$

where we wrote for the external energy term

$$\rho \dot{Q}_{\text{ext}} \equiv \rho T \left. \frac{\partial S}{\partial t} \right|_{\text{ext}} \quad (6-6)$$

This term may be split into a source term representing mechanical heating produced by the shock wave, and a sink describing radiative losses.

$$\rho \dot{Q}_{\text{ext}} = \rho \dot{Q}_{\text{mech}} - \rho \dot{Q}_{\text{rad}} \quad (6-7)$$

In steady state there is no explicit time dependence and we obtain from (2-1)

$$\nabla \cdot \rho \vec{u} = 0 \quad (6-8)$$

Hence,

$$\rho \dot{Q}_{\text{mech}} = \rho \vec{u} \cdot \left\{ \nabla \left(\frac{1}{2} u^2 + H \right) + \vec{g} \right\} - \nabla k \nabla T + \rho \dot{Q}_{\text{rad}} \quad (6-9)$$

This equation agrees with Field's [31] result, (see Appendix H).

After the passage of a shock an amount of energy dD/dx is deposited per cm^3 . If we have v_0 shocks per second,

$$\rho \dot{Q}_{\text{mech}} = v_0 \frac{dD}{dx} \quad (6-10)$$

Thus with Eq. (4-32)

$$\rho \dot{Q}_{\text{mech}} = v_o \rho \frac{x^2}{x_o} \frac{c^2}{\gamma(\gamma-1)} \ln \phi \theta^{-\gamma} \quad * \quad (6-11)$$

Radiative losses $\rho \dot{Q}_{\text{rad}}$ are not so easy to treat and will be discussed in detail in Section 7.

b) Treatment without conduction

In spherical geometry and using the dimensionless height variable r : Eq. (2-7), we get using Eqs. (6-9), (6-11), (2-9)

$$v_o \frac{c^2}{\gamma(\gamma-1)} \ln \phi \theta^{-\gamma} \cdot r^2 = \frac{Mc}{r_o} \left(Mc^2 \frac{dM}{dr} + \frac{M^2}{2} \frac{dc^2}{dr} + \frac{dH}{dr} + \frac{g_o r_o}{r^2} \right) + \frac{\rho \dot{Q}_{\text{rad}}}{\rho} \quad (6-12)$$

With the aid of the flow equation (2-14) we obtain

* Eq. (6-11) can be compared with Bird's [14] work, noting that for small shock Mach numbers $\phi \rightarrow 1$, $\theta \rightarrow 1$ and

$$\ln \phi \theta^{-\gamma} = \gamma \ln((\phi^{1/\gamma} \theta^{-1} - 1) + 1) \approx \gamma(\phi^{1/\gamma} \theta^{-1} - 1),$$

or

$$\rho \dot{Q}_{\text{mech}} = \frac{x^2}{x_o} \frac{\gamma RT}{\gamma(\gamma-1)\mu} \gamma(\phi^{1/\gamma} \theta^{-1} - 1) v_o.$$

This relation was used by Bird with the molecular weight $\mu = 1$.

$$\frac{v_o r_o}{Mc} \frac{1}{\gamma-1} \ln \phi \theta^{-\gamma} \cdot r^2 = \frac{\gamma M^2}{r \gamma M^2} \left(\frac{1}{c^2} \frac{dc^2}{dr} - \frac{1}{\gamma} \frac{d\gamma}{dr} \right) + \frac{\gamma}{c^2} \frac{dH}{dV}$$

$$+ \frac{\gamma}{1-\gamma M^2} \frac{g_o r_o}{c^2 r^2} - \frac{\gamma M^2}{1-\gamma M^2} \frac{2}{r} + \frac{r_o \gamma \rho \dot{Q}_{rad}}{\rho M c^3} \quad (6-13)$$

Now

$$p = \rho \frac{c^2}{\gamma} \quad (6-14)$$

and since γ , c^2 , H depend only on T ,

$$\frac{\gamma}{c^2} \frac{dH}{dr} = \frac{\gamma}{c^2} c_p \frac{dT}{dr} = \frac{\gamma}{(\gamma-1)T} \frac{dT}{dr}, \quad \frac{d\gamma}{dr} = \frac{d\gamma}{dT} \frac{dT}{dr} \text{ etc.} \quad (6-15)$$

Thus we can solve for the temperature derivative and obtain

$$\frac{dT}{dr} = \frac{\frac{v_o r_o}{Mc} \frac{1}{\gamma-1} \ln \phi \theta^{-\gamma} \cdot r^2 - \frac{r_o \gamma \rho \dot{Q}_{rad}}{M c p} - \frac{\gamma M^2}{1-\gamma M^2} \left(\frac{g_o r_o}{M^2 c^2 r^2} - \frac{2}{r} \right)}{\frac{\gamma M^2}{1-\gamma M^2} \left(\frac{1}{c^2} \frac{dc^2}{dT} - \frac{1}{\gamma} \frac{d\gamma}{dT} \right) + \frac{\gamma}{(\gamma-1)T}} \quad (6-16)$$

c) Treatment with conduction

We note that with the identities

$$\vec{\rho u} \cdot \hat{g}_x = \vec{\rho u} \cdot \frac{g_o x_o^2}{x^2} \hat{x} = - \nabla \cdot \vec{\rho u} \frac{g_o x_o^2}{x}, \quad (6-17)$$

and writing the loss term in (6-9) on the left hand side, we can express the entire right hand side as a divergence:

$$\rho \dot{Q}_{\text{mech}} - \rho \dot{Q}_{\text{rad}} = \nabla \cdot \left\{ \rho \vec{u} \left(\frac{1}{2} u^2 + H - \frac{g_0 x_0^2}{x} \right) - K \nabla T \right\}, \quad (6-18)$$

where we used (6-8).

Integrating Eq. (6-18) over the volume of a cone of unit solid angle which is limited by the spherical surfaces $x = x$ and $x = x_0$ we can transform the right hand side into a surface integral

$$\int_{x_0}^x (\rho \dot{Q}_{\text{mech}} - \rho \dot{Q}_{\text{rad}}) x^2 dx = \left\{ \rho M c \left(\frac{1}{2} M^2 c^2 + H - \frac{g_0 x_0^2}{x} \right) - K \frac{dT}{dx} \right\} x^2 - \left\{ \rho_0 M_0 c_0 \left(\frac{1}{2} M_0^2 c_0^2 + H_0 - g_0 x_0 \right) - K \frac{dT_0}{dx} \right\} x_0^2 \quad (6-19)$$

Contributions over the sides of the cone vanish as

$$\vec{u}, \nabla T \parallel \hat{x}.$$

Going over to the variable r (2-7) and using (2-17)

$$\rho M c r^2 = \rho_0 M_0 c_0 = \text{constant} \quad (6-20)$$

Hence we have

$$\int_1^r r_0 (\rho \dot{Q}_{\text{mech}} - \rho \dot{Q}_{\text{rad}}) r^2 dr = \left\{ \rho M_0 c_0 \left(\frac{1}{2} M^2 c^2 + H - \frac{g_0 r_0}{r} \right) - \frac{K}{r_0} \frac{dT}{dr} r^2 \right\} - \left\{ \rho_0 M_0 c_0 \left(\frac{1}{2} M_0^2 c_0^2 + H_0 - g_0 r_0 \right) - \frac{K}{T_0} \frac{dT_0}{dr} \right\}$$

and upon solving for dT/dr :

$$\frac{dT}{dr} = \frac{r_o}{K_o T_o^{5/2}} \frac{1}{r^2} \left\{ \text{FLOW} - \text{DISS} + \text{RAD} + \frac{K_o}{r_o} T_o^{5/2} \frac{dT_o}{dr} \right\} \quad (6-21)$$

The symbolic notations FLOW, DISS, RAD are defined by:

$$\text{RAD} = \int_1^r r_o \rho \dot{Q}_{\text{rad}} r^2 dr \quad (6-22)$$

$$\text{DISS} = \mp \cdot \int_1^r r_o v_o p \frac{1}{\gamma-1} \ln \phi \theta^{-\gamma} r^4 dr \quad (6-23)$$

$$\text{FLOW} = \rho_o M_o c_o \left\{ \left(\frac{1}{2} M_o^2 c_o^2 + H - \frac{g_o r_o}{r} \right) - \left(\frac{1}{2} M_o^2 c_o^2 + H_o - g_o r_o \right) \right\} \quad (6-24)$$

The origin of the factor \mp in (6-23) will be discussed in Section 12.

We used for the thermal conductivity the conventional [82]

$$K = K_o T^{5/2} = 6 \cdot 10^{-7} T^{5/2} \text{ ergs/cm}^2 \text{ sec} \quad (6-25)$$

Finally writing

$$\text{COND} = \frac{K_o}{r_o} \left(T^{5/2} \frac{dT}{dr} r^2 - T_o^{5/2} \frac{dT_o}{dr} \right) \quad (6-26)$$

we obtain the balance relation

$$\text{COND} = \text{FLOW} + \text{RAD} - \text{DISS} \quad (6-27)$$

The physical interpretation of the quantities RAD, DISS, FLOW, and COND is that they represent the total energies (per cm^2 of the initial surface) that are radiated, dissipated transformed into stellar wind and conducted, respectively per second within the column bounded by $r = 1$ and $r = r$. (They are therefore energy fluxes).

From (6-27) we see that the conduction term acts as a reservoir from which we can borrow energy to radiate or increase the thermal and kinetic energy of the stellar wind in case that the shock dissipation is not yet sufficient to compensate for the losses. (DISS < FLOW + RAD)

However ultimately the dissipation term must equal the sum of flow and radiation terms, if the energy to drive the stellar wind and to provide for radiation losses comes from within the star and not from an external reservoir.

This condition of a "shock dominated solution" is discussed below in detail.

Section 7. Radiative Losses

Of all the physical parameters that determine ultimately the structure of our solutions, the amount and distribution of radiative losses is least known. Again as in the case of the adiabatic coefficient a truly self-consistent method would require an iterative procedure that is excluded by considerations of numerical labor. And again it subsequently turned out that our solutions are not very sensitive to the detailed knowledge of the amount and distribution of the radiative losses.

We therefore decided to use the radiation rates given in the literature and use the ones that seem most appropriate for our problem.

Since we have to expect a rather large margin of error, we consider two cases which we call "strong" and "weak" case and settle for a "medium" case in the actual computations.

a) Temperatures below 7000 °K

The region above the photosphere at these temperatures is optically thin for wave lengths above the Lyman limit, emitting mostly subordinate H continua and the H⁻ continuum, while the Ly and Ba lines are optically thick. For this region we treat the hydrogen continua in LTE.

1) Weak Case

Noting that metal lines can be included by multiplying the hydrogen contribution by a factor of 2 (P. K. Raju [88]) we can estimate the radiation loss using the equilibrium emission with

the Rosseland mean absorption coefficient [110]

$$4\pi\epsilon = 4 \bar{\kappa} \sigma T^4 \quad (7-1)$$

The actual values have to be reduced by the contribution of scattering. The numerical values were computed from tables given by L. Oster [74], [75].

2) Strong case.

An alternate procedure has been suggested by Weymann [114] (strong case), based on calculations by Seaton [96] for coal interstellar gas. In this calculation all continua and resonance lines are treated as optically thin. The ionization is calculated in the coronal approximation (Sec. 5).

This case predicts much higher radiation losses because of the contribution by (optically thin) resonance lines. We considered this "strong" case as an upper limit. Where the LTE calculations exceeded this upper limit they were cut off.

b) Temperatures exceeding 7000 °K

1) Weak case.

Here we adopted Weymann's [114] weak case that includes only the bound-free continua of H and He in addition to bremsstrahlung. Such a spectrum can be considered as a lower limit.

2) Strong case.

Here Doherty and Menzel's [24] computation was taken as an upper limit as it exceeded other estimates such as Pottasch's [84] and Raju's [88].

c) Adopted loss function

After some preliminary numerical checks, we decided to use the following loss function.

For temperatures below 7000°K we use the LTE values as discussed under a). These values may still be somewhat too high as departures from equilibrium keep the ground state overpopulated thus reducing Balmer and Paschen-continua.

For temperatures exceeding 7000°K we divided Doherty and Menzel's values by 5 to 10 to account for the optical thickness of resonance lines. In the very hot regions our adopted curve goes over into the strong case.

The following graphs Figs. 11-12 give the energy loss $\rho\dot{Q}_{\text{rad}}$ (labeled M) in $\text{ergs}/\text{cm}^3\text{sec}$ as function of temperature, the logarithm of the gas pressure being a parameter.

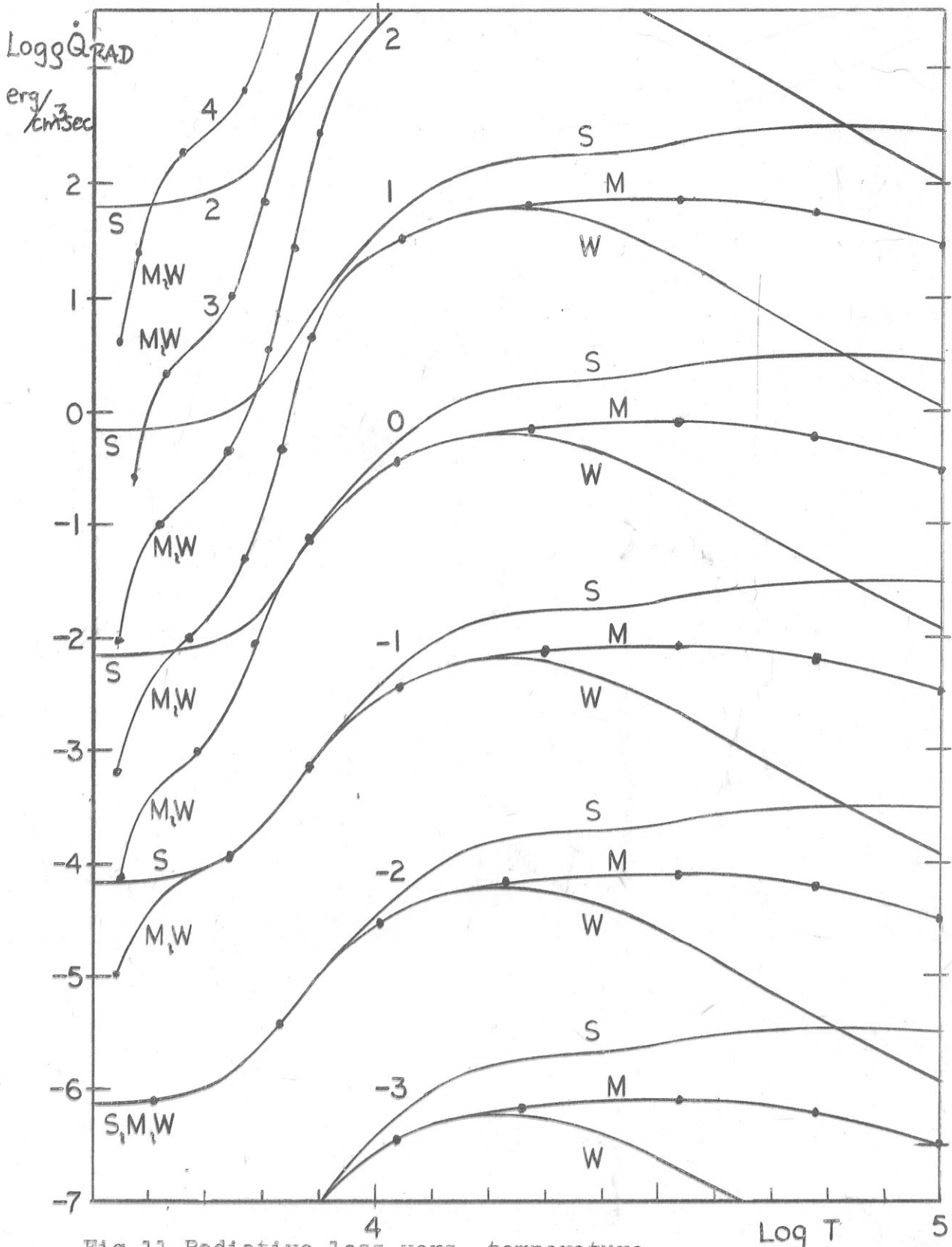


Fig.11 Radiative loss vers. temperature

with $\text{Log } p_{\text{gas}}$ as parameter. \bullet M \bullet Adopted case.

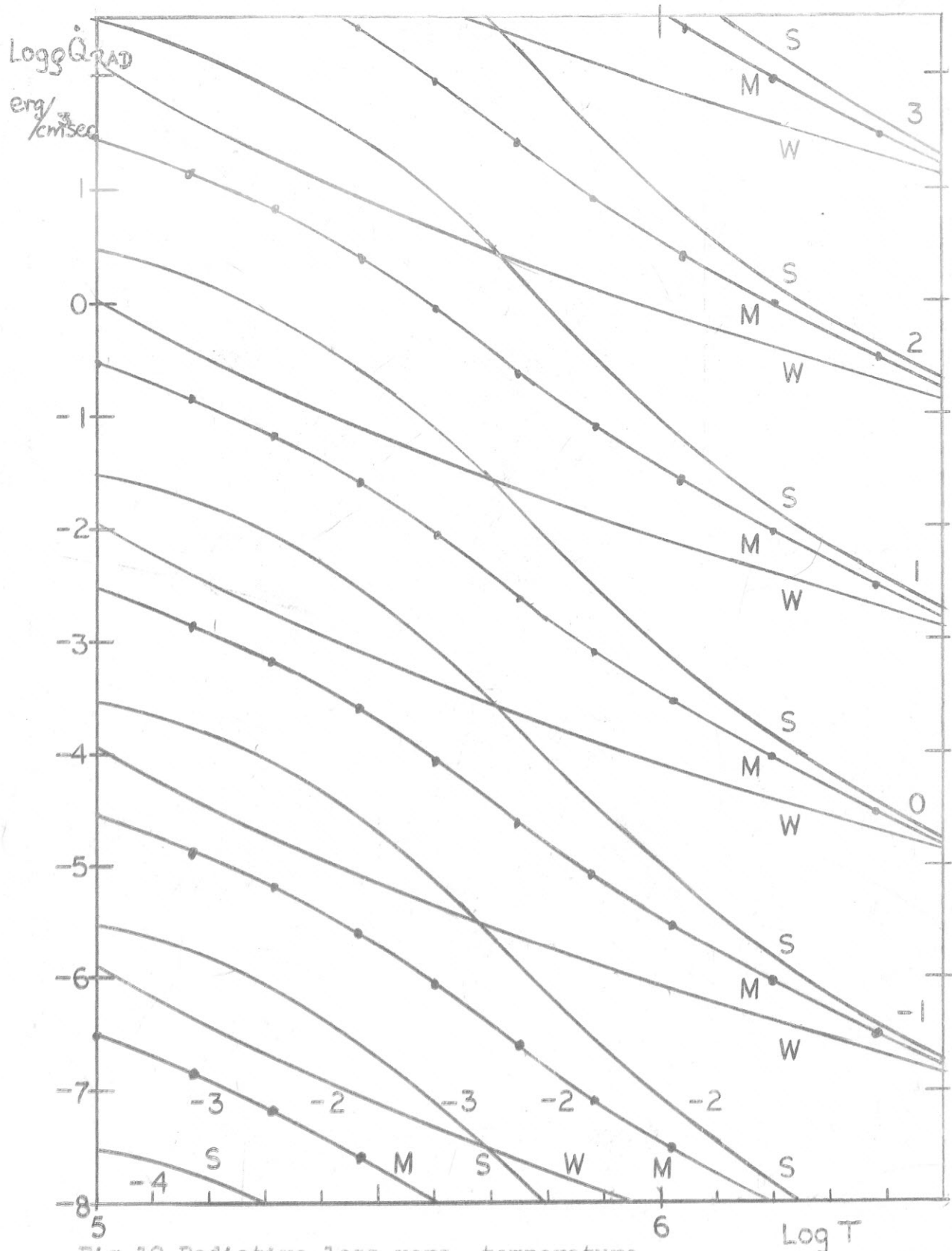


Fig.12 Radiative loss vers. temperature
with $\text{Log } P_{\text{gas}}$ as parameter. —●— M —●— Adopted case.

Section 8. Computation of Noise Energy Production
from Böhm-Vitense's Models.

We now want to make the physical connection between the internal structure of the star and its outer atmosphere. The quantity of major importance is the mechanical energy input from the convection zone through the photosphere.

a) Velocities

The mean velocities \bar{v} of the rising or falling turbulence elements in 15 stellar models have been calculated by Böhm-Vitense [16],[111]. We obtained \bar{v} from these models. Since the effective gravitational acceleration

$$g_{\text{eff}} = g_{\text{grav}} - g_{\text{rad}} - g_{\text{turb}} \quad (8-1)$$

arising from gravitational, radiative and turbulent pressures was not known from the beginning, an iterative procedure was employed using the tables for μ , c_p , $\bar{\alpha}$, v_{ad} collected by Unsöld [105].

It was found that in our 4 cases the effects of radiative and turbulent acceleration are negligible against g_{grav} .

We adopted the following models. (Spectral classes have been adopted by Allen [2]. They differ somewhat from those given by Unsöld [105])

Spectral class	$T_{\text{eff}} \text{ } ^\circ\text{K}$	Surface grav. $\log g \text{ cm/sec}^2$
Sun G2 V	5800	4.45
K1 III	4400	2.50
G3 III	5000	3.00
G7 V	5000	4.45

Table 2. The four stars for which models were calculated.

b) Production of acoustic noise energy

Following Lighthill [59],[60] and Osterbrock [76] we can write for the rate of generation of acoustical noise:

$$A_1 = \bar{\alpha} \rho \frac{\bar{v}^8}{c^5 l} \quad (8-2)$$

where $\bar{\alpha}$ is a constant, which depends on the spectrum of the turbulence and has the value 38 for the Heisenberg spectrum [86], l is the mixing length. It is customary to identify it with the scale height [16],[111],[76], i.e., to set

$$l = H_s \quad (8-3)$$

The values of $A_1(h)$ are given in Figs. 13-16. The total noise energy can be computed from the relation

$$\pi F_{mo}^+ = \frac{1}{2} \int A_1(h) dh \quad (8-4)$$

where we have assumed that all the noise directed upwards escapes, while all the noise directed downwards is absorbed.

The values of πF_{mo}^+ are given in Table 3.

c) Frequency spectrum of the noise

The frequency spectrum is obtained from Osterbrock's [76] method. The maximum of the frequency spectrum reads

$$\nu_0 = \frac{\bar{v}}{H_s} \quad (8-5)$$

We assume ν_0 to be the frequency of our sound waves.

The frequencies are given in Table 3.

d) The cut-off frequency

Kuperus [54], Moore and Spiegel [65] and others have shown that there is a cut-off frequency for sound waves at low frequencies, where the pressure gradient of the atmosphere becomes equal to the pressure gradient in the profile of the sound wave [54]. We have

$$\nu_{\text{cut-off}} = \frac{\gamma E}{4\pi c} \quad (8-6)$$

The values of $\nu_{\text{cut-off}}$ and γ at the layer with maximum noise production are summarized in Table 3.

The comparison with ν_0 shows that the frequency of the noise produced is above the cut-off frequency, however within a factor of 2 to 4 from $\nu_{\text{cut-off}}$.

Star	$\frac{\pi F^+}{\text{ergs/cm}^3 \text{sec}}$	$\nu_0 \frac{1}{\text{sec}}$	$\nu_{\text{cut-off}} \frac{1}{\text{sec}}$	γ	Scale heights H_s cm
Sun G2 V	$1.6 \cdot 10^7$	$9.0 \cdot 10^{-3}$	$3.3 \cdot 10^{-3}$	1.22	$2.0 \cdot 10^7$
K1 III	$1.6 \cdot 10^7$	$1.5 \cdot 10^{-4}$	$3.9 \cdot 10^{-5}$	1.15	$1.5 \cdot 10^9$
G3 III	$3.4 \cdot 10^7$	$5.0 \cdot 10^{-4}$	$1.2 \cdot 10^{-4}$	1.13	$5.1 \cdot 10^8$
G7 V	$3.0 \cdot 10^6$	$7.9 \cdot 10^{-3}$	$3.6 \cdot 10^{-3}$	1.25	$1.7 \cdot 10^7$

Table 3. Noise production

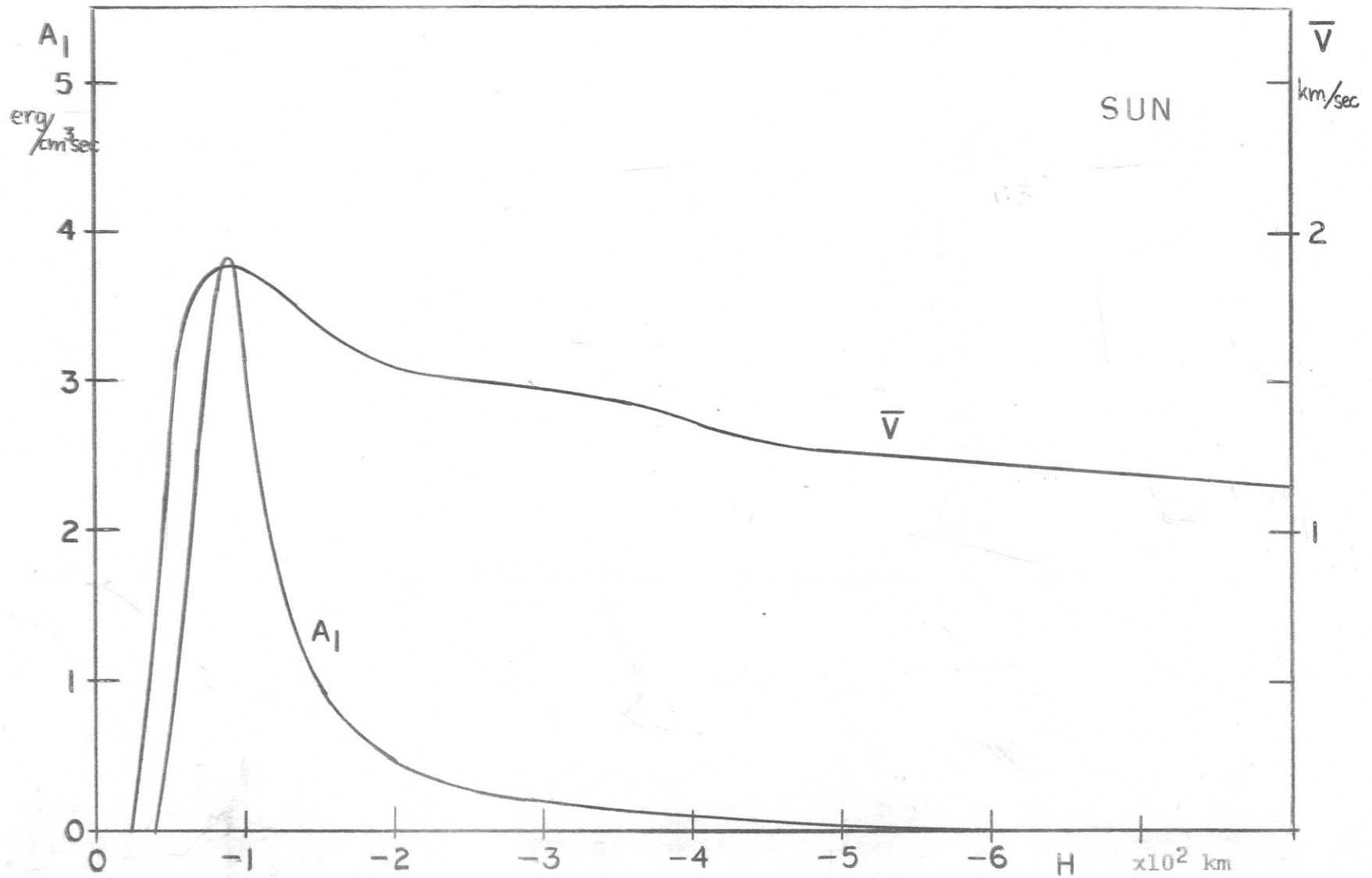


Fig.13 Noise energy production and mean velocity versus height.

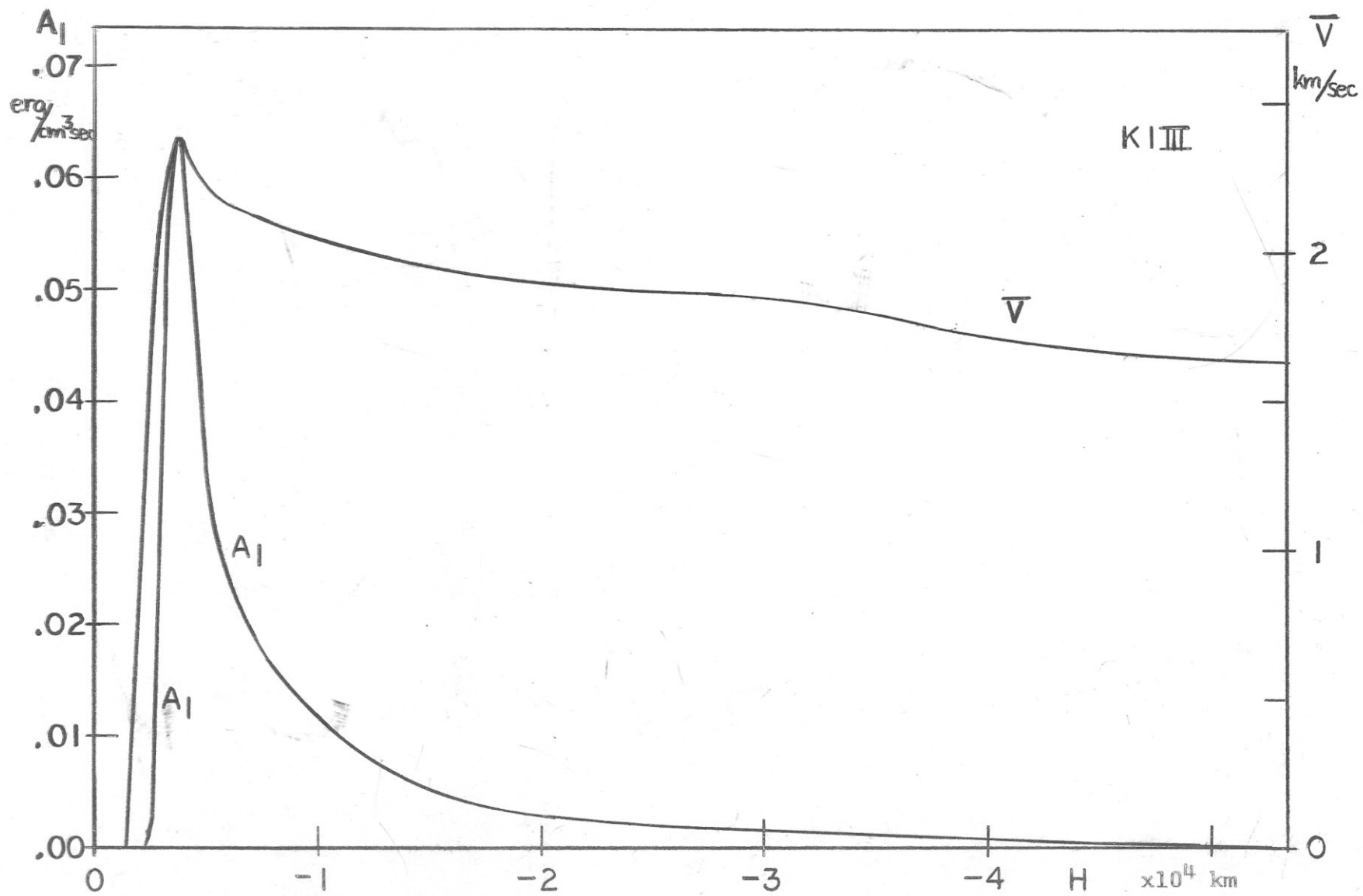


Fig.14 Noise energy production and mean velocity versus height.

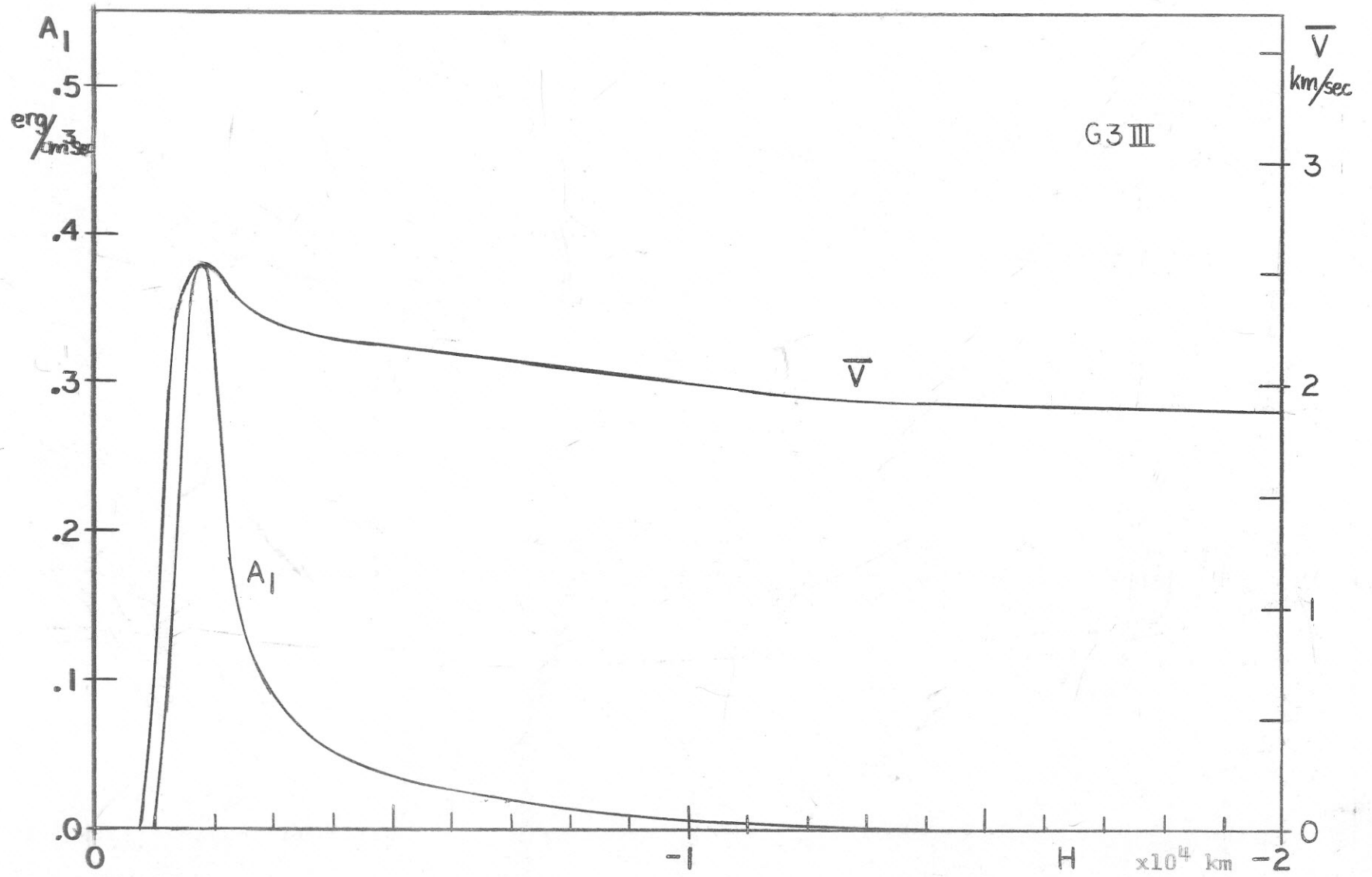


Fig.15 Noise energy production and mean velocity versus height.

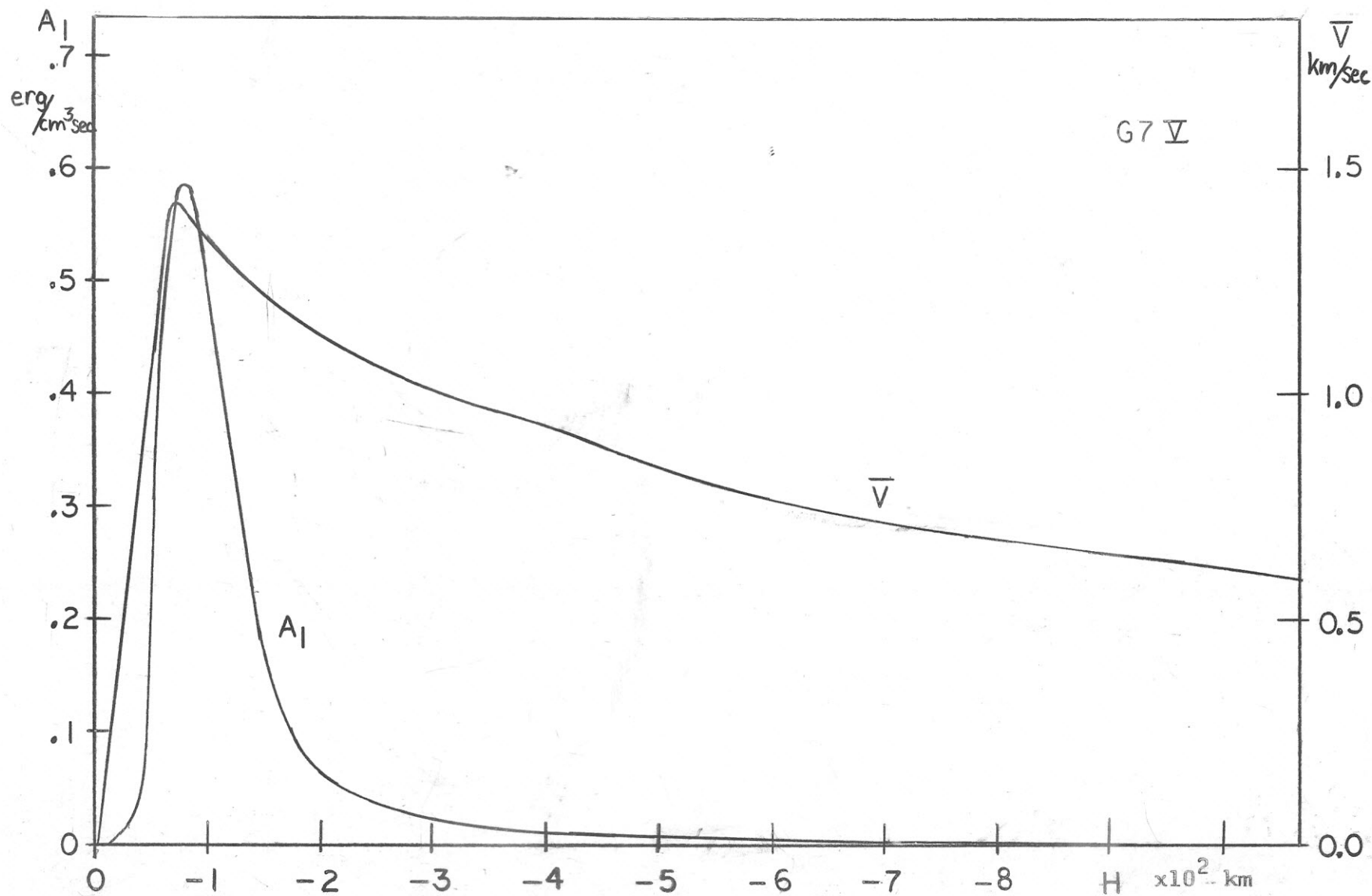


Fig.16 Noise energy production and mean velocity versus height.

Section 9. Initial Conditions and the Photosphere

We are now ready to derive the boundary conditions from which we start our model calculations.

a) The height at which the shock forms.

Sound waves of frequency ν_0 containing flux πF_{m0}^+ travel in an outward direction down the density gradient and so long as viscous dissipation and heat conduction can be neglected (see [59, p. 567]) will grow in amplitude to conserve flux.

This growth will lead to larger and larger velocity amplitudes. A large velocity amplitude however will distort the sinusoidal shape of the sound wave [59, p. 366] and the hills and valleys will melt into each other to form a shock wave [76].

To describe this situation quantitatively, we first write [58, p. 250]

$$\pi F_{m0}^+ = \rho_0 u_0^2 c_0 = \rho u^2 c \quad (9-1)$$

or

$$\frac{u}{c} = \sqrt{\pi F_{m0}^+} / \sqrt{\gamma p c} \quad (9-2)$$

where again

$$c^2 = \gamma \frac{p}{\rho} \quad (9-3)$$

Let H_p be the height (in the height scale given by Böhm-Vitense's models) at which maximum noise production occurs, and H_T the height at which the shock is formed. The condition that the

hills catch up with the valleys (Fig. 17)

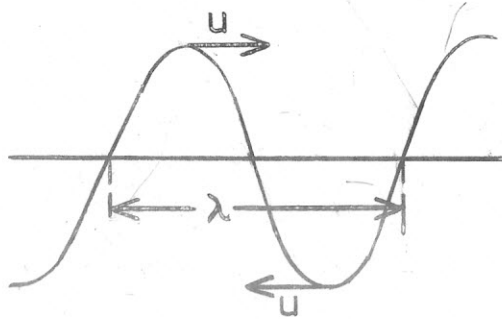


Fig. 17. Velocity amplitudes in a sound wave

then becomes

$$\int_{t(H_p)}^{t(H_F)} u \, dt = \frac{\lambda}{4} \quad \text{or} \quad \int_{H_p}^{H_F} \frac{u}{c} \, dh = \frac{c}{4v_0} \quad (9-4)$$

With the aid of (9-2) we thus have

$$4v_0 \sqrt{\pi F_{m0}^+ / \gamma} \int_{H_p}^{H_F} 1/\sqrt{pc} \, dh = c. \quad (9-5)$$

Eq. (9-5) determines H_F provided that a model of the stellar photosphere is available.

b) Models of stellar photospheres

The photospheric models we used were based on the data by Böhm-Vitense [16]. From $\bar{\tau} = .01$ on they were continued isothermally and this established a boundary temperature T_0 (See Fig. 19). This approximation is justified in cases where viscosity and radiative effects could be neglected [94]. We will come back to this point under d).

c) Initial pressures

Several calculations with the aid of (9-5) were performed with different πF_{m0}^+ and for different stars. It was found that we obtain a result which is within 2% of these calculations if we just use (9-2) and put down the condition for getting a shock as

$$u = c_0 \quad (9-6)$$

Using this new condition we have

$$p = \pi F_{m0}^+ / \gamma c_0, \quad (9-7)$$

where

$$c_0 = \sqrt{\gamma RT_0 / \mu_0} \quad (9-8)$$

d) Shape compression factor

It was shown by Schirmer [94] that there is a fairly large difference between the growth of a sinusoidal sound wave without viscosity and radiative cooling, and the case with those effects included. This means that the sound wave will in reality travel to much greater height before becoming a shock wave. We introduce a factor \star by

$$p = p_0 \star \quad (9-9)$$

where p is the pressure as calculated from (9-7) and p_0 the pressure at which the sound wave in reality transforms into a shock wave.

The quantity κ is called "shape compression factor" as it is a measure of how much the wave profile is distorted from the free case by viscosity and radiation.

Thus the initial pressure p_0 finally reads

$$p_0 = \pi F_{mo}^+ / \kappa \gamma c_0 \quad (9-10)$$

For our models $\kappa = 4.91$ was fitted see below (Sec. 14b- 3) and 4)).

e) Initial heights

- 1) The height H_p of the layer of maximum noise production can be taken from Figs. 13 to 16 in terms of the height scale of Böhm-Vitense.
- 2) The height H_1 of the layer at which $\bar{\tau} = .01$ can be obtained by numerical integration of the hydrostatic equation for the values of p, T given in Böhm-Vitense's models.

$$H_1 - H_p = \int_{p_0}^{p_1} \frac{RT}{\mu_0 g p} dp \quad (9-11)$$

- 3) The height H_F of shock formation can finally be computed from the barometric formula.

$$H_F - H_1 = H_s \ln \frac{p_1}{p_0} \quad (9-12)$$

p_1 is the pressure at H_1 , p_0 the pressure at H_F given by Eq. (9-7) and

$$H_s = \frac{c_0^2}{\gamma g} = \frac{RT_0}{\mu_0 g} \quad (9-13)$$

is the scale height.

f) The zero reference level

For all stars other than the sun we have assumed that H_1 is the reference level whose distance from the center of the star is r_0 .

For the sun the customary $\bar{\tau} = .003$ was retained. The interpolation of the $\bar{\tau}$ values for $\bar{\tau} = .003$ is given in Fig. 19. It was found

$$H_{\bar{\tau}=.003} = + 270 \text{ km}$$

$$H_{\bar{\tau}=.0046} = + 263 \text{ km}$$

as measured in Böhm-Vitense's height scale.

g) Initial shock Mach numbers

From Eq. (4-33) we have defining

$$H_0 = H_F - H_1 \quad (9-14)$$

$$\pi F_{m0}^+ = v_0 D(H_0) = \left(1 + 2 \frac{H_0}{r_0}\right) (\phi - 1) p_0 \xi c_0 \quad (9-15)$$

With $H_0 \approx 10^{-3} r_0$, definitions of ϕ and ξ and assuming a triangle pulse (See Fig. 18) Eq. (9-15) becomes

$$\pi F_{m0}^+ = c_0 p_0 \frac{(M_{s_0}^2 - 1)}{M_{s_0}} \frac{4\gamma}{(\gamma+1)^2} \cdot \frac{1}{6} \quad (9-16)$$

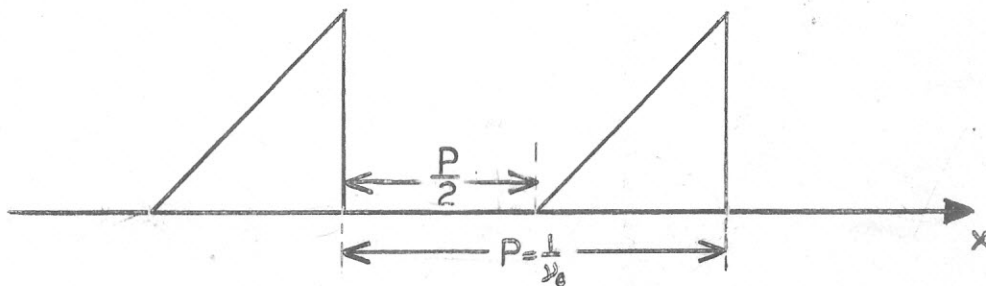


Fig. 18. Shock form at shock formation.

We use positive pulses of triangular shape in comparison with the sawtooth profile customary in papers where small shock Mach numbers are employed ($M_s \approx 1$). The reason is that for large M_s -values, say of the order of 4, the negative pulse of a symmetric sawtooth would result in a negative pressure. Hence the major portion of the energy must be transported in the positive part of the sawtooth for which the triangle shape is a good approximation. Behind strong shocks the pressure is indeed increased by typically an order of magnitude (See Eq. (4-9)).

From Eqs. (9-10) and (9-16) follows

$$\frac{(M_{s_0}^2 - 1)^2}{M_{s_0}} = \frac{\epsilon \gamma}{\frac{4\gamma}{(\gamma+1)^2} \cdot \frac{1}{6}} = 10.68 \cdot \epsilon \quad (9-17)$$

With $\epsilon = 4.91$ that is

$$M_{s_0} = 3.91 \quad (9-18)$$

for all stars.

h) Summary of initial values

Star	T_0 °K	p_0 dyn/cm ²	$H_0 = H_F - H_1$ km	H_p km	$H_1 - H_p$ km	M_{s_0}	r_0 km
Sun G2 V	4064	3.2	668.3	-90	3.30	3.91	$6.953 \cdot 10^5$
K1 III	3069	3.67	29120	-3981	26239	3.91	$4.937 \cdot 10^6$
G3 III	3793	7.08	12680	-1698	7148	3.91	$3.337 \cdot 10^6$
G7 V	3793	.619	789.7	-75	260	3.91	$4.867 \cdot 10^5$

Table 4. Initial values

i) Comparison of photospheric models

For the sun we compared our photospheric model following Böhmer-Vitense with other data. As an illustration we quote a recent model given by Heintze [33]. (See Fig. 19)

Using Heintze's model we find the level of shock formation ($p_0 = 3.2 \text{ dyn/cm}^2$) at 1330 km on the Böhmer-Vitense scale, or at 1060 km on the conventional scale. ($H_{\bar{\tau}=.003} = 0$) Hence $H_0 = H_F - H_1 = 1090 \text{ km}$.

For the sun we summarize below the different heights defined on Böhmer-Vitense scale which sets the zero level of height at the upper end of the convection zone:

Symbol	Height km.	Definition
H_p	-90	Level of max. noise prod.
H_1	+240	Level at which $\bar{\tau} = .01$
$H_{\bar{\tau}=.0046}$	+263	Zero level of Heintze [33]
$H_{\bar{\tau}=.003}$	+270	Conventional zero level
H_F	+913.3	Level of shock form our photosph.

H_F Heintze	+1330	Level of shock form. Heintze
H_0		$H_F - H_1$ Initial height
H_s		RT/ μ g Scale height

Table 5. Height definitions

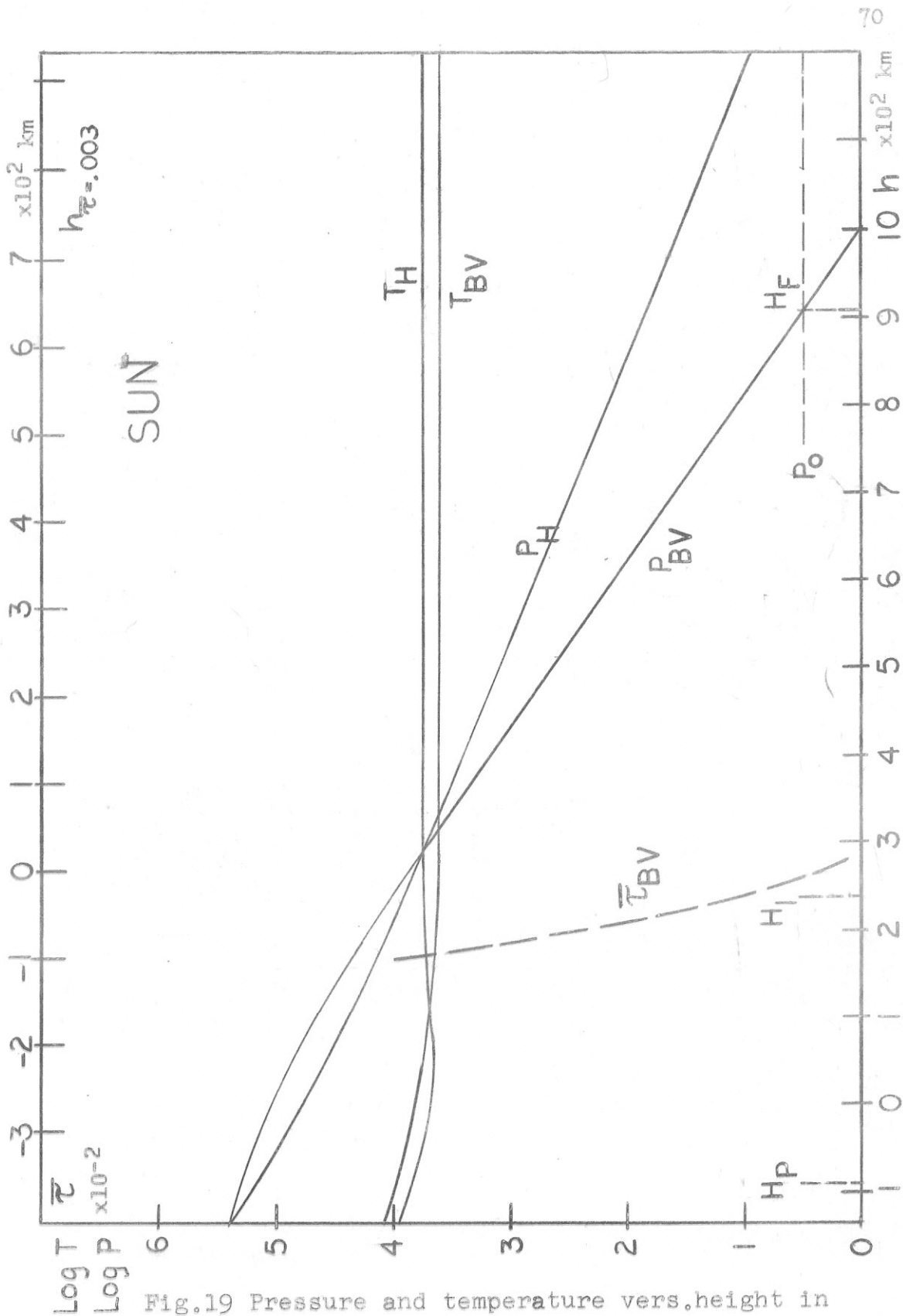


Fig.19 Pressure and temperature vers.height in the photosphere.Heintze(H) and Böhm-Vitense(BV) models.

Section 10. The Complete Set of Equations
and the Type of Solutions

a) Summary of the mathematical problem

From the discussions in the previous sections we can summarize the mathematical problem by stating the three differential equations for the unknown quantities M , M_s , T :

The flow equation (2-14):

$$\frac{dM}{dr} = f\left(M, \frac{dy}{dr}, \gamma, \frac{dc^2}{dr}, c^2, r\right) \quad (10-1)$$

The shock equation (4-40):

$$\frac{dM_s}{dr} = f\left(M_s, M, \frac{dy}{dr}, \gamma, \frac{dc^2}{dr}, c^2, r\right) \quad (10-2)$$

The energy equation (6-21) or (6-27):

$$\frac{dT}{dr} = f\left(T, M_s, M, c^2, \gamma, H, \rho \dot{Q}_{\text{rad}}, p, r\right) \quad (10-3)$$

The radiative loss from Sec. 7:

$$\rho \dot{Q}_{\text{rad}} = f(T, p) \quad (10-4)$$

The thermal properties from Sec. 5:

$$c^2 = \gamma \frac{RT}{\mu}, \quad H = f(T), \quad \gamma = f(T), \quad \mu = f(T) \quad (10-5)$$

$$\frac{dc^2}{dr} = \frac{df(T)}{dT} \frac{dT}{dr}, \quad \frac{d\gamma}{dr} = \frac{df(T)}{dT} \frac{dT}{dr} \quad (10-6)$$

The pressure finally follows from Eq. (2-18)

$$p = \text{const.} \frac{T}{\mu M c r^2} \quad (10-7)$$

With the initial conditions of Sec. 9, Eqs. (10-1) to (10-7) represent a closed set of equations.

b) Types of solutions

1) Conduction and shock dominated solutions (CD, SD).

We first note that the shock equation (10-2) enters the other 2 differential equations (10-1) and (10-3) only through the dissipation term DISS in the energy equation (10-3). We can therefore treat (10-2) as a more or less independent equation which provides the term DISS to the energy equation.

The relative magnitudes of the two gain terms DISS and COND, and the two loss terms RAD and FLOW in (10-3) (defined via Eqs. (6-22) to (6-26)) tells us the nature of the energy balance, such that we can define a region to be conduction dominated when the main energy gain is due to conduction and to be shock dominated when the main energy gain is due to shock dissipation.

The groups of solutions of the flow equation (10-1) thus can be classified as either shock dominated (SD) or conduction dominated (CD) solutions.

2) Super- and sub-critical solutions

To investigate the flow equation (10-1) we use it in one for this purpose more convenient form Eq. (2-13):

$$\frac{1-\gamma M^2}{M} \cdot \frac{dM}{dr} = \frac{1+\gamma M^2}{2c^2} \frac{dc^2}{dr} - \frac{1}{\gamma} \frac{d\gamma}{dr} + \frac{\gamma g_o r_o}{c^2 r^2} - \frac{2}{r}, \quad (10-8)$$

or in short

$$A \cdot B = C \quad . \quad (10-9)$$

We see that the singularity in (10-1) for $M = \gamma^{-1/2}$ is of no consequence because with A in Eq. (10-9) C vanishes at the same time.

For a very small initial flow Mach number M_i , A is relatively large and B relatively small for the same C. The distance r grows faster than M and in C the r^{-1} term will become larger than r^{-2} at great distances, leading to $C = 0$. If $A \neq 0$ at this point, then $B = 0$, and the flow Mach number M will decrease again, leading to a subsonic flow at all distances. This case is called subcritical solution.

For a very large initial flow Mach number M_i ($M_i < \gamma^{-1/2}$), A is relatively small and B relatively large. M grows faster than the distance r leading to $A = 0$. If $C \neq 0$ at this point, B has to be infinite, which means that $M(r)$ swings back in r to become a multivalued function of r. This case is called super-critical solution and has to be excluded because no physical meaning can be attributed to a multivalued flow.

The case where A and C vanish the same time leaving $B > 0$ is called critical solution. The flow Mach number M can continue to grow and ultimately gives rise to supersonic flow.

This is the solution which we need on physical grounds for stellar winds as supersonic velocities are observed at least in case of the sun [81].

This behavior of the flow equation is well-known and has been discussed by Parker [82], Noble and Scarf [70], [71] for CD solutions and by Bird [12], [14] for SD solutions.

3) The three critical solutions (CDC, SDCF, SDCR)

If we use the full energy equation (10-3) we get three critical solutions. For comparison Parker, Noble and Scarf who assumed COND = FLOW, and Bird who assumed DISS = FLOW obtained only one.

We have Eq. (10-3)

$$\text{COND} = \text{FLOW} + \text{RAD} - \text{DISS} .$$

a) Starting off with a very high value of M_1 we find

$$\text{DISS}, \text{RAD} \ll \text{FLOW}$$

and obtain the CD critical solution (CDC).

This will be the only solution if everywhere

$$\text{DISS} < \text{RAD}$$

b) When, at the other hand

$$\text{DISS} > \text{RAD}$$

we obtain SD solutions by lowering M_1 . If M_1 is still large, then

$$\text{DISS} > \text{FLOW} > \text{RAD}$$

we say that we have a SD critical solution where the flow is dominant. (SDCF)

If M_1 is small, then

$$\text{DISS} > \text{RAD} > \text{FLOW}$$

we get a SD critical solution where radiation is dominant. (SDCR)

c) Selection of the solutions

From the three solutions CDC, SDCF, SDCR which are possible if we insist on supersonic stellar wind velocities* [81] we can exclude CDC as this solution depends on a heat source outside the star. The SDCR solution is ruled out by the physical arguments stated below. The remaining SDCF solution is therefore the only object of our attention.

* Otherwise we would have a infinite multitude of subcritical solutions.

Section 11. Computer Program

The numerical calculations were performed on the IBM 7094 computer of the Yale Computer Center in Fortran IV-Language.

- 1) The quantities

$$\rho \dot{Q}_{\text{rad}}(T, p)$$

and

$$\left(\frac{dc^2}{dT}, c^2, \frac{d\gamma}{dT}, \gamma, \mu, H \right) = f(T)$$

were treated as subroutines interpolating from tables of the radiative loss function of Sec. 7, and the calculations of Sec. 5.

- 2) Another subroutine computed the various numerical factors in the shock and energy equation that depend on M_s and M .
- 3) The integrals DISS and RAD were performed with an integration-interpolation formula [1, p. 888] (Bodes Law).
- 4) The system of three first order differential equations was numerically integrated with a 5th order Runge Kutta method [121] where the 6th order term was kept to regulate the stepsize. Root mean square values of this 6th order term were kept smaller than a certain externally adjustable size. If this error exceeded the permitted limit, the step was rejected. A second order auxilliary formula predicted the next step size on the basis of the last 2 accepted steps.

For the first few steps we used r as independent variable, so that formally

$$\frac{dM}{dr} = f_M, \quad \frac{dM_s}{dr} = f_{M_s}, \quad \frac{dT}{dr} = f_T, \quad \frac{dr}{dr} = 1.$$

Because of the initial steep rise in temperature we changed then over to T as being the independent variable, so that formally

$$\frac{dM}{dT} = \frac{f_M}{f_T}, \quad \frac{dM_s}{dT} = \frac{f_{M_s}}{f_T}, \quad \frac{dT}{dT} = 1, \quad \frac{dr}{dT} = \frac{1}{f_T}.$$

At greater heights we went back to r as the independent variable.

The machine time required to complete one star model with the final program was approximately one hour.

Section 12. The Principle of Similarity Invariance
and the Condition of Complete Shock Dissipation

When we first tried the computer program as outlined in the last section with $\frac{1}{2} \approx 1$ in Eq. (6-23) we found the conduction dominated (CD) solutions and could iterate to the critical CDC solution.

Lowering the initial flow Mach number M_i , however, to search for the shock dominated critical solutions, did not bring us into the shock dominated region. This failure was soon realized to be caused by the fact that at 1/10 solar radii still only a few percent of the original noise energy had been dissipated. In other words, as

$$\text{DISS} \ll \text{FLOW} + \text{RAD} \quad (12-1)$$

we obtained

$$\text{COND} \approx \text{FLOW} + \text{RAD} \quad (12-2)$$

and consequently higher and higher temperatures.

This behavior in turn increased the thermal energy of the gas (that is the FLOW-term) to make the DISS-term even smaller compared to the sum $\text{FLOW} + \text{RAD}$ in Eq. (12-1).

Artificially increasing the dissipation rate beyond Brinkley and Kirkwood's value (by multiplying both Eqs. (4-39) and DISS in Eq. (6-23) by an arbitrary factor) did not help the problem. Extensive checks then showed that the origin was the principle of shape similarity invariance.

This principle as explained in Appendix B states that $\mu v = \frac{1}{6v_0} = \text{const}$, or in other words, that once we have chosen a certain shock profile, in our case a triangle pulse, it stays a triangle pulse through all regions it passes until the shock energy is completely dissipated.

We therefore are led to the conclusion that this product μv apparently does not remain constant.

It should be kept in mind that the principle of shape similarity invariance was developed for underwater explosions where there were no sharp density and temperature gradients.

In our case, the product μv seems to change to a degree sufficient to invalidate our solution.

To understand how μv may change we use Eq. (4-24)

$$D = p'_m u_m \mu v \quad (12-3)$$

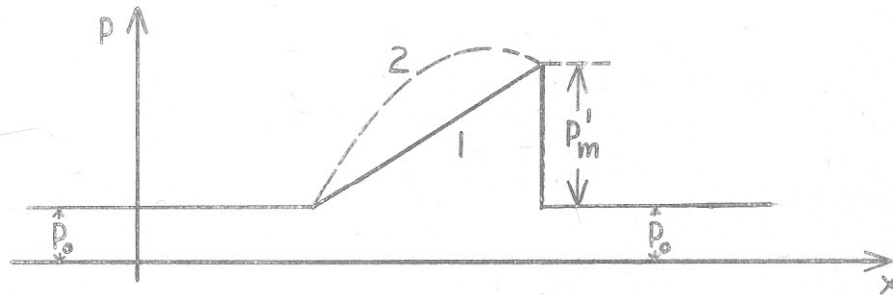


Fig. 20. Change of shock profile

and Fig. 20. Changing the shape from our profile 1 in Fig. 20, to profile 2, μv increases considerably.

The correct procedure would thus be to develop a detailed theory of the growth of the profile behind the shock, similar to the work done by Schirmer [94] for sound wave profiles in the photosphere, and to include this feature in the computer program. Obviously this is beyond present possibilities.

By assuming a shock profile different from the triangular shape, practically any value of πv can be obtained. In order to exclude arbitrariness, we now postulate that all initial shock energy is dissipated once the shock Mach number M_s has reached unity again at great distance from the stars surface.* In the case of the sun

$$\text{DISS} = 1.6 \cdot 10^7 \text{ ergs/cm}^2\text{sec for } M_s \rightarrow 1.$$

In numerical terms, the condition of complete shock dissipation determines the actual value of the product πv , that is the factor \mp with which the term DISS alone has to be multiplied. (See Sec. 6, Eq. (6-23))

We found this factor by plotting the energy at $M_s \rightarrow 1$ vs. \mp (each time iterating to the critical SDCF solution) and then interpolated to the \mp value at which the dissipated energy/cm²sec is πF_{mo}^+ . See Fig. 21.

This was done for the sun and the star G7 V to 1%, however for the stars G3 III and K1 III only to 17.8% and 15.6%

* One might object to this condition on grounds that there might be some energy left over in the form of sound waves when $M_s \rightarrow 1$ and therefore not all the energy reappears in DISS. This possibility can however be excluded as the decrease in density always tends to establish a new shock front.

respectively because it was not felt to warrant the amount of machine time involved to reduce the remaining difference.

Especially because a comparison of the effects of different factors \pm for the case of the sun (Fig. 22) shows that the change in the temperature profile is very slight. All the factors \pm have approximately the numerical value 9.

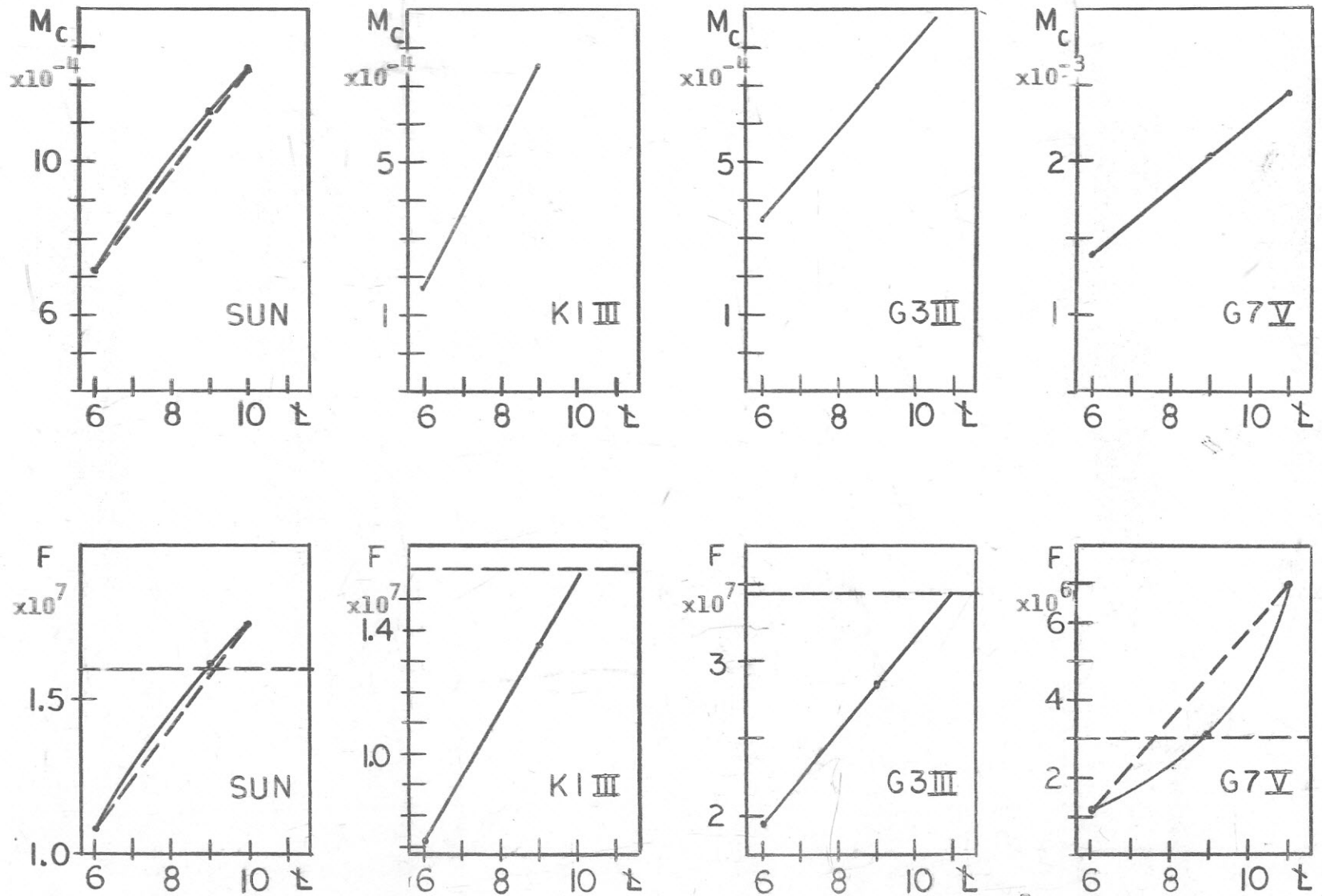


Fig.21 Critical flow Mach numbers and total dissipated energies (in erg/cm^2) per sec as function of the multiplication factor L .

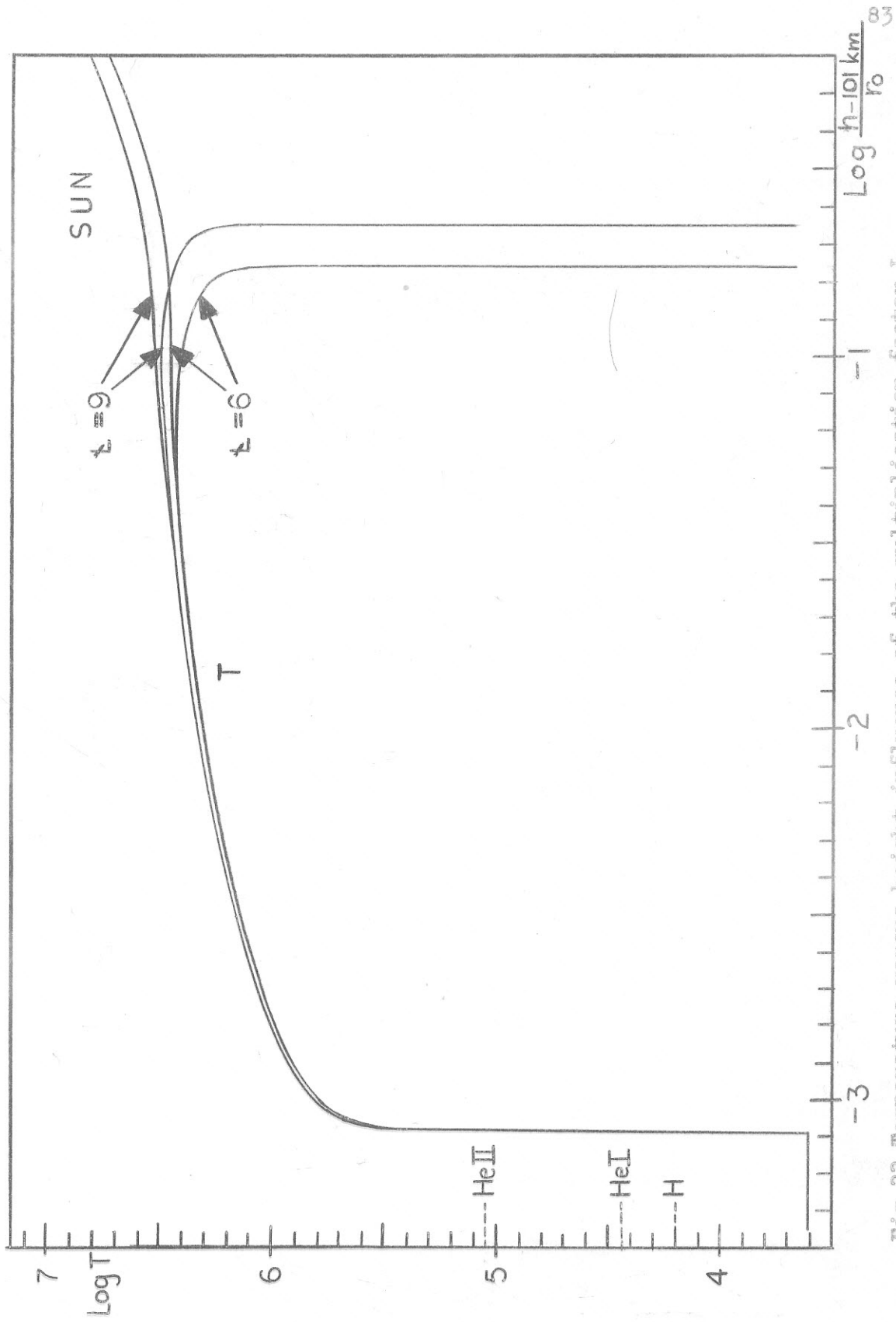


Fig.22 Temperature versus height, influence of the multiplication factor b .

Section 13. Numerical Results

a) Recalculation of Bird's results

Leaving out the terms RAD and COND in the energy equation (6-27) and using a factor $\pm = 1$ in the DISS term as well as changing the shock equation to Bird's form (Sec. 4d), we recalculated one case of Bird's work [14]. We found very good agreement in the behavior of the solution, and fairly good agreement* of our critical solution with Bird's. (See Fig. 23)

b) Survey of the different solutions with the full set of equations.

Figs. 24 and 25 show the different nature of the solutions met in the process of searching for the critical solutions. These solutions are for the sun and the multiplication factor \pm is six for all solutions. Only the initial flow Mach number is changed.

For high M_1 -values the conduction dominated solutions (CD) are obvious in Fig. 25 by their persistent positive temperature gradient. From Fig. 24 we conclude that the critical CD-solution (CDC) has the critical initial flow Mach number

$$M_1 = 3.5 \cdot 10^{-3} \pm 50\%$$

For a smaller M_1 , we find the shock dominated solutions (SD) with their negative temperature gradients (Fig. 25). The

* We used a mean molecular weight $\mu = .672$, while Bird had $\mu = 1$. This may explain the remaining difference.

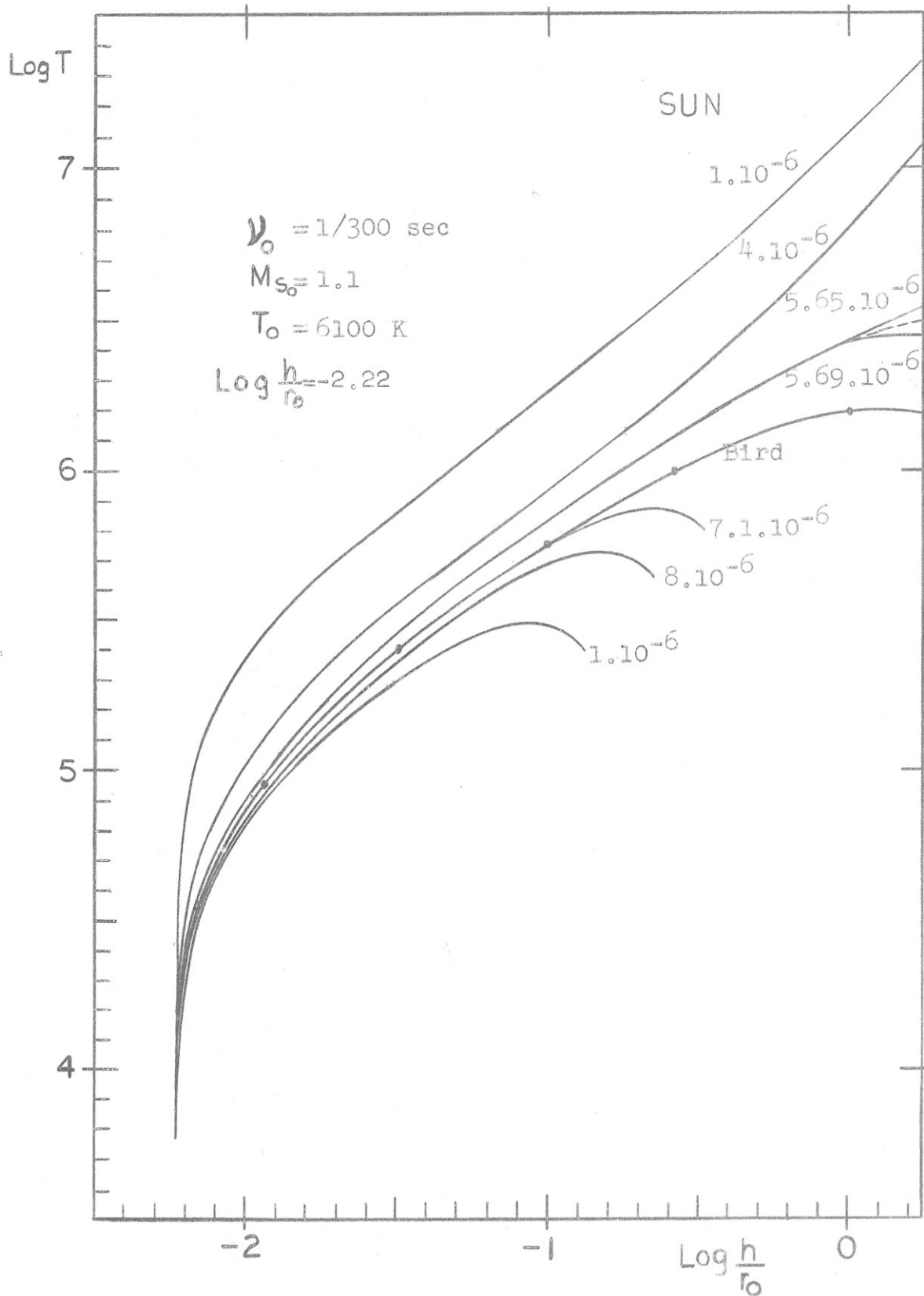


Fig.23 Temperature vers. height, M_1 as parameter.

Comparison with Bird's work.

critical SDCF solution has been approached by iteration, and we deduced the critical flow Mach number $M_i = 7.195 \cdot 10^{-4} \pm .34\%$. The two solutions bounding this value are almost identical up to a certain height from where on they behave according to their supercritical and subcritical nature, respectively. This point (where dM/dr becomes infinite) lies the higher in the atmosphere, the closer we have come to the critical initial flow Mach number.

For very small M_i the supercritical nature of the solutions becomes more predominant until $M_i = 5 \cdot 10^{-6}$. At $M_i = 1.06 \cdot 10^{-7}$ approaching the SDCR solution, we discontinued the survey because the initial step size became unrealistically low, namely, in numbers $\Delta r = 2 \cdot 10^{-13} r_\odot$, which corresponds to a temperature gradient of about 5000° per cm. The reason for this behavior is that at very low heights conduction is not yet important, so that the dissipation term in Eq. (6-16):

$$\frac{v_0^2 r_0}{Mc} \frac{1}{\gamma-1} \ln \phi \theta^{-\gamma} \cdot r^2 \quad (13-1)$$

(where c , ϕ , θ , γ are approximately constants) with its M^{-1} dependence dominates the temperature derivative.

We did not investigate the SDCR solution further because of this physically unlikely behavior. We note however, that qualitatively the solution predicts an extended atmosphere of coronal type with a temperature of a few million degrees K in the same manner as the SDCF solution. Since the initial flow Mach number M_i is much smaller, the amount of matter flowing away from the star is much less, giving rise to much reduced solar or stellar winds.

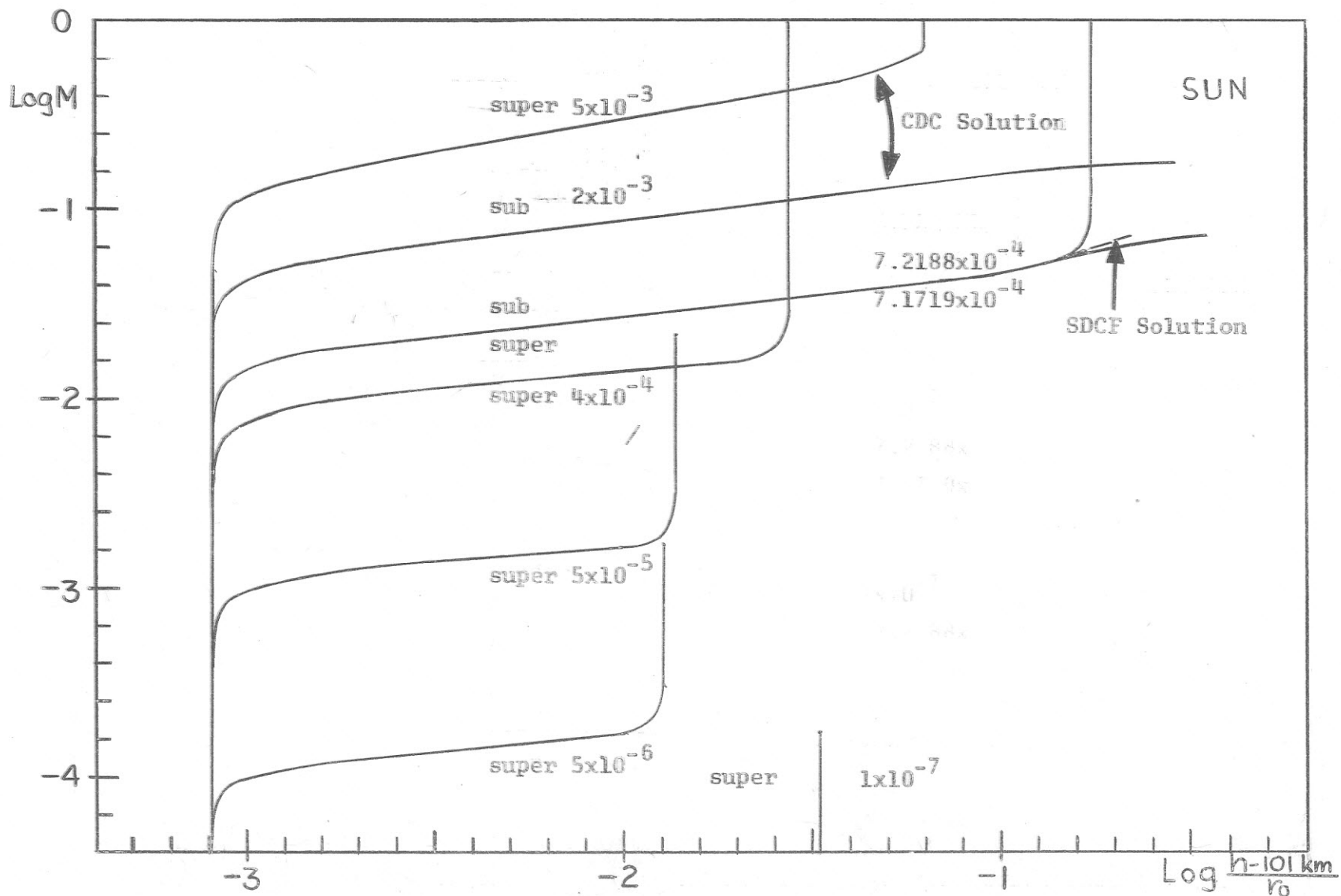


Fig.24 Flow Mach number versus height, iteration to the critical solutions. $L = 6$.
Initial flow Mach number as parameter.

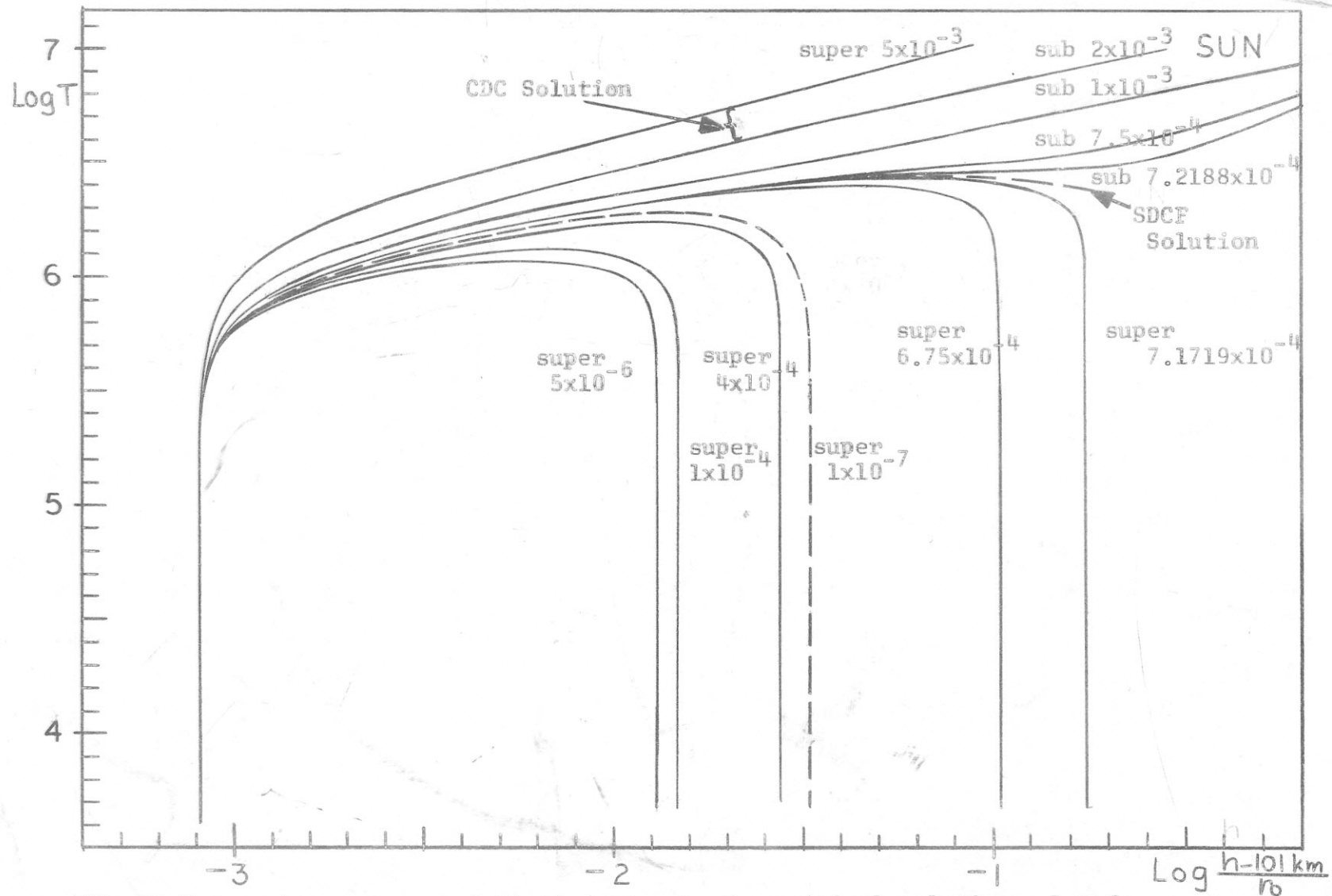


Fig.25 Temperature versus height, iteration to the critical solutions. $L = 6$.
Initial flow Mach number as parameter.

c) The models.

The numerical results of the correct critical SDCF solutions for our four stellar models are exhibited in Figs. 26 to 38 and Tables 6-8. The comparison with available observations and model calculations is given in the next two sections.

Star	T_{corona} $^{\circ}\text{K}$	M_i critical
Sun G2 V	$3.16 \cdot 10^6$	$1.136 \cdot 10^{-3} \pm .38\%$
K1 III	$2.76 \cdot 10^6$	$7.468 \cdot 10^{-4} \pm .42\%$
G3 III	$3.53 \cdot 10^6$	$6.968 \cdot 10^{-4} \pm .45\%$
G7 V	$1.74 \cdot 10^6$	$2.036 \cdot 10^{-3} \pm .38\%$

Table 6. Coronal temperatures and initial flow Mach numbers.

Temp	Sun km	K1 III km	G3 III km	G7 V km
T_0	0	0	0	0
$7 \cdot 10^3$.056			
$1 \cdot 10^4$.062	.02	.01	.017
$2 \cdot 10^4$.085			
$5 \cdot 10^4$.25	.23	.13	.65
$1 \cdot 10^5$	1.15	1.05	.54	4.18
$2 \cdot 10^5$	5.54			
$5 \cdot 10^5$	65.5	54.7	30.1	261
$1 \cdot 10^6$	493	470	253	2350

Table 7. Temperature rise in the transition layer. The heights given are heights above the level of shock formation.

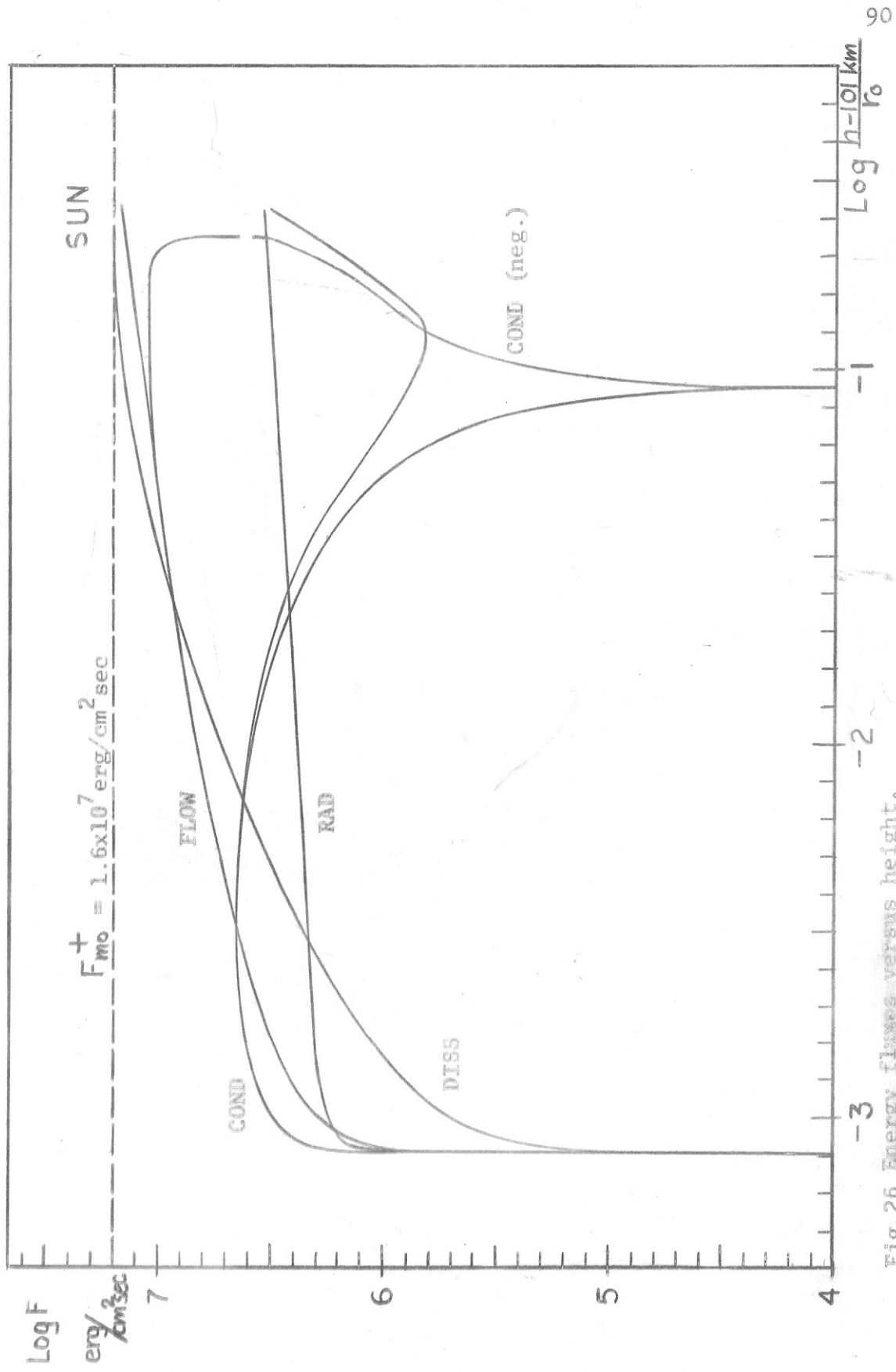


Fig.26 Energy fluxes versus height.

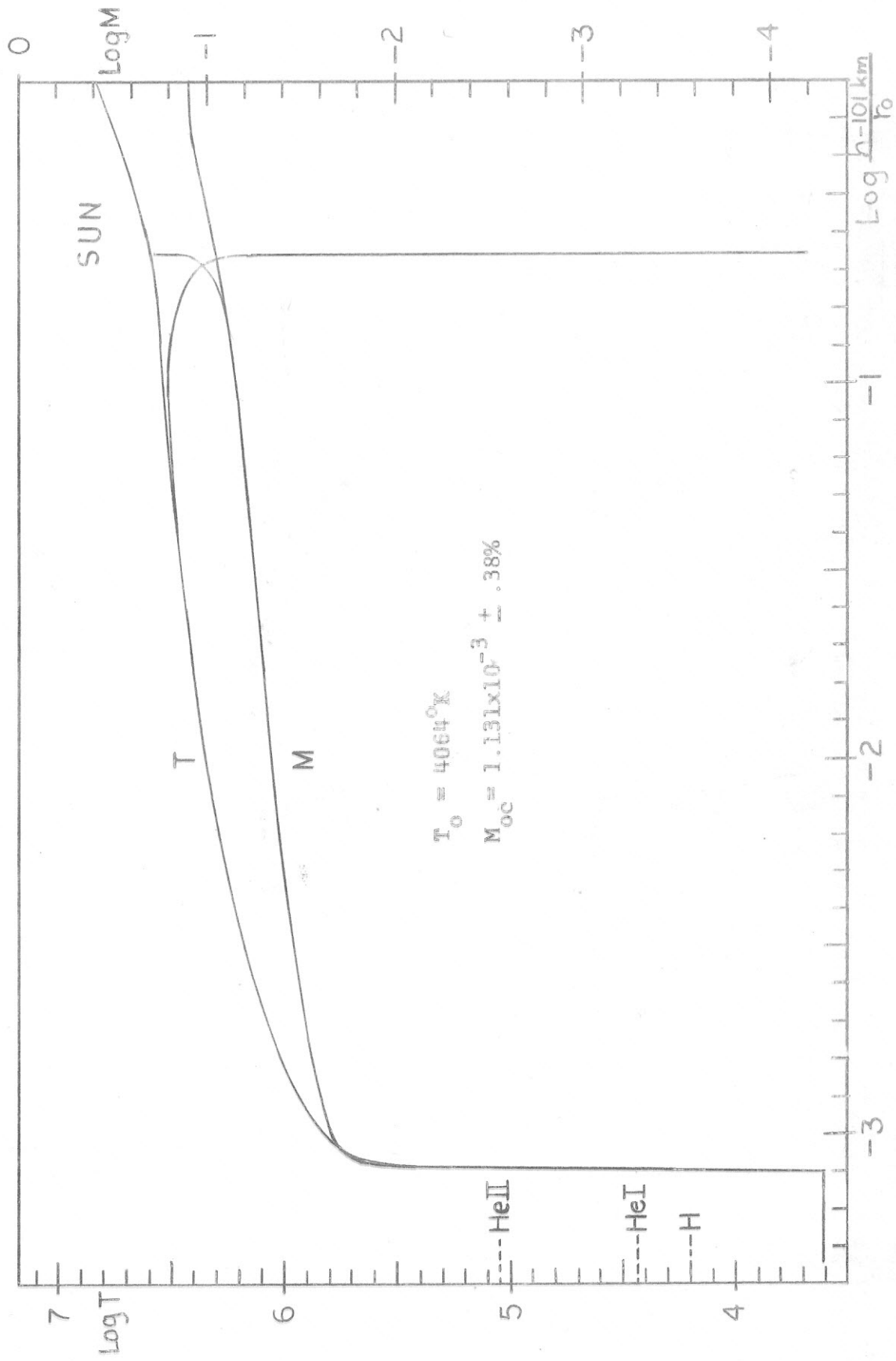


Fig.27 Temperature and flow Mach number versus height.

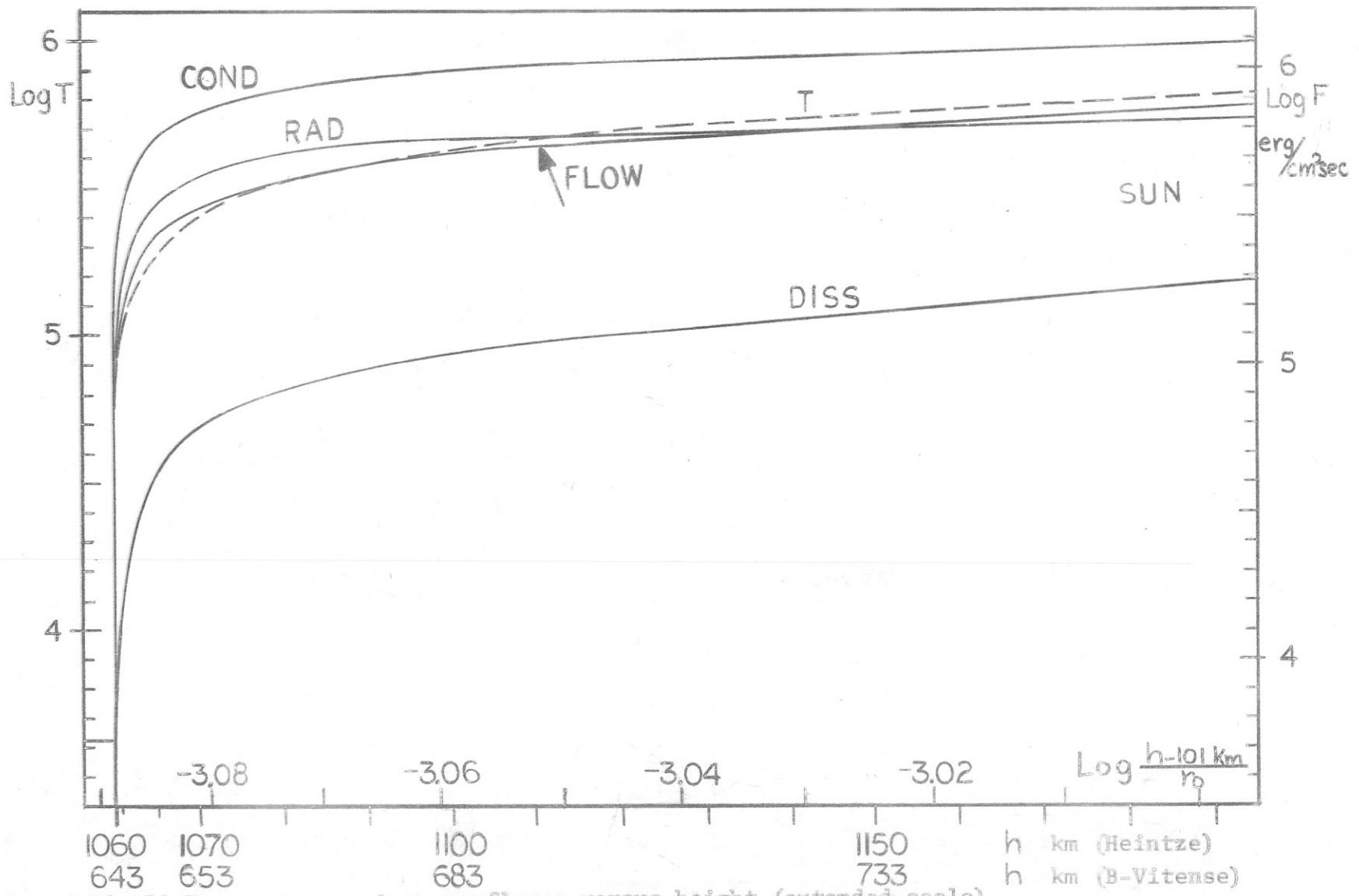


Fig.28 Temperature and energyfluxes versus height.(extended scale)

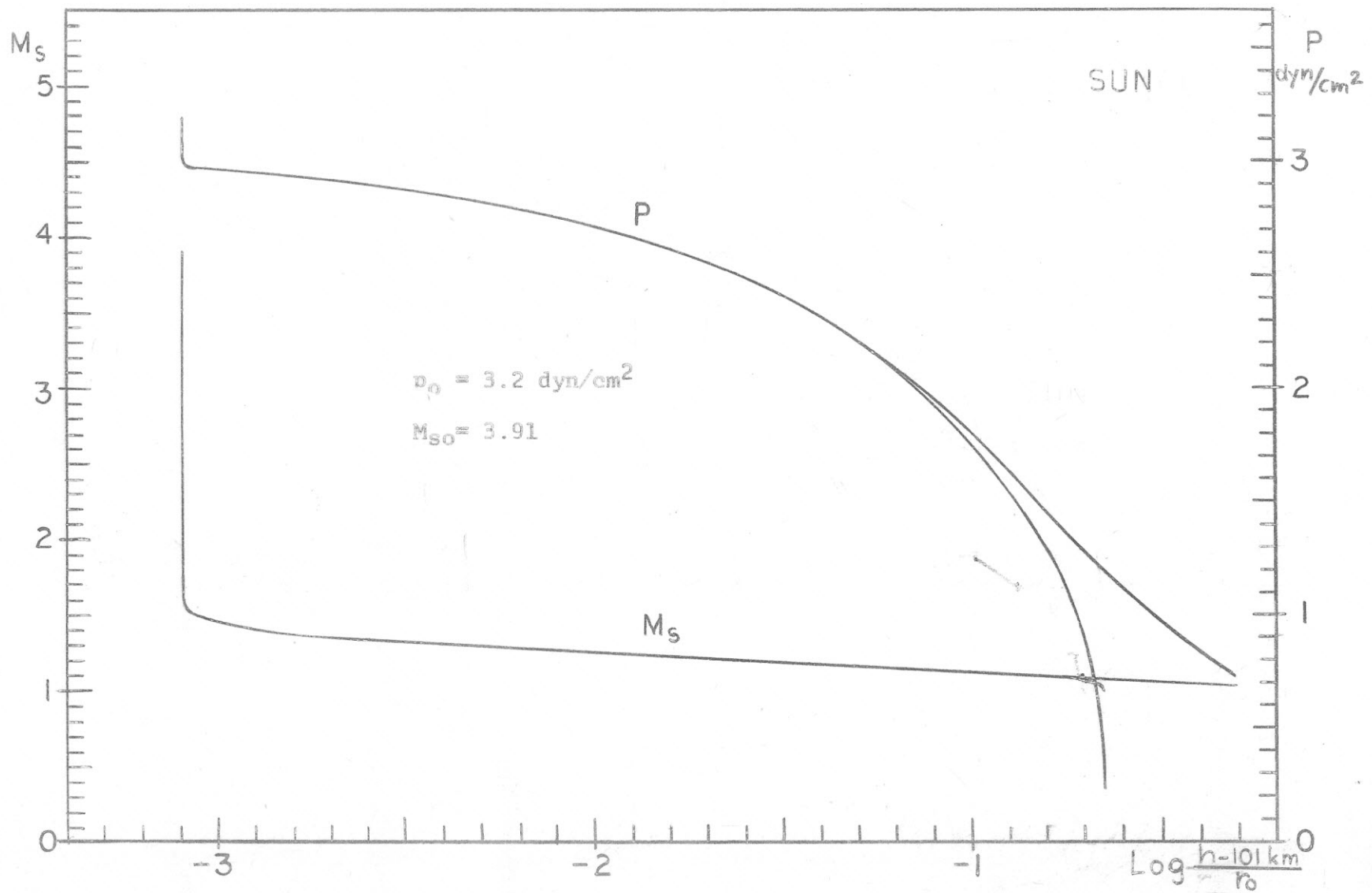


Fig.29 Pressure and shock Mach number versus height.

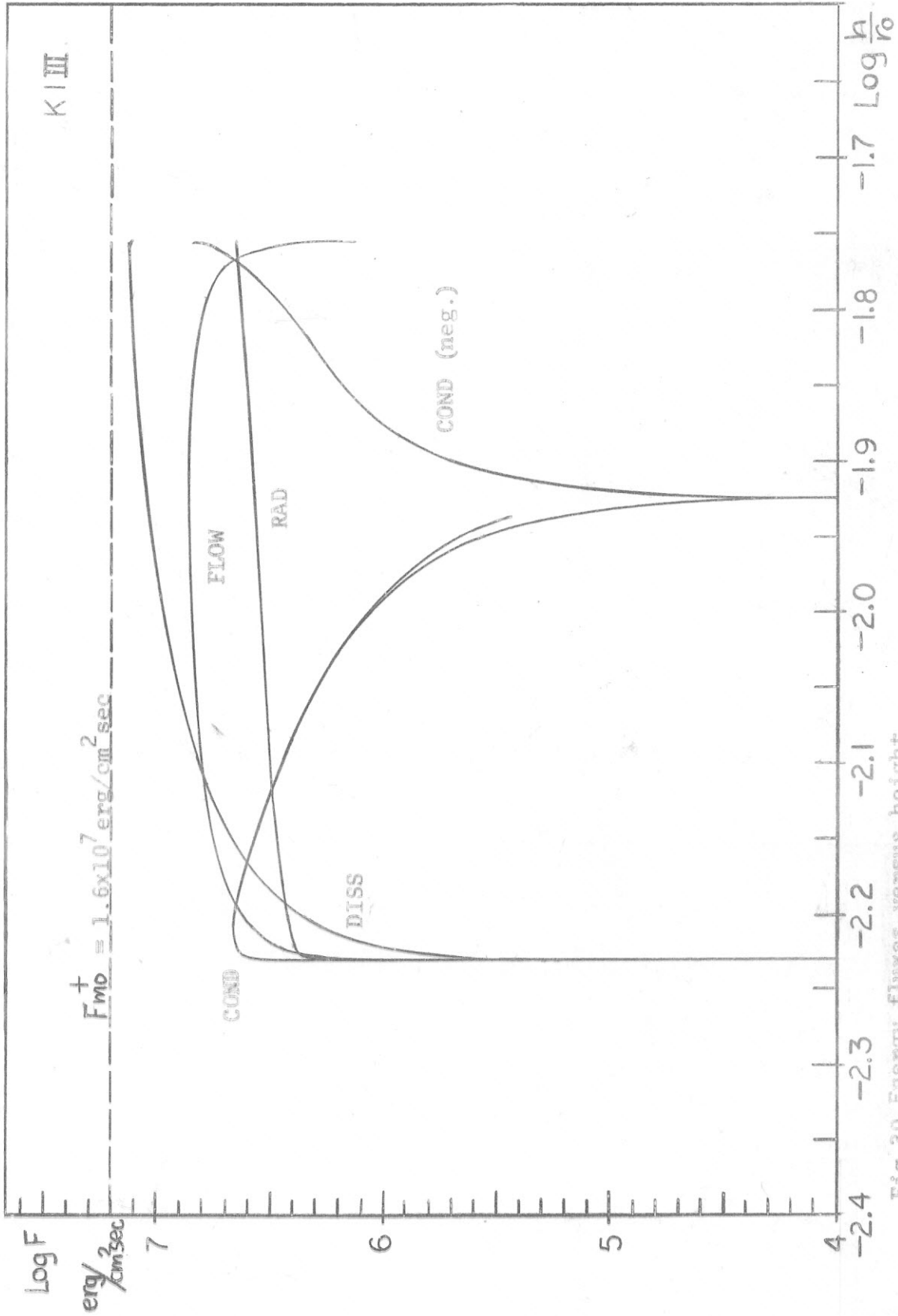


Fig.30 Energy fluxes versus height.

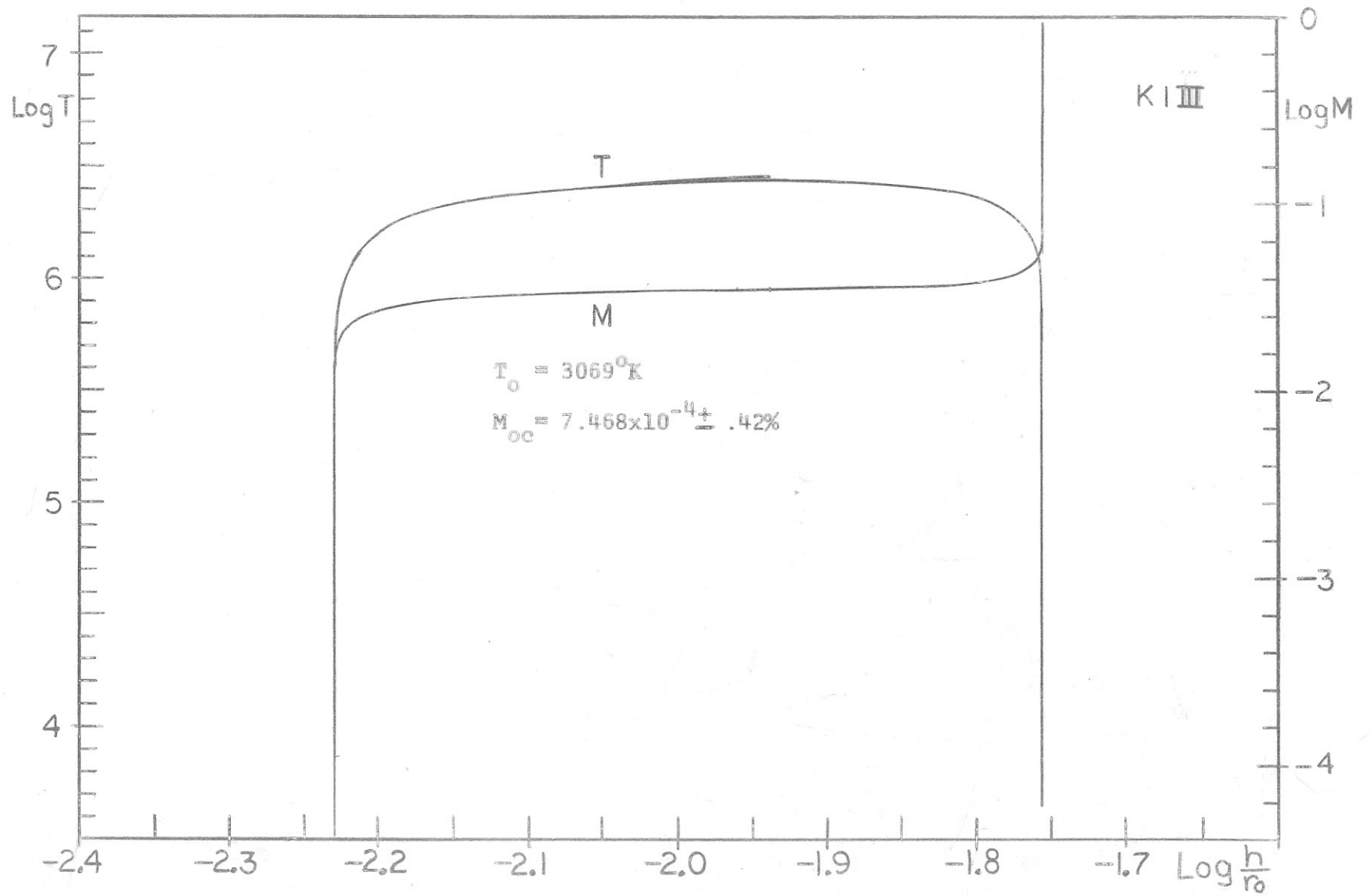


Fig.31 Temperature and flow Mach number versus height.

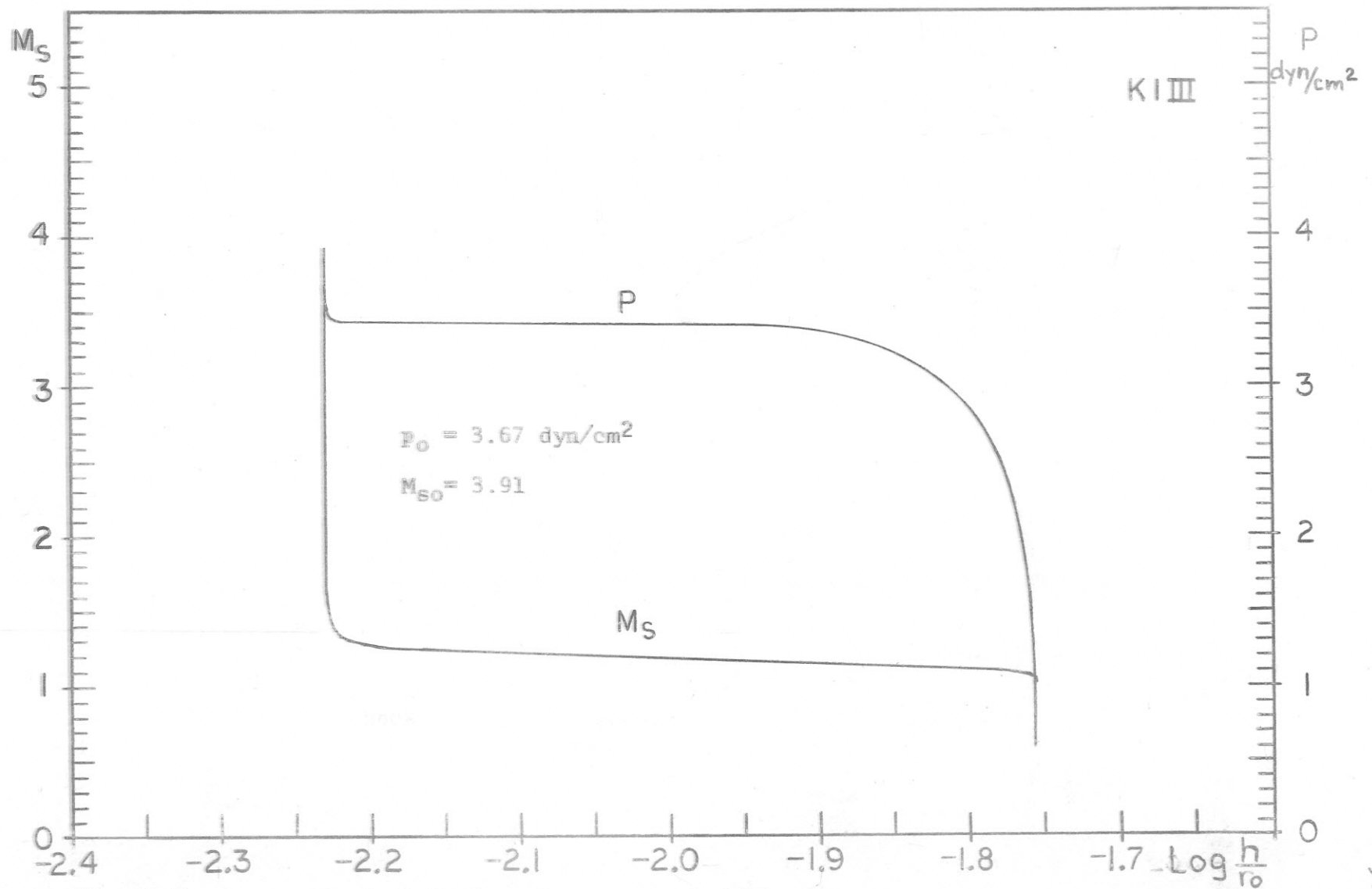


Fig.32 Pressure and shock Mach number versus height.

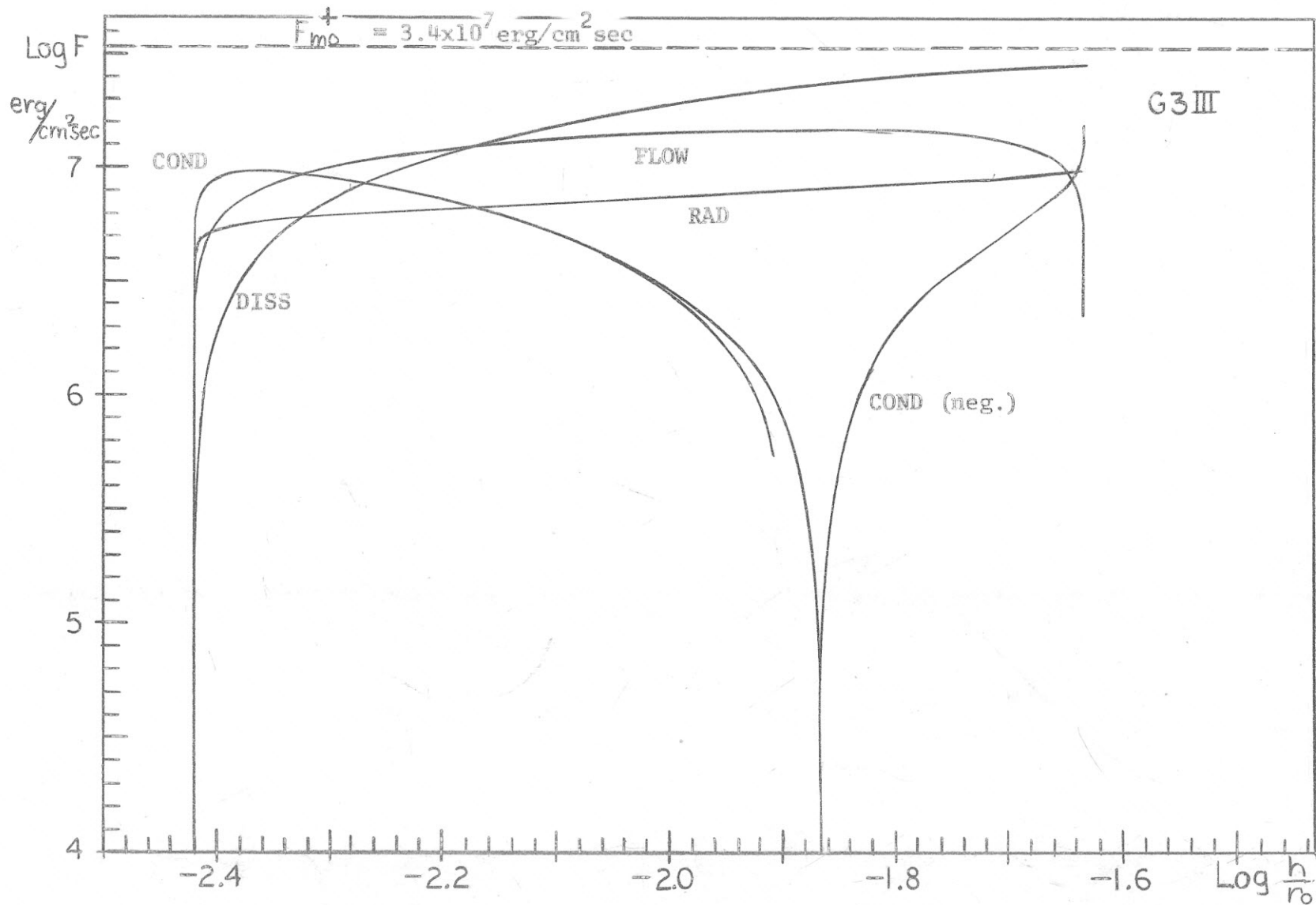


Fig.33 Energy fluxes versus height.

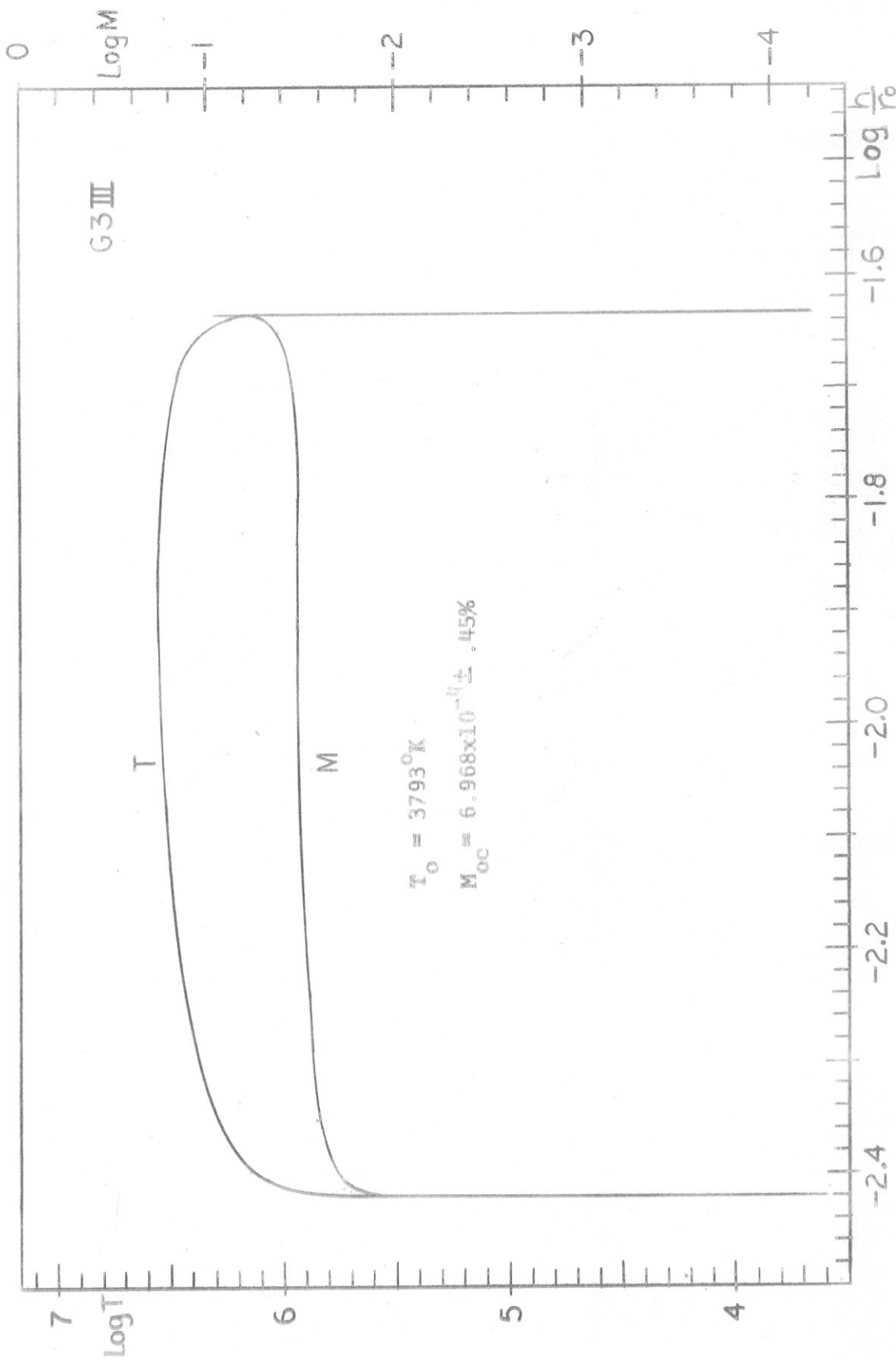


Fig.34 Temperature and flow Mach number versus height.

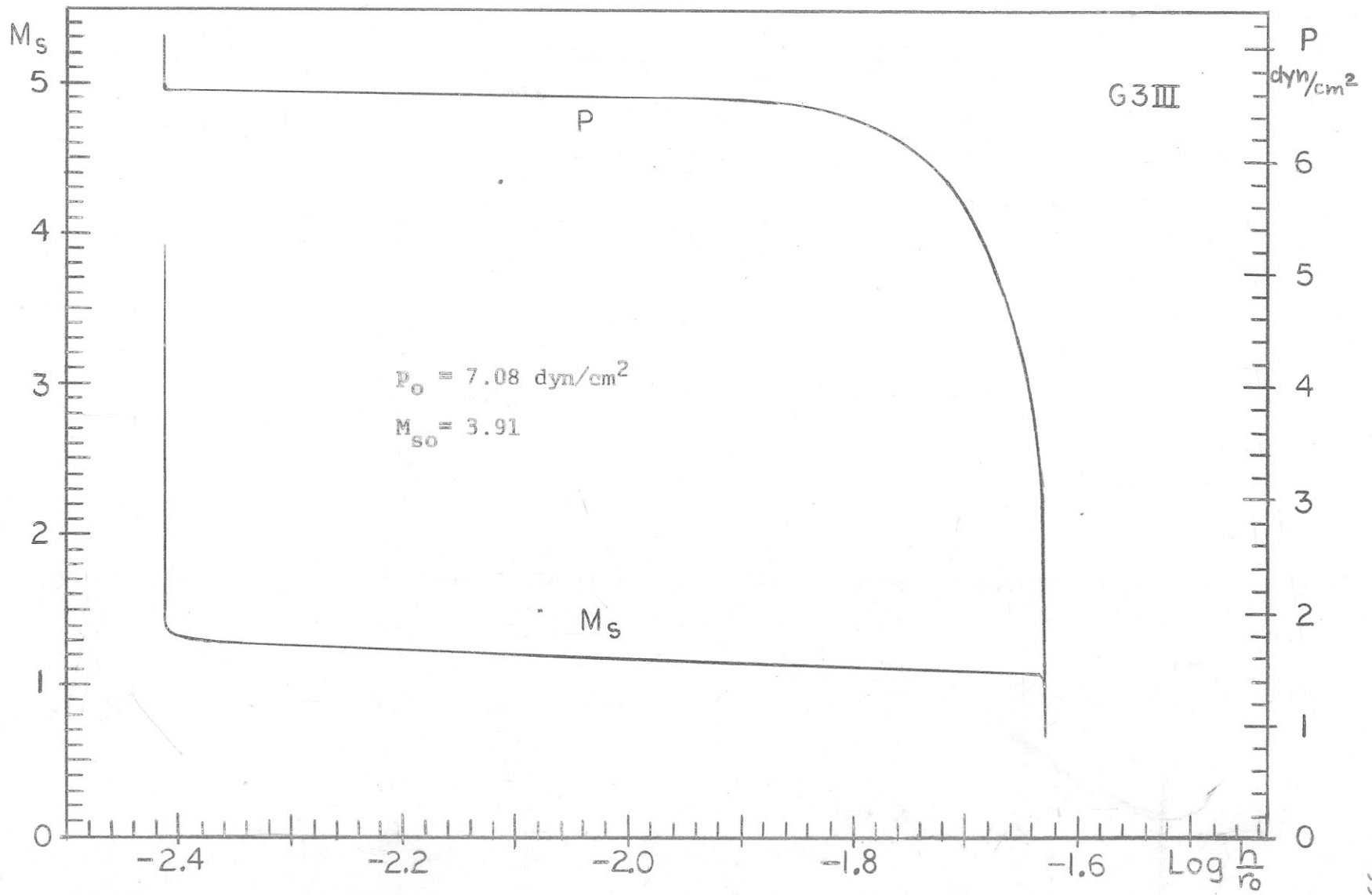


Fig.35 Pressure and shock Mach number versus height.

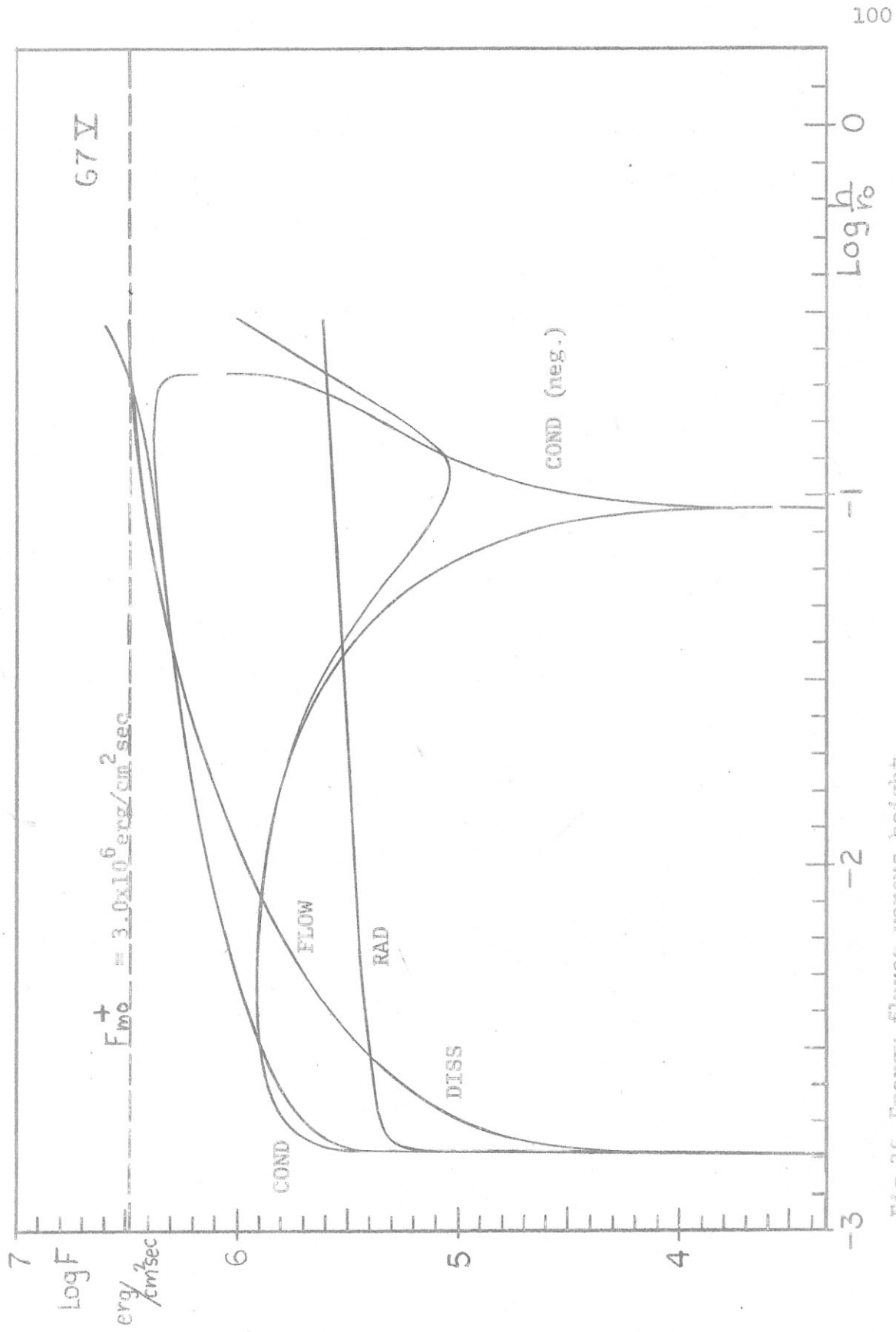


Fig.36 Energy fluxes versus height.

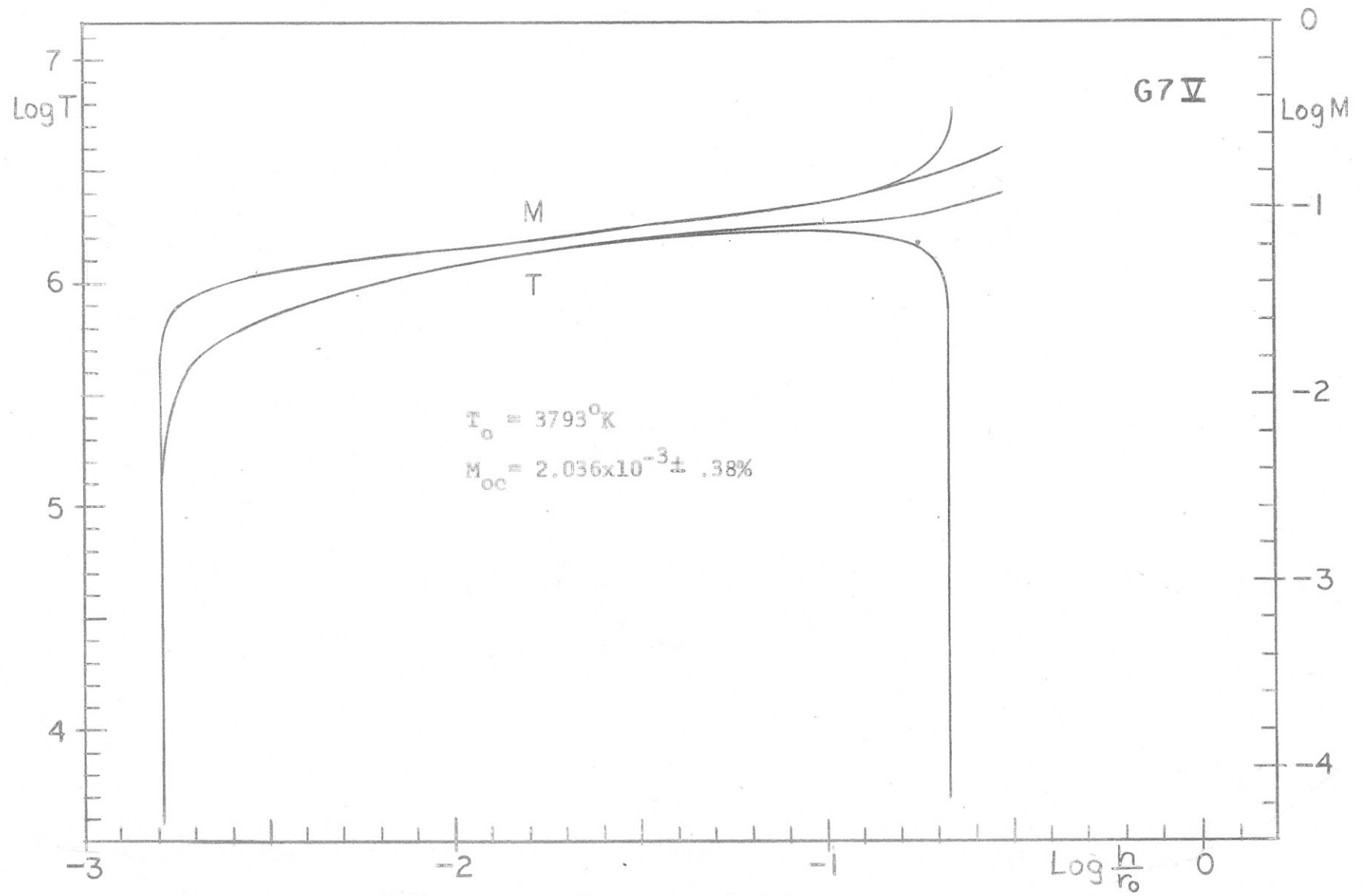


Fig.37 Temperature and flow Mach number versus height.

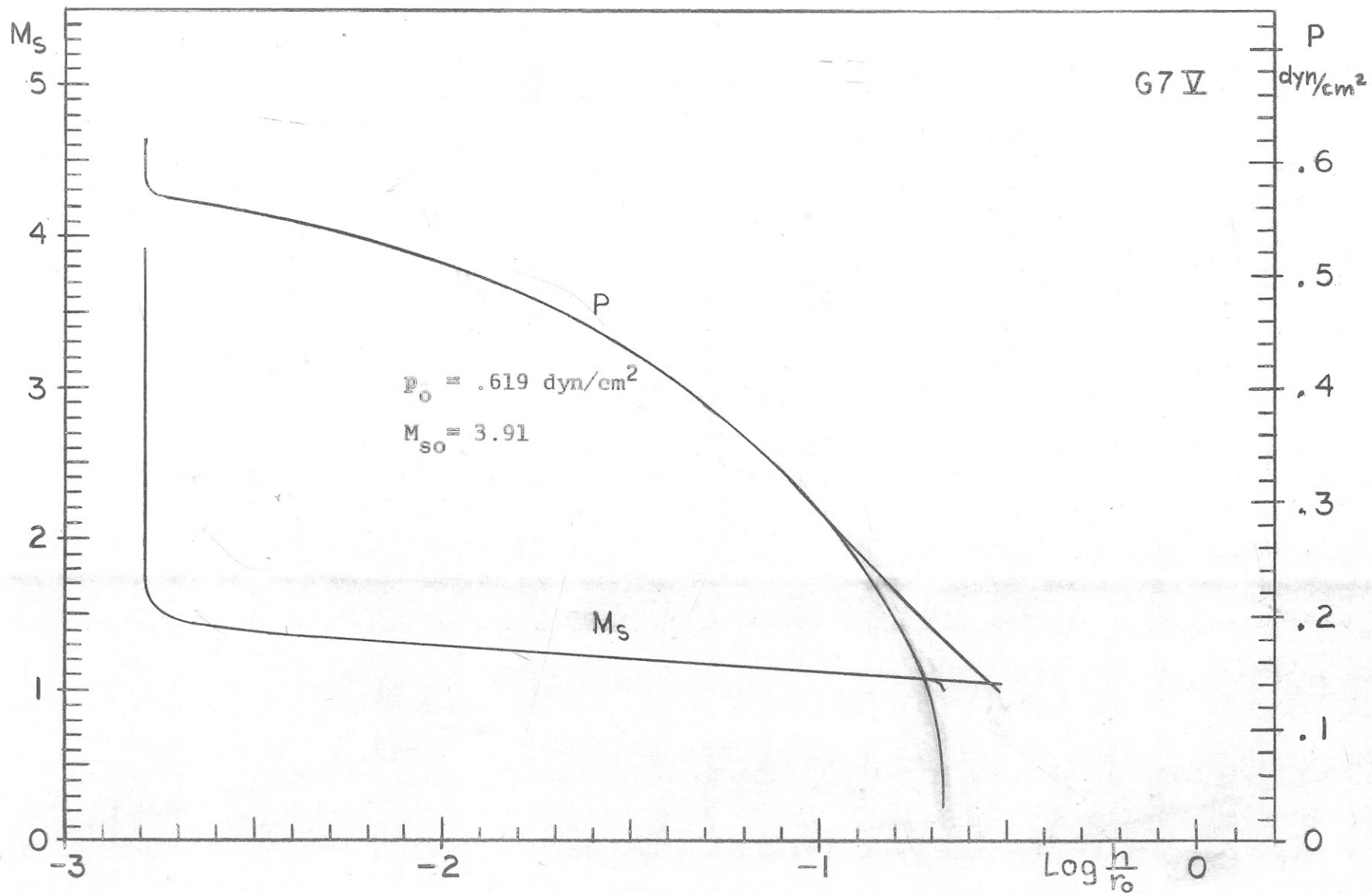


Fig.38 Pressure and shock Mach number versus height.

Section 14. Discussion of the Solar Results

a) Discussion of the model

As soon as the shock has formed, shock energy is dissipated (DISS) very rapidly. (See Eqs. (6-16) and (13-1)) The energy serves primarily to heat the gas (balance the FLOW term) while conduction is not yet important:

$$\text{DISS} = \text{FLOW} + \text{RAD} \quad (14-1)$$

The temperature rise will bring the gas quickly into a temperature region where the radiative losses (RAD) increase rapidly by approximately 4 orders of magnitude. (Sec. 7, Fig. 11) The comparatively slowly varying dissipation term (DISS) can not compete any more with the radiative losses and the energy must be supplied by conduction (COND). The more energy is radiated out, the steeper the temperature gradient must be in order to balance this radiation via conduction:

$$\text{COND} = \text{RAD} + \text{FLOW} \quad (14-2)$$

This behavior can be illustrated by a comparison with Bird's [14] solar model (see Figs. 23 and 28) that balances dissipation (DISS) against thermal and kinetic energy in the solar wind (FLOW).

$$\text{DISS} = \text{FLOW} \quad (14-3)$$

Bird finds the same steep initial temperature rise due to the large shock dissipation. However, as conduction is neglected as well as the radiative loss, the steepening influence of a large

conduction term balancing a large radiation term is not experienced and his model temperatures rise very much less steeply further out.

The temperature region of extremely large radiative losses is thus passed with a very steep temperature gradient which limits the amount of radiative losses by reducing the total gas mass in this region.

At higher temperatures we see that the flow energy (FLOW) which incidentally consists primarily of the thermal energy of the gas and not of kinetic energy, dominates over the radiative contribution (See Figs. 26 and 28). This flow term increases slowly.

Conduction finally becomes small compared with shock dissipation and vanishes with vanishing temperature gradient when the dissipated shock energy balances the sum of flow and radiated energies.

$$\text{DISS} = \text{FLOW} + \text{RAD} \quad (14-4)$$

At this point we have to consider the influence of viscosity whose importance in solar wind calculations has been shown by Noble and Scarf [70], [71]. As the effect of viscosity is proportional to v^2 and $v \frac{dv}{dr}$ (cf. Noble and Scarf Eq. (11)) we see that it will become important whenever the flow energy dominates.

Hence at lower heights where the flow energy and especially its kinetic part is negligible viscosity will play a minor role and our temperature profile will not be altered. The more the

flow term dominates at greater heights the more the viscosity will influence the model. This is especially true where the temperature of the corona has decreased and the kinetic part of the then supersonic flow is more important than the thermal part.

However, at heights beyond $0.1 r_{\odot}$ our model becomes unreliable at any rate because of the disparity of the supercritical and subcritical solutions.

b) Comparison with observations and other models.

1) Coronal temperature

Our coronal temperature of $T_{\text{cor}} = 3.16 \cdot 10^6$ °K (Table 6) may be compared with recent observations summarized in Table 8.

T_{cor}	Year	Nature of Observation	Author
$2 \cdot 10^6$	1965	radio	Cronyn [22]
$8 \cdot 10^5$	1964	radio, x-ray	Kundu [52], de Jager [42]
$2.6 \cdot 10^6$	1963	line width	Billings and Lilliequist [10]
$1.5 \cdot 10^6$	1961	x-ray	Elwert [27]
$3.2-3.5 \cdot 10^6$	1961	line width	Jarrett and Von Klüber [44]
$2 \cdot 10^6$	1959	line width	Billings [9]

Table 8. Observations of coronal temperature.

Recent model calculations of the solar wind by Parker [82] and Noble and Scarf [71] give coronal temperatures of $1.2-1.9 \cdot 10^6$ °K and $2 \cdot 10^6$ °K respectively.

Our result is somewhat higher than most determinations, but clearly within a reasonable range.

2) Pressure and electron density

Our values of N_e versus height are shown (see Fig.39) in a graph adopted from Kuperus [54]. The curves refer to the following authors.

Designation	Region	Author
1	normal	de Jager (1959) [41]
2		
3		
4		
5		
6	active	Kakinuma and Swarup (1962) [47]
7		Kawabata (1960) [48]
8		Christionsen <u>et. al.</u> (1960) [20]
9		Newkirk (1961) [69]
10		Hiei (1962) [36]
11	quiescent prominence	Koelbloed and Kuperus (1963) [51]
12	normal	Ulmschneider solar model
13		Ulmschneider solar model $p_0 = 16 \text{ dyn/cm}^2$

Table 9. Origin of electron density data.

3) Shape compression factor

Comparing Figs. 1 and 3 of Schirmer's [94] article we find a shape compression factor of $\# = 6.5/2.5 = 2.6$. A shape compression factor of $\# = 1$, on the other hand, yields according to our Eq. (9-10) an initial pressure $p_0 = 16 \text{ dyn/cm}^2 \text{sec}$. From

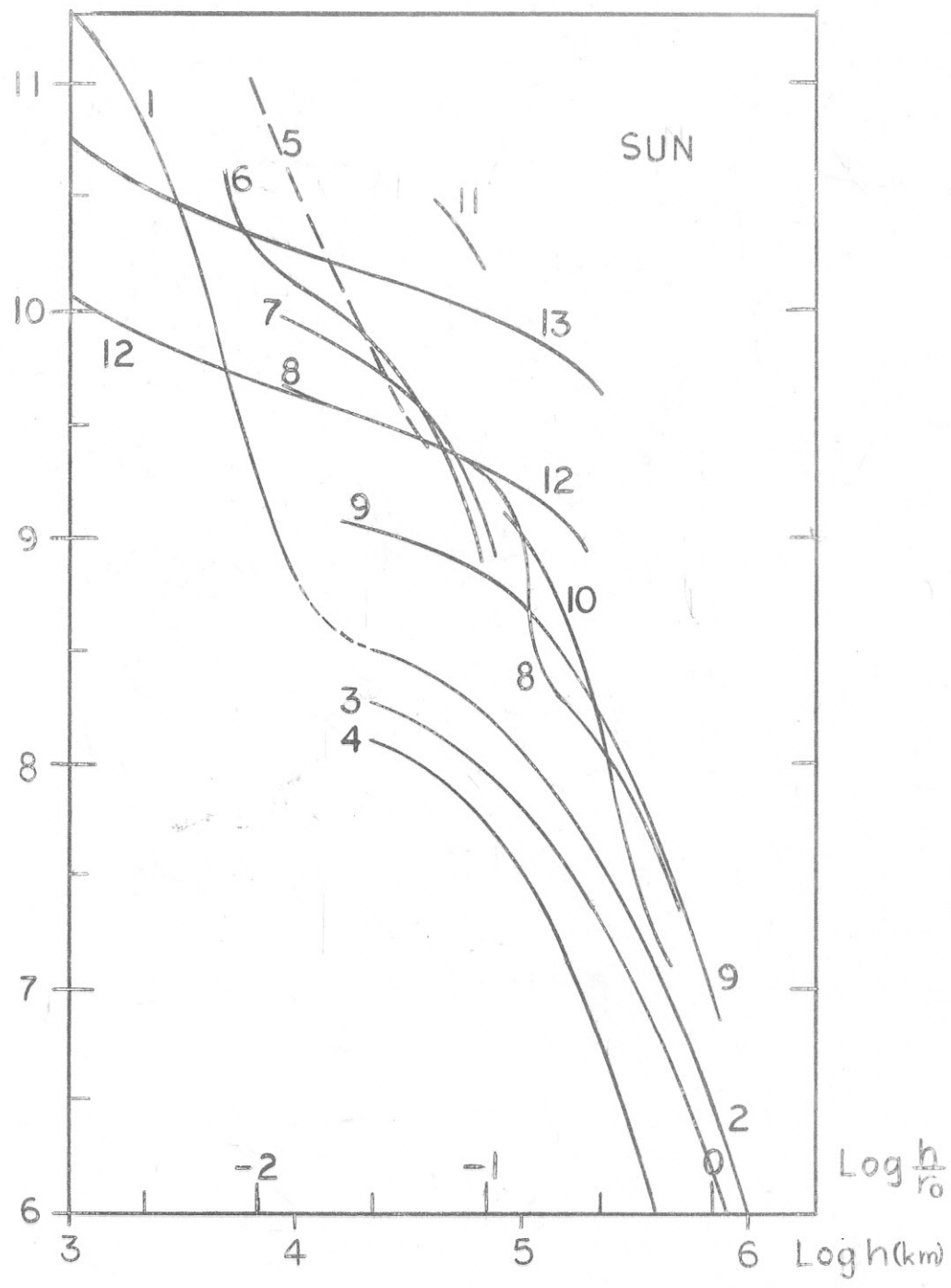


Fig.39 Electron density (cm^{-3}) versus height.

Authors see Table 9.

this pressure the solar model 13 in Fig. 39 is derived. It requires clearly too high density values.

Therefore a shape compression factor $\kappa = 4.91$, that is dividing p_0 by 5, was adopted leading to the solar model 12 with $p_0 = 3.2 \text{ dyn/cm}^2$. (See also 4))

4) Total emission of transition layer and corona

Recent theoretical estimates of the total emission of chromosphere and corona are given in Table 10.

F_r temp/cm ² sec	year	Author
$2 \cdot 10^7$	1961	Osterbrook [76]
$2.5 \cdot 10^5$	1959	de Jager [41]

Table 10. Total emission of chromosphere and corona.

Our result is $3.48 \cdot 10^6 \text{ ergs/cm}^2 \text{sec}$. It has to be noted, however, that the radiated energy is directly proportional to the pressure as can be seen from Table 11. For the energy radiated from the transition region below $1 \cdot 10^6 \text{ }^\circ\text{K}$ we obtained the following values:

initial pressure p_0	energy radiated	Model
160	$1.25 \cdot 10^8$	Sun
16	$1.26 \cdot 10^7$	$M_i = 1.35 \cdot 10^{-4}$
1.6	$1.27 \cdot 10^6$	$\kappa = 10$
.16	$1.28 \cdot 10^5$	

Table 11. Influence of initial pressure p_0 on the radiative losses.

The above value lies well within the presently available data.

5) Mass flow

a) Using a discussion of coronal line profiles Billings and Lilliequist [10] obtained data on the velocities close to the solar surface. They quote at a distance:

$$r = 1.03 \quad \text{velocity} \quad v = 6.6 \text{ km/sec}$$

In our model we find for this point (see Fig. 27)

$$\log \frac{h}{r_0} = -1.52, \quad T = 2.75 \cdot 10^6 \text{ } ^\circ\text{K}, \quad M = 5.6 \cdot 10^{-2}, \quad c = 2.4 \cdot 10^7$$

We obtain a solar wind velocity of

$$v = Mc = 13.4 \text{ km/sec}$$

within a factor of two of the observed value.

b) Observations of the solar wind at the orbit of the earth by Mariner II and values given by recent model calculations are listed in Table 12.

N_e (cm^{-3})	velocity km/sec	year	Method	Author
2	500	1962	Mariner II	Neugebauer and Snyder [68], Coleman <u>et. al.</u> [21]
1	300		$\rho v^2 = B^2/8\pi$	
20 - 40	440 - 730	1965	Solar wind	Parker [82]
6.75	352	1963	Solar wind	Noble and Scarf [71]

Table 12. Mass flux observations and model results at the earth's orbit.

Using the equation of mass conservation

$$\rho_0 M_i c_0 = \rho v^2 r^2$$

$$\rho_0 = 1.2 \cdot 10^{-11} \text{ gram/cm}^3, c_0 = 6.1 \cdot 10^5 \text{ cm/sec}, r = 214$$

we obtain from Mariner II observations $M_i = 2.1 \cdot 10^{-6}$ and from Parker's values $M_i = 8.1 \cdot 10^{-5}$. These values do not compare favorably with our $M_i = 1.1 \cdot 10^{-3}$. However, the same discrepancy results for the observations of Billings and Lilliequist. The reason is presumably that the Mariner II results are strongly influenced by coronal inhomogeneities.

6) Mechanical energy input

The input of mechanical energy into the outer atmosphere has been calculated by Osterbrock [76] on the basis of the earlier model of the solar convection zone given by Vitense [111]. An independent minimum estimate from calculations of the convection zone can be obtained in the following way:

From the fact that there exists a supersonic solar wind at a distance of $r \approx 1$ and that the coronal temperature is $\approx 2 \cdot 10^6$ °K we get with Eq. (6-24):

$$\text{FLOW} \approx \rho_0 M_0 c_0 \left\{ \left(\frac{1}{2} M^2 c^2 + H \right) - \left(\frac{1}{2} M_0^2 c_0^2 + H_0 \right) \right\}$$

using $\rho_0 = 1.2 \cdot 10^{-11} \text{ gram/cm}^3$, $c_0 = 6.1 \cdot 10^5 \text{ cm/sec}$, $M_0 = 1.1 \cdot 10^{-3}$, $M = 1$, $c = 2.1 \cdot 10^7 \text{ cm/sec}$, and the data collected in Fig. 10, we find

$$\text{FLOW} = 6.7 \cdot 10^6 \text{ ergs/cm}^2 \text{ sec}$$

Radiation losses will increase this value so that this estimate represents a minimum estimate. A summary of values is given in Table 13.

πF_{mo}^+ ergs/cm ² sec	Author	Nature
$3.3 \cdot 10^7$	Osterbrock [76]	Convection zone
$1 \cdot 10^5$	Sturrock [100]	estimate
$1 \cdot 10^6$	Saito [91]	estimate
$1.6 \cdot 10^7$	Ulmschneider	Convection zone
$6.7 \cdot 10^6$	Ulmschneider	estimate (solar wind alone)

Table 13. Noise energy production data

7) Comparison with recent models of the transition layer.

The most recent solar models quoted in the literature, Allen's [3] and Kanno and Tominaga's [46], are not yet published in full form.

a) Allen [3] reports calculations that result in a very sharp temperature transition with a rise in temperature from $\log T = 4.5$ to 5.3 over a distance of only 100 km. Our calculation (See Table 7) predicts this rise over 5.4 km, is therefore steeper by a factor of 20.

b) Kanno and Tominaga [46] quoted in an article by Pottasch [83] also give a very sharp temperature rise from $\log T = 4.5$ to 5.3 in 48 km. Our calculation is a factor of 9 times steeper.

c) A quite steep temperature gradient was also predicted on general grounds by Unsöld [107] and by Weymann [114].

- d) From observational arguments Zirin and Dietz [120] came to the same result.
- e) Calculations of Kuperus and de Jager [53] and Kuperus [54] performed with a shock dissipation theory, restricted to small shock Mach numbers and excluding the solar wind flow, also show a very steep temperature gradient. However, only corona temperatures of $6.5 \cdot 10^5$ °K to $7.8 \cdot 10^5$ °K were obtained. This is probably due to the fact that a larger amount of shock energy instead of conductive energy is used to balance radiation losses, leading to a premature exhaustion of the shock energy.
- f) Finally the model of Uchida [104] shows a steep rise ($\log T$ from 3.8 to 5.0 in 200 km). The corona temperature is $1 \cdot 10^6$ °K and the solar wind flow is taken into account, but not based on a supersonic critical solution as in our case. The initial wind velocity v_0 of 3 km/sec does not compare very well with our 50 cm/sec.

Section 15. Discussion of the Stellar Models

Our stellar models behave in a very similar manner as the solar model (See Figs. 30 to 38) except that, of course, none of the data could be checked against observations. A comparison will be given however with the only available model calculation given by Kuperus [54].

- a) The amount of convective noise energy produced by different stars.

The amount of noise energy produced by a convection zone depends strongly on the value of the mean velocity \bar{v} in the turbulent velocity field. For very hot stars ($T_e \gtrsim 15000^\circ$) and stars with very low surface gravity ($\log g \approx 1$) the inner ionization zone of hydrogen occurs already in the outer radiative equilibrium layer of the star and thus does not start a convection zone as is the case in cooler and more dense stars. With no convective motion no noise is produced by the processes considered in this paper.

It is readily seen from Eq. (8-2) and Figs. 13 to 16 that the noise production is important only in a narrow region around the maximum of the velocity curve. It is limited towards the stellar interior by the increase of the sound velocity and toward the outer atmosphere by the sharp decrease of the turbulent velocity.

Noting that very close to the layer of maximum noise production the total flux πF of the star is carried completely by convection, as is shown by Vitense [111] Fig. 5, we can understand the amount

of noise energy produced by a star as function of the effective temperature T_{eff} and the surface gravite as follows:

As the convective flux πF_k is proportional to \bar{v} and the density ρ , we can write for a point shortly before the velocity maximum \bar{v}_{max} is reached:

$$\sigma T_e^4 = \pi F = \pi F_k \sim \rho \bar{v} \quad (15-1)$$

Now consider two stars with effective temperatures T_{eff_1} , T_{eff_2} and surface gravities g_1 , g_2 .

If $g_1 = g_2$ and $T_{\text{eff}_1} > T_{\text{eff}_2}$ the size of star 1 is the same as star 2, or possibly a little larger. That means that the density in star 1 is the same, or possibly a little smaller. From Eq. (15-1) we see that then $\bar{v}_1 > \bar{v}_2$, and the noise production in star 1 is greater than in star 2.

If $g_1 < g_2$ and $T_{\text{eff}_1} = T_{\text{eff}_2}$, the star 1 is less dense. Eq. (15-1) shows that then $\bar{v}_1 > \bar{v}_2$ and the noise production in star 1 is again greater than in star 2. We find therefore

T.1. The higher T_{eff} and the smaller g the larger, therefore, the noise energy production.

This statement is valid only when a convection zone of reasonable size can develop in a star, however, it is consistent with all our models as well as those given by Kuperus [54, p. 63] (See Tables 2 and 3). *A summary of our conclusions is given in Fig. 40.*

b) Coronal temperatures and temperature gradients in the transition layers for different stars.

The height at which the shock is formed is determined entirely by the flux of noise energy and the scale height H_s of the atmosphere (Eqs. (9-10) and (9-12)). The temperature of the upper

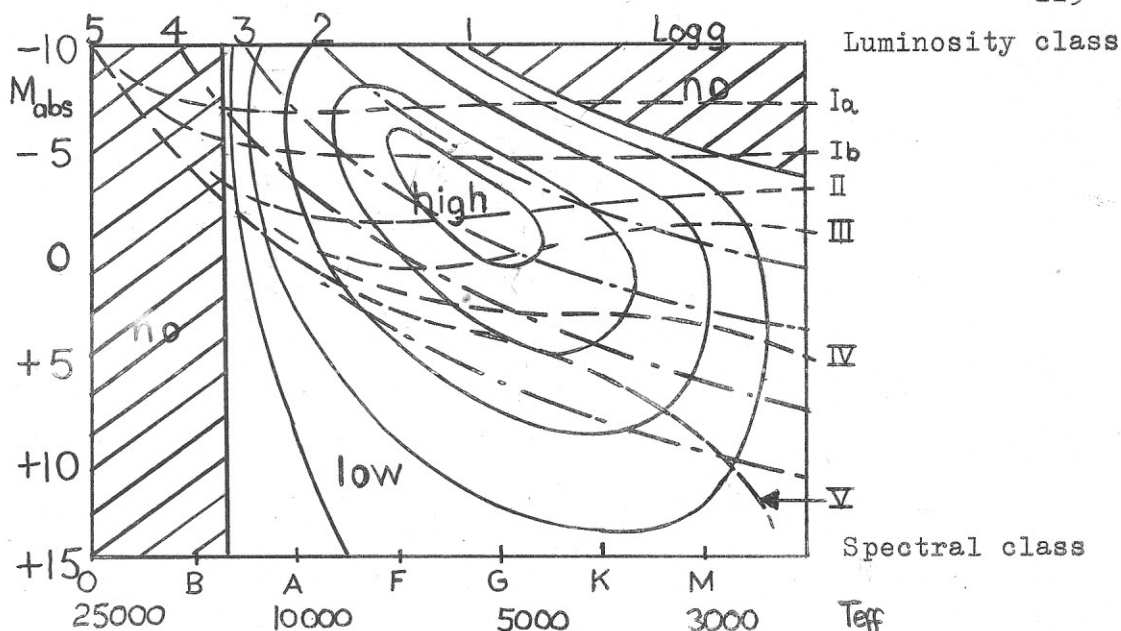


Fig. 40. Hertzsprung-Russel diagram and lines of equal noise production (Schematic)

photosphere of the stars is roughly the same (3500°K to 4500°K). The less the noise flux and the lower the surface gravity the more extended the upper photosphere.

Most important for our considerations, however, is the pressure p_0 at the height of shock formation. Considering the similarity of boundary temperatures T_0 , and that this value enters Eq. (9-10) only as $\sqrt{T_0}$, we can make the following statement, keeping this limitation in mind: (See Tables 3 and 4)

T.2. The pressures p_0 at the level of shock formation are directly proportional to the noise fluxes.

As we already found for the sun that the radiative losses are directly proportional to p_0 (see Table 11), we conclude in general:

T.3. The amount of radiative losses in a star is directly proportional to the amount of noise energy produced.

This can be ascertained in our models by comparing the "RAD"-profiles of our 4 stars (Figs. 26, 30, 33, 36) and correcting

them by the factors $p_{o \text{ star}}/p_{o \text{ sun}}$. All curves can approximately be brought to coincide with the solar curve.

The lines of equal noise production in Fig. 40 are lines of equal radiative losses from the transition layers of stars, or in other words, lines of equal UV radiation from the star.

Another important conclusion can be drawn from statements T2 and T3 by remembering that conduction (COND) is balancing the radiative losses (RAD) at the heights where most of the radiative losses occur. If the RAD-term is very large, the COND-term has to be very large and, consequently, the temperature gradient very steep. We can state therefore:

T.4. The steepness of the temperature gradient in the transition layer is directly proportional to the amount of noise produced.

This can be checked from a comparison of Tables 7 and 3. However, the temperature gradient must be measured at temperatures above 10^4 °K because at lower temperatures the assumption $\text{COND} = \text{RAD}$ is not valid as can be seen in Table 7. Again the lines of equal noise production in Fig. 40 are lines of equal steepness of the transition layer.

From Fig. 21, invoking the similarity of the stellar boundary temperatures, keeping the limitations of this statement in mind, and using the equation

$$\text{mass flux} = \rho_o c_o M_{cr}$$

where M_{cr} is the critical flow Mach number of the supersonic stellar wind flow, we can say:

T.5. The larger the noise flux the larger the mass flux due to stellar wind from the star.

We have again that the lines of equal noise production in Fig. 40 are lines of equal mass flux due to stellar winds.

Finally we deduce the statement

T.6. The larger the noise flux the higher the coronal temperature of the star.

The lines of equal noise flux in Fig. 40 are then again lines of equal coronal temperatures. To prove this statement, we just note that because a higher noise flux means higher mass fluxes, higher radiative losses and steeper temperature gradients, so that conduction may balance the radiative term, then, the temperature has already reached a higher value when the shock dissipation finally catches up with the FLOW and RAD terms.

c) Comparison with Kuperus

The comparison with Kuperus's [54] models is shown in Table 14.

	Sun	K1 III	G3 III	G7 V	Author
F_{mo}^+	$2.6 \cdot 10^7$	$4.8 \cdot 10^7$	$7.9 \cdot 10^7$	$4.7 \cdot 10^6$	Kuperus
	$1.6 \cdot 10^7$	$1.6 \cdot 10^7$	$3.43 \cdot 10^7$	$3 \cdot 10^6$	Ulmschneider
T_{cor}	$7.8 \cdot 10^5$	$1.2 \cdot 10^6$	$1.4 \cdot 10^6$	$3.7 \cdot 10^5$	Kuperus
	$3.16 \cdot 10^6$	$2.76 \cdot 10^6$	$3.53 \cdot 10^6$	$1.74 \cdot 10^6$	Ulmschneider

Table 14. Comparison with Kuperus [54].

There is general agreement in the behavior of both the noise energies produced and the coronal temperatures. In addition our statements T.1 and T.6 agree very well with Table 9 in Kuperus' paper.

The energy production is bigger by a factor 2-3 due probably to Kuperus' more approximate method of computing it.

The coronal temperatures are by a factor of 3-4 lower which, as already noted in Sec. 14, is probably due to the exhaustion of shock energy at greater heights because his theory depends on small shock Mach numbers and uses up more shock energy at lower heights in order to balance radiation.

Section 16. References

1. M. Abramowitz and I. E. Stegun Hdbook of Math. Funct.
New York: Dover, (1965).
2. C. W. Allen Astrophysical Quantities. London: Athlone (1964).
3. C. W. Allen Space Sci. Rev. 4, 91 (1965).
4. L. H. Aller Astrophysics. New York: Ronald (1963).
5. H. Alfvén Cosmic Electrodynamics. Oxford: Claredon (1963).
6. R. G. Athay and D. H. Menzel Ap. J. 123, 285 (1956).
7. R. G. Athay and R. N. Thomas Ap. J. 123, 299 (1956).
9. D. E. Billings Ap. J. 130, 961 (1959).
10. D. E. Billings and C. G. Lilliequist Ap. J. 137, 16 (1963).
11. G. A. Bird J. Fluid. Mech. 11, 180 (1961).
12. G. A. Bird Ap. J. 139, 675 (1964).
13. G. A. Bird Ap. J. 139, 684 (1964).
14. G. A. Bird Ap. J. 141, 1455 (1965).
15. E. Böhmer-Vitense Z. f. Ap. 36, 145 (1955).
16. E. Böhmer-Vitense Z. f. Ap. 46, 108 (1958).
17. S. R. Brinkley and J. G. Kirkwood Phys. Rev. 71, 606 (1947).
19. S. Chapman Ap. J. 120, 151 (1954).
20. W. N. Christiansen *et. al.* Ann. Ap. 23, 75 (1960).
21. P. I. Coleman *et. al.* Science 138, 1099 (1962).
22. W. M. Cronyn M.S. Thesis, Univ. of Michigan (1965).
24. L. R. Doherty and D. H. Menzel Ap. J. 141, 251 (1965).
27. G. Elwert J. Geoph. Res. 66, 391 (1961).
30. J. Faulkner to be published in the Ap. J. 1966.
31. G. B. Field Ap. J. 142, 531 (1965).

33. J. R. W. Heintze *Rech. Ast. de l'obs. Utrecht* 17(2) (1965).
34. L. L. House *Ap. J. Suppl.* 8, 307 (1964).
35. H. C. Van de Hulst *The Sun*, ed. G. Kuiper (Chicago) (1953).
36. E. Hiei *Jour. Phys. Soc. Japan* 17, 227 (1962).
39. G. S. Ivanov Kholodnyi and G. M. Nikolskii *Sov. Ast.* 5,
31 (1961).
41. C. de Jager *Handbuch der Physik* 52, 80 (1959).
42. C. de Jager *Res. in Geoph.* 1, 1 (1961): MIT Press, Cambridge,
Mass.
43. C. de Jager and L. Neven *Utrecht Publ.* 13 (1957).
44. A. H. Jarrett and H. Von Klüber *M. N.* 122, 223 (1961).
46. M. Kanno and S. Tominaga quoted in Pottasch [83].
47. T. Kakinuma and G. Swarup *Ap. J.* 136, 975 (1962).
48. K. Kawabata *Publ. Ast. Soc. Japan* 12, 513 (1960).
49. A. E. Kingston *Ap. J.* 140, 736 (1964).
51. D. Koelbloed and M. Kuperus *Proc. Kon. Ned. Ak. v. Wet.*
B 66, 36 (1962).
52. M. R. Kundu *Univ. Mich. Rad. Ast. Obs. Report No.* 64-4
(1964).
53. M. Kuperus and C. de Jager *B. A. N.* 16, 71 (1961).
54. M. Kuperus *Rech. Ast. de l'Obs. d'Utrecht* 17(1) (1965).
57. H. Lamb *Hydrodynamics*, Cambridge: Cambridge (1932).
58. L. D. Landau and E. M. Lifshitz *Fluid Mechanics*, New York:
Pergamon (1959).
59. M. J. Lighthill *Proc. Roy. Soc.* A211, 564 (1952).
60. M. J. Lighthill *Proc. Roy. Soc.* A222, 1 (1952).
61. R. Lüst *Space Sci. Rev.* 1, 522 (1962).

64. D. Mihalas Ap. J. 141, 564 (1965).
65. D. W. Moore and E. A. Spiegel Ap. J. 139, 48 (1964).
68. M. Neugebauer and F. L. Snyder Science 138, 1095 (1962).
69. G. Newkirk Ap. J. 133, 983 (1961).
70. L. M. Noble and F. L. Scarf Ap. J. 138, 1169 (1963).
71. L. M. Noble and F. L. Scarf Ap. J. 141, 1479 (1965).
74. L. Oster Z. f. Ap. 44, 26 (1957).
75. L. Oster Ap. J. 143, 928 (1966).
76. D. E. Osterbrock Ap. J. 134, 347 (1961).
77. K. Oswatitsch and G. Kuerti Gas Dynamics, New York: Acad. Press (1956).
80. E. N. Parker Interpl. Dyn. Proc., New York: Interscience (1963).
81. E. N. Parker Ap. J. 141, 1463 (1965).
82. E. N. Parker Space Sci. Rev. 4, 666 (1963).
83. S. R. Pottasch Space Sci. Rev. 3, 816 (1964).
84. S. R. Pottasch B. A. N. 18, 7 (1965).
85. S. R. Pottasch and R. N. Thomas Ap. J. 132, 195 (1960).
86. I. Proudman Proc. Roy. Soc. A214, 119 (1952).
88. P. K. Raju Ph.D. Thesis, Yale University (1966).
89. A. Rosa and A. Unsöld Z. f. Ap. 25, 20 (1948).
91. M. Saito Publ. Ast. Soc. Japan 16, 179 (1964).
92. W. C. Saslow and M. Schwarzschild Ap. J. 142, 1468 (1965).
93. E. Schatzmann Ann. d'Ap. 12, 203 (1949).
94. H. Schirmer Z. f. Ap. 27, 132 (1950).
95. M. Schwarzschild Struct. and Evol. of Stars, Princeton: Princeton (1958).

96. M. J. Seaton *Ann. d'Ap.* 18, 188 (1955).
97. A. J. Skalafuris *Ap. J.* 142, 351 (1965).
99. M. R. Spiegel *Vector Analysis*, New York: Schaum (1959).
100. P. A. Sturrock *Nature* 203, 285 (1964).
104. Y. Uchida *Publ. Ast. Soc. Japan* 15, 376 (1963).
105. A. Unsöld *Phys. der Sternatm.*, Springer (1955).
106. A. Unsöld *Z. f. Ap.* 24, 355 (1947).
107. A. Unsöld *Z. f. Ap.* 50, 57 (1960).
110. E. Vitense *Z. f. Ap.* 28, 81 (1951).
111. E. Vitense *Z. f. Ap.* 32, 135 (1953).
114. R. Weymann *Ap. J.* 132, 381 (1960).
115. R. Weymann *Ap. J.* 132, 452 (1960).
116. G. B. Whitham *J. Fluid Mech.* 4, 337 (1958).
117. C. A. Whitney and A. J. Skalafuris *Ap. J.* 138, 200 (1963).
120. H. Zirin and R. D. Dietz *Ap. J.* 138, 664 (1963).
121. J. A. Zonneveld *Autom. Num. Integr.*, Math. Centr., Amsterdam (1964).

Section 17. Acknowledgments

I would like to thank Dr. Ludwig Oster for suggesting this investigation and for continuous encouragement and helpful criticisms.

The friendship and continuous discussion of many basic questions with N. Paul Patterson have proven invaluable to me.

I would also like to thank Dr. James Hunter for many discussions and criticisms.

Financial support during the course of this work was provided by the Aerospace Research Laboratories of the Office of Aerospace Research, United States Air Force, Wright-Patterson AFB, Ohio.

Funds for computer time were provided by Yale University and by the National Science Foundation through Yale University and are gratefully acknowledged.

Appendix A

Derivation of the shock equation

Inserting Eqs. (4-9) to (4-15) into (4-8), we obtain

$$\frac{dp\theta}{dr} + \rho c \theta \rho \frac{d(\zeta+M)c}{dr} + \frac{\zeta c \cdot \theta \rho}{(\xi+M)c + \zeta c} \left(\frac{g_o r_o}{r^2} + \frac{2\zeta c(\xi+M)c}{r} \right) = 0 \quad (1)$$

Using

$$c^2 = \gamma \frac{p}{\rho}$$

to eliminate ρ , multiplying Eq. (1) by $(p\gamma\theta)^{-1}$ and using Eqs. (2-15) and (4-13), we get:

$$\begin{aligned} \frac{1}{\gamma\theta} \frac{d\theta}{dr} + \zeta \frac{d\xi}{dr} &= \frac{\zeta^2}{c^2} \left(Mc \frac{dMc}{dr} + \frac{g_o r_o}{r^2} \right) - \frac{\zeta(\xi+M)}{2c^2} \frac{dc^2}{dr} \\ &- \zeta \frac{dM}{dr} - \frac{1}{c^2} \frac{\zeta}{(\xi+\zeta+M)} \left(\frac{g_o r_o}{r^2} + c^2 \frac{2\zeta(\xi+M)}{r} \right) \\ &= (\zeta^2 M^2 - \zeta M) \frac{1}{M} \frac{dM}{dr} + \frac{\zeta^2 M^2 - \zeta(\xi+M)}{2c^2} \frac{dc^2}{dr} \\ &+ \frac{\zeta^2(\xi+\zeta+M) - \zeta}{c^2(\xi+\zeta+M)} \frac{g_o r_o}{r^2} - \frac{\zeta^2(\xi+M)}{\xi+\zeta+M} \frac{2}{r} \end{aligned} \quad (2)$$

Now, from Eqs. (4-9) to (4-13) follows

$$\frac{1}{\gamma\theta} \frac{d\theta}{dr} = 4 \frac{(\gamma-1)M_s^2 + 2}{(\gamma+1)^2 M_s} \frac{dM_s}{dr} + \frac{\xi M_s}{\gamma(\gamma+1)\theta} \frac{d\gamma}{dr}, \quad (3)$$

$$\zeta \frac{d\xi}{dr} = \frac{2\zeta}{\gamma+1} \frac{M_s^2+1}{M_s^2} \frac{dM_s}{dr} = \frac{\zeta\xi}{(\gamma+1)} \frac{d\gamma}{dr} \quad (4)$$

and from Eqs. (3) and (4) for the left side of (2):

$$\frac{1}{\gamma\theta} \frac{d\theta}{dr} + \zeta \frac{d\xi}{dr} = \frac{1}{\eta} \frac{1}{M_s} \frac{dM_s}{dr} + \frac{\xi}{\gamma+1} \left(\frac{M_s}{\gamma\theta} - \zeta \right) \frac{d\gamma}{dr} \quad (5)$$

If we now use Eq. (2-14) in (2), and if we take $\zeta/(1-\gamma M^2)$ out of the right hand side of (2), we find

$$\begin{aligned} \frac{1}{M_s} \frac{dM_s}{dr} &= \frac{\zeta\eta}{1-\gamma M^2} \left\{ (-\xi-2M+(\gamma\xi+2\zeta)M^2) \frac{1}{2c^2} \frac{dc^2}{dr} \right. \\ &\quad \left. + \frac{1}{\xi+\zeta+M} \left\{ (\zeta(\xi+\zeta)-1+(\zeta-\gamma(\xi+\zeta))M) \frac{g_{or}}{c^2 r^2} - \right. \right. \\ &\quad \left. \left. - (\zeta\xi-\xi M+(\zeta^2-1-(\gamma-1)\zeta\xi)M^2-(\gamma-1)\zeta M^3) \frac{2}{r} \right\} \right. \\ &\quad \left. - (\delta-M+(\zeta-\gamma\delta)M^2) \frac{1}{\gamma} \frac{d\gamma}{dr} \right\} \quad (6) \end{aligned}$$

where:

$$\eta = \frac{(\gamma+1)/2}{\frac{2}{\gamma+1} \left((\gamma-1)M_s^2+2 \right) + \zeta \left(\frac{M_s^2+1}{M_s} \right)} \quad (7)$$

$$\delta = \frac{\xi}{\gamma+1} \cdot \left(\frac{M_s}{\theta\zeta} - \gamma \right) \quad (8)$$

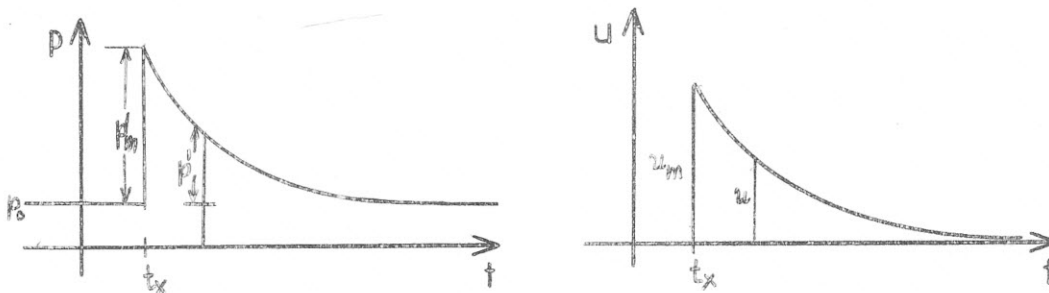
This is the desired shock equation.

Appendix B

1) Principle of shape similarity invariance.

To illustrate the principle of shape similarity invariance, we take as example an exponential behavior of pressure as function of time:

$$p'(t) u'(t) \approx p_m' u_m' e^{-t/\mu} \quad (1)$$



We want to calculate

$$D = \int_{t_x}^{\infty} p' u dt$$

For this purpose, we

1) Normalize to unity initial shock strength:

$$\frac{p' u}{p_m' u_m} \approx e^{-t/\mu} \quad (2)$$

$$D = p_m' u_m \int_{t_x}^{\infty} \frac{p' u}{p_m' u_m} dt \approx p_m' u_m \int_{t_x}^{\infty} e^{-t/\mu} dt \quad (3)$$

2) Normalize to unity initial slope:

$$D = p_m' u_m \underbrace{\int_{t_x}^{\infty} f(t) dt}_{\nabla} \approx p_m' u_m \underbrace{\int_0^{\infty} e^{-\tau} d\tau}_{\nabla} \quad (4)$$

From Eq. (1) follows:

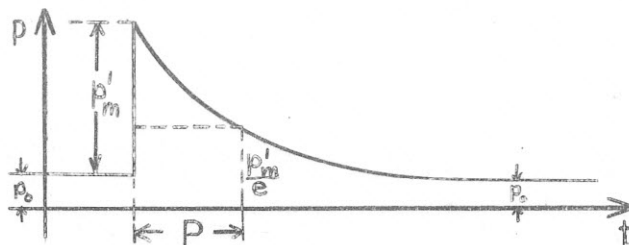
$$\frac{1}{\nabla} = - \frac{\partial}{\partial t} \ln p'u \Big|_{t=t_x} \quad (5)$$

The principle of shape similarity invariance now states that the integral ∇ over the shape of this normalized shock remains the same during propagation.

2) Time scales ∇ and form factors ∇

On several occasions, we used in the main body of the text the quantities ∇ and ∇ related to specific shock forms. Their derivation is briefly reviewed in the following.

a) Exponential pulse:



We know from Eq. (4):

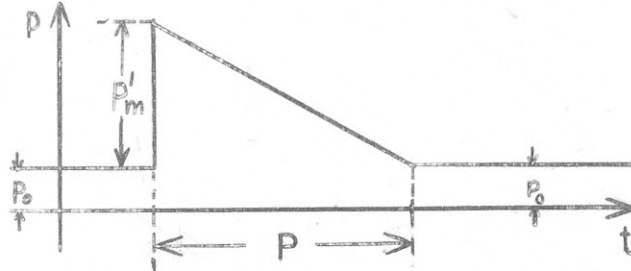
$$\nabla = 1 \quad (6)$$

If p_m' and u_m have the same time behavior, we have

$$p' = p_m' e^{-t/2\tau} = p_m' e^{-t/P}$$

$$\tau = P/2 \quad (7)$$

b) Triangle pulse:



Assuming:

$$u = u_m \left(1 - \frac{t}{P}\right); \quad p' = p_m' \left(1 - \frac{t}{P}\right)$$

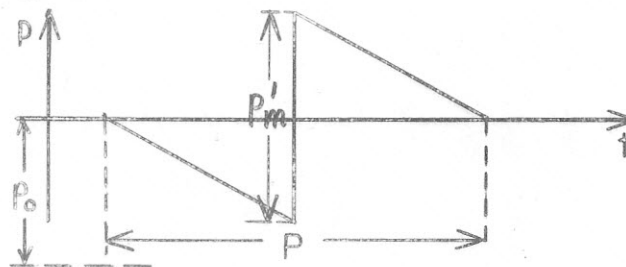
we find

$$\frac{1}{\tau} = - \frac{\partial}{\partial t} \ln p_m' u_m \left(1 - \frac{t}{P}\right)^2 \Big|_{t=0} = \frac{2}{P} \quad (8)$$

$$D = \int_0^P p' u \, dt = p_m' u_m \tau \nu$$

$$\nu = \int_0^P \frac{2}{P} \left(1 - \frac{t}{P}\right)^2 dt = \frac{2}{3} \quad (9)$$

c) Sawtooth pulse



Assuming:

$$u = \begin{cases} -\frac{u_m}{2} \left(1 - \frac{2t}{P}\right) & -\frac{P}{2} \leq t \leq 0 \\ \frac{u_m}{2} \left(1 - \frac{2t}{P}\right) & 0 \leq t \leq P/2 \end{cases}$$

$$p' = \begin{cases} -\frac{p_m'}{2} \left(1 - \frac{2t}{P}\right) & -\frac{P}{2} \leq t \leq 0 \\ \frac{p_m'}{2} \left(1 - \frac{2t}{P}\right) & 0 \leq t \leq P/2 \end{cases}$$

we find the results

$$\frac{I}{\pi} = - \left. \frac{\partial \ln p'u}{\partial t} \right|_{t=0} = \frac{4}{P} \quad (10)$$

$$D = 2 \int_0^{P/2} \frac{p_m'}{2} \cdot \frac{u_m'}{2} \left(1 - \frac{2t}{P}\right)^2 dt = p_m' u_m' \pi \nu$$

$$\nu = \int_0^{P/2} \left(1 - \frac{2t}{P}\right)^2 \frac{2dt}{P} = \frac{1}{3} \quad (11)$$

Appendix C

Entropy difference

In a gas with $\gamma = \text{const.}$ and $\mu = \text{const.}$,

$$p = \rho \frac{RT}{\mu} \quad v = \frac{1}{\rho} \quad \text{spec. vol. per gram} \quad (1)$$

From the 1st and 2nd law of thermodynamics, we have

$$TdS = c_v dT + pdV, \quad (2)$$

$$dS = c_v \frac{dT}{T} + \frac{R}{\mu} \frac{dV}{V}, \quad (3)$$

or upon integration,

$$\Delta S = c_v \ln \frac{T}{T_0} + \frac{R}{\mu} \ln \frac{V}{V_0} \quad (4)$$

With

$$c_p - c_v = \frac{R}{\mu}$$

from Sec. 5 and with Eq. (1)

$$\Delta S = c_v \ln \frac{p}{p_0} - c_p \ln \frac{\rho}{\rho_0}. \quad (5)$$

Thus

$$\Delta S = c_v \ln \frac{p}{p_0} \left(\frac{\rho}{\rho_0} \right)^{-\gamma} \quad (6)$$

with

$$\gamma = c_p / c_v \quad (7)$$

as usual.

Appendix D

Expansions for small shock Mach numbers $M_s = 1 + \alpha$

$$\text{Eq. (4-9): } \phi = 1 + \frac{4\gamma}{\gamma+1} \alpha + \frac{2\gamma}{\gamma+1} \alpha^2 \quad (1)$$

$$\text{Eq. (4-10): } \theta = 1 + \frac{4\alpha}{\gamma+1} + \left(1 - 4 \frac{\gamma-1}{\gamma+1} - \frac{\gamma-1}{\gamma+1} + 4 \frac{(\gamma-1)^2}{(\gamma+1)^2}\right) \alpha^2 \quad (2)$$

$$\text{Eq. (4-13): } \rho = 1 + 2 \frac{\gamma-1}{\gamma+1} \alpha + \frac{1}{2} \frac{\gamma-1}{\gamma+1} \alpha^2 \quad (3)$$

$$\text{Eq. (4-15): } \zeta = \frac{4\alpha}{\gamma+1} - \frac{2\alpha^2}{\gamma+1} \quad (4)$$

$$\text{Eq. (4-18): } \eta = \frac{\gamma+1}{8} - \frac{1}{4}(\gamma-1)\alpha + \frac{1}{16} \left(\frac{6\gamma^2 - 17\gamma + 9}{\gamma+1}\right) \alpha^2 \quad (5)$$

$$\zeta\eta = \frac{\gamma+1}{8} - \frac{\gamma}{16} \alpha^2 \quad (6)$$

$$\zeta(\zeta+\xi) = 1 + \frac{4\gamma}{\gamma+1} \alpha + \frac{5\gamma-7}{\gamma+1} \alpha^2 \quad (7)$$

$$\zeta\eta \left(\frac{\zeta(\xi+\zeta)-1}{\zeta+\xi}\right) = \frac{\gamma}{2} \alpha - \frac{3\gamma+7}{8} \alpha^2 \quad (8)$$

Now:

$$\ln(\phi \theta^{-\gamma}) = \ln \phi - \gamma \ln \theta \quad (9)$$

and correct to terms of third order,

$$\ln(\phi \theta^{-\gamma}) = \frac{16}{3} \frac{\gamma(\gamma-1)}{(\gamma+1)^2} \alpha^3 \quad (10)$$

Also,

$$3M_s^2 - 2 - \frac{1}{M_s^2} = 8\alpha \quad (11)$$

and from Eq. (4-38):

$$\chi = \frac{2}{3} \alpha^2 \quad (12)$$

If γ is constant, if we use plane geometry, and if there is no mass flow, we get from Eqs. (4), (6), (8), (12) and (4-40)

$$\frac{d\alpha}{dr} = (1+\alpha) \left\{ - \left(\frac{1}{4} \alpha - \frac{1}{8} \alpha^2 \right) \frac{1}{c} \frac{dc^2}{dr} + \left(\frac{\gamma}{2} \alpha - \frac{3\gamma+7}{8} \alpha^2 \right) \frac{r_0}{\gamma H} \right\} - \frac{1}{6} \frac{\alpha^2 r_0}{c r v}$$

or

$$\frac{1}{\alpha} \frac{d\alpha}{dr} = - \left(\frac{1}{4} + \frac{1}{8} \alpha \right) \frac{1}{c} \frac{dc^2}{dr} + \left(\frac{1}{2} + \frac{\gamma-7}{8\gamma} \alpha \right) \frac{r_0}{H} - \frac{1}{6} \frac{\alpha r_0}{c r v} \quad (13)$$

Appendix E

Equation of Energy Conservation

From the identity

$$\frac{\partial}{\partial t} \left(\frac{1}{2} \rho u^2 + \rho E \right) = \frac{1}{2} u^2 \frac{\partial \rho}{\partial t} + \rho \vec{u} \cdot \frac{\partial \vec{u}}{\partial t} + \frac{\partial \rho E}{\partial t}$$

we have with Eqs. (2-1), (2-2)

$$= - \frac{1}{2} u^2 \nabla \rho \vec{u} - \rho \vec{u} (\vec{u} \cdot \nabla) \vec{u} - \rho \vec{u} \cdot \frac{\nabla p}{\rho} - \rho \vec{u} \cdot g \vec{x} + \frac{\partial \rho E}{\partial t}$$

or

$$= -\frac{1}{2} \nabla \rho \vec{u} - \rho \vec{u} \nabla \left(\frac{1}{2} u^2 + H \right) + \rho \vec{u} \cdot \nabla s - \rho \vec{u} \cdot \vec{g} + \frac{\partial \rho E}{\partial t} \quad (1)$$

Now:

$$d\rho E = E d\rho + \rho dE = E d\rho + \rho T ds + \frac{p}{\rho} d\rho = \rho T ds + H d\rho \quad (2)$$

where we used Eq. (6-2) and (6-3). Hence, with Eqs. (2-1) and (2-3),

$$\frac{\partial \rho E}{\partial t} = H \frac{\partial \rho}{\partial t} + \rho T \frac{\partial s}{\partial t} = -H \nabla \rho \vec{u} - \rho T \vec{u} \cdot \nabla s + \rho T \frac{\partial s}{\partial t} \Big|_{\text{ext}}$$

or

$$= -\left(\frac{1}{2} u^2 + H \right) \nabla \cdot \rho \vec{u} - \rho \vec{u} \nabla \left(\frac{1}{2} v^2 + H \right) - \rho \vec{u} \cdot \vec{g} + \rho T \frac{\partial s}{\partial t} \Big|_{\text{ext}}$$

and finally,

$$\frac{\partial}{\partial t} \left(\frac{1}{2} \rho u^2 + \rho E \right) = -\nabla \cdot \rho \vec{u} \left(\frac{1}{2} u^2 + H \right) - \rho \vec{u} \cdot \vec{g} + \rho T \frac{\partial s}{\partial t} \Big|_{\text{ext}}$$

Appendix F

Shock behavior under energy conservation.

1) Isothermal gravitational atmosphere.

The conservation of energy flux of a weak shock wave can be written in the form:

$$\rho u^2 c = \rho_0 u_0^2 c_0 \quad (1)$$

Now in a weak shock the propagation velocity

$$U \approx c.$$

Using this fact and Eqs. (4-42) and (3-21) we get:

$$\frac{v_2}{v_1} = \frac{u-U}{-U} = 1 - \frac{u}{c} = 1 - \bar{\eta}$$

or

$$u = \bar{\eta} c \quad (2)$$

With the aid of the relations

$$c = c_0 ; \quad \rho = \rho_0 e^{-h/H_0}$$

where $H_s = RT/\mu g$ is the scale height, we have

$$\bar{\eta}^2 = \bar{\eta}_0^2 e^{h/H_s} \quad (3)$$

or

$$\frac{1}{\bar{\eta}} \frac{d\bar{\eta}}{dh} = \frac{1}{2H_s} \quad (4)$$

2) Isobaric atmosphere, no gravitation

Using

$$c^2 = \gamma \frac{p}{\rho}$$

and Eqs (2) and (1) we get:

$$p \bar{\eta}^2 c = p_0 \bar{\eta}_0^2 c_0 \quad (5)$$

Now if $p = p_0$,

$$\bar{\eta}^2 = \frac{\bar{\eta}_0^2 c_0}{c} \quad (6)$$

Hence

$$\frac{1}{\bar{\eta}} \frac{d\bar{\eta}}{dh} = - \frac{1}{4c^2} \frac{dc^2}{dh} \quad (7)$$

Appendix G

Importance of the bound state energy.

To check the importance of bound state populations in computing internal energies we have calculated the bound energy for an atmosphere consisting of 84% ($v_1 = .84$) Hydrogen, the remainder being some unionized gas.

To specify the physical conditions in the atmosphere, in particular the pressure vers. temperature behavior, we used the

"working model for the chromosphere" by Aller [4, p. 507] (interspicule case). The partition functions were taken from de Jager and Neven [43] and Aller [4, p. 116].

1) LTE Case

The ionization was calculated from tables given by Unsöld [105, p. 87].

2) Non-LTE Case

We assumed $b_1 = 10^9$, $b_2 = b_3 = \dots = 1$. The ionization was calculated according to House [34]. The results were:

1) LTE case.

The contribution of the bound energy is negligible.

2) Non-LTE case

The contribution of the bound states may exceed at times the other contributions. But only in certain temperature ranges. We feel that the inclusion of this effect is not worth the tremendous mathematical labor involved, especially as it subsequently turned out that the variation of γ is unimportant for our calculations.

The influence of the bound energies is shown in Fig. 8 in terms of the variation of γ .

Appendix H

Agreement with G. B. Field's result.

Eq. (6-9) agrees with Field's [31] result, as can be seen in the following manner:

Firstly from (6-9) we have

$$\rho \vec{u} \left\{ \nabla \left(\frac{1}{2} u^2 + H \right) + g \hat{x} \right\} - \nabla K \nabla T + \rho \dot{Q}_{\text{rad}} - \rho \dot{Q}_{\text{mech}} = 0 \quad (1)$$

Secondly with Eq. (2-2) in steady state:

$$(\vec{u} \cdot \nabla) \vec{u} = - \frac{1}{\rho} \nabla p - g \hat{x} \quad (2)$$

and from Sec. 5 with constant γ :

$$H = \frac{\gamma}{\gamma-1} \frac{p}{\rho} \quad (3)$$

or

$$\nabla H = \frac{\gamma}{\rho(\gamma-1)} \nabla p - \frac{\epsilon p}{(\gamma-1)\rho^2} \nabla \rho \quad (4)$$

Using

$$\nabla \frac{1}{2} u^2 = (\vec{u} \cdot \nabla) \vec{u} \quad (5)$$

we obtain

$$\rho \vec{u} \cdot \left\{ \frac{\gamma}{\rho(\gamma-1)} \nabla p - \frac{\gamma p}{(\gamma-1)\rho^2} \nabla p - \frac{1}{\rho} \nabla p \right\} - \nabla K \nabla T + \rho \dot{Q}_{\text{rad}} - \rho \dot{Q}_{\text{mech}} = 0$$

or

$$\frac{1}{\gamma-1} \vec{u} \cdot \nabla p - \frac{\gamma}{\gamma-1} \frac{p}{\rho} \vec{u} \cdot \nabla \rho + (\rho \dot{Q}_{\text{rad}} - \rho \dot{Q}_{\text{mech}}) - \nabla K \nabla T = 0 \quad (6)$$

This is the steady state form of Field's Eq. (9).